



HAL
open science

Studies of the dynamics of dry-friction-damped blade assemblies

Jérôme Guillen

► **To cite this version:**

Jérôme Guillen. Studies of the dynamics of dry-friction-damped blade assemblies. Mechanics [physics.med-ph]. University of Michigan-Ann Arbor, 1999. English. NNT: . tel-00365016

HAL Id: tel-00365016

<https://theses.hal.science/tel-00365016>

Submitted on 2 Mar 2009

HAL is a multi-disciplinary open access archive for the deposit and dissemination of scientific research documents, whether they are published or not. The documents may come from teaching and research institutions in France or abroad, or from public or private research centers.

L'archive ouverte pluridisciplinaire **HAL**, est destinée au dépôt et à la diffusion de documents scientifiques de niveau recherche, publiés ou non, émanant des établissements d'enseignement et de recherche français ou étrangers, des laboratoires publics ou privés.

STUDIES OF THE DYNAMICS OF DRY-FRICTION-DAMPED BLADE ASSEMBLIES

by
Jérôme Guillen

A dissertation submitted in partial fulfillment
of the requirements for the degree of
Doctor of Philosophy
(Mechanical Engineering)
in The University of Michigan
1999

Doctoral Committee:

Professor Christophe Pierre, chairman
Assistant Professor Karl Grosh
Professor A. Galip Ulsoy
Assistant Professor Nickolas Vlahopoulos
Marc Berthillier, SNECMA

Mai, o bellasso! au mai t'aluque,
Au mai, pecaire! m'emberluque! . . .
Veguère uno figuiero, un cop, dins moun camin,
Arrapado à la roco nuso
Contro la baumo de Vau-Cluso:
Maigro, pecaire! i lagramuso
Ié dounarié mai d'ombro un clot de jaussemin!

Un cop pèr an vers si racino
Vèn flouqueja l'ondo vesino;
E l'aubret secarous, à l'aboundouso font
Que mounto à-n-éu pèr que s'abéure
Tant que n'en vóu, se bouto à béure . . .
D'acò tout l'an n'a proun pèr viéure.
Coume à l'anèu la pèiro, à iéu acò respond.

F. M.

© Jérôme Guillen 1999
All Rights Reserved

ACKNOWLEDGEMENTS

I wish to express my profound gratitude to Prof. Christophe Pierre for his guidance and his trust. Additionally, I would like to thank Marc Berthillier and La Société Nationale D'Étude et de Construction de Moteurs d'Aviation (SNECMA) for their support and input, Nicolas Boivin for his mentorship when I started this dissertation, Jonathan Cherry and Thomas Lagrange for their help with the codes and the computational runs, and Ronnie Bladh and Matt Castanier for their insights. Finally, many thanks to my friends in Ann Arbor who supported me throughout my years at the University of Michigan.

TABLE OF CONTENTS

ACKNOWLEDGEMENTS	ii
LIST OF FIGURES	vi
LIST OF TABLES	xv
CHAPTER	
I. INTRODUCTION	1
1.1 Foreword	1
1.2 Literature review	4
1.3 Dissertation outline	7
II. SINGLE-HARMONIC BASED METHODS	9
2.1 Introduction	9
2.2 Single-Degree of Freedom Systems	10
2.2.1 System Model	10
2.2.2 Force-displacement relation	10
2.2.3 Single-harmonic approximation	12
2.2.4 Improvement to the single-harmonic approximation	14
2.2.5 Results	17
2.3 Multi-DOF systems with a single friction damper	20
2.3.1 System model	20
2.3.2 Reduction of the number of equations	22
2.3.3 Single-harmonic approximation	23
2.3.4 Results	24
2.4 Multi-DOF systems with multiple friction dampers	31
2.5 Conclusion	33
III. MULTI-HARMONIC, HYBRID FREQUENCY/TIME METHOD	35
3.1 Introduction	35
3.2 Friction force treatment	36

3.3	Frequency domain treatment	38
3.4	Solving the nonlinear equations in the frequency domain . . .	40
3.4.1	QR vs. LU decomposition	41
3.4.2	Broyden method	42
3.5	Overview of the multi-harmonic, hybrid frequency/time method	45
3.6	Conclusion	47
IV. SELECTED FORCED RESPONSE RESULTS		48
4.1	Introduction	48
4.2	Forced response of beam system	49
4.2.1	System model and influence of force amplitude . . .	49
4.2.2	Influence of the damper stiffness	53
4.3	Forced response of turbine blade system	55
4.4	Performance of the hybrid frequency/time method	62
4.5	Large-scale tuned and mistuned beam assemblies	65
4.6	Conclusion	72
V. FREE RESPONSE AND STABILITY		78
5.1	Introduction	78
5.2	Free response of single-DOF systems	78
5.2.1	Single-harmonic approximation	79
5.2.2	Multi-harmonic method	85
5.2.3	Influence of the friction damper stiffness, k_d	91
5.3	Free response of multi-DOF system	93
5.3.1	Equations of motion and multi-harmonic solution method	93
5.3.2	Multiplicity of solutions	96
5.4	Stability considerations for multi-DOF systems	106
5.4.1	Stability of SNECMA beam with all three modes negatively damped	106
5.4.2	Stability of SNECMA beam with a single negatively damped mode	117
5.5	Conclusion	120
VI. ADVANCED FRICTION DAMPERS		126
6.1	Introduction	126
6.2	Friction force for elementary damper model	127
6.3	Friction force for advanced structure-like dampers	129
6.3.1	New force update for elementary damper	130
6.3.2	New update for structure-like dampers	131
6.3.3	Time-marching procedure for structure-like dampers	133

6.3.4	Initial conditions	139
6.4	Results for an example system	140
6.4.1	Time histories	140
6.4.2	Frequency response results	145
6.5	Conclusions and Future work	153
VII. CONCLUSIONS		155
7.1	Main contributions	155
7.2	Direction for future work	157
BIBLIOGRAPHY		161

LIST OF FIGURES

Figure

1.1	Blade assembly model [Kruse and Pierre, 1996].	2
1.2	Blade model [Berthillier et al., 1998a].	3
2.1	Single-DOF system with attached flexible dry-friction damper . . .	11
2.2	Force transmitted by the damper as a function of the mass DOF displacement	12
2.3	Damper displacement predicted by Griffin's single-harmonic solution [Griffin, 1980], by the improved single-harmonic approximation and by full time integration, $P = 0.5F_d$, $\omega = 225 \text{ rad/s}$	16
2.4	Mass displacement and damper displacement for a single-DOF system using numerical time integration and improved single-harmonic approximation. External force $P = 0.5F_d$	18
2.5	Mass displacement and damper displacement for a single-DOF system using numerical time integration and improved single-harmonic approximation. External force $P = 2F_d$	19
2.6	Mass displacement for a single-DOF system using the improved single-harmonic approximation. The frequency responses are scaled by the force amplitude.	21
2.7	Three-DOF beam of length L , with an attached flexible friction damper at $0.239L$	21
2.8	Beam displacement amplitude at the damper location and damper displacement for a 3-DOF system using numerical time integration and improved single-harmonic approximation. External force $P = 16.563N$	25

2.9	Tip beam displacement amplitude for a 3-DOF system using numerical time integration and improved single-harmonic approximation. External force $P = 16.563N$	28
2.10	Beam displacement amplitude at the damper location for a 3-DOF system using the improved single-harmonic approximation. The frequency responses are normalized by the force amplitudes.	29
2.11	Tip beam displacement for a 3-DOF system using the improved single-harmonic approximation. The frequency responses are normalized by the force amplitudes.	30
3.1	Model of the i -th friction damper.	37
4.1	Time histories of displacement at the damper location, x_1 , and damper displacement, x_d , for the 3-DOF SNECMA beam, for a force amplitude of $20.313N$, at $170rad/s$, as predicted by the 19-harmonic hybrid frequency/time method (Broyden), and numerical time integration.	50
4.2	Time histories of displacement at the damper location, x_1 , and damper displacement, x_d , for the 3-DOF SNECMA beam, for a force amplitude of $25.0N$, at $200rad/s$, as predicted by the 19-harmonic hybrid frequency/time method (Broyden), and numerical time integration.	51
4.3	Frequency responses at the damper location, for the 3-DOF SNECMA beam, for various force amplitudes, as predicted by the 15-harmonic hybrid frequency/time method.	52
4.4	Frequency responses at the tip of the beam, for the 3-DOF SNECMA beam, for various force amplitudes, as predicted by the 15-harmonic hybrid frequency/time method.	53
4.5	Beam frequency response at the damper location, x_1 , for the 3-DOF SNECMA beam, for various damper stiffnesses, k_d , as predicted by the 15-harmonic hybrid frequency/time method, and for force amplitude $P = 20.313N$	54
4.6	Beam frequency response at the tip, x_2 , for the 3-DOF SNECMA beam, for various damper stiffnesses, k_d , as predicted by the 15-harmonic hybrid frequency/time method, and for force amplitude $P = 20.313N$	55

4.7	Beam frequency response at the damper location, x_1 , for the 3-DOF SNECMA beam, for various damper stiffnesses, k_d , as predicted by the 15-harmonic hybrid frequency/time method, and for force amplitude $P = 20.313N$	56
4.8	Beam frequency response at the tip, for the 3-DOF SNECMA beam, x_2 , for various damper stiffnesses, k_d , as predicted by the 15-harmonic hybrid frequency/time method, and for force amplitude $P = 20.313N$	57
4.9	18-mode turbine blade model [Berthillier et al., 1998a]. Friction dampers are inserted between the blade and the platform.	59
4.10	Blade frequency response at the damper location, normalized by the peak amplitude when the damper is totally stuck, for various levels of maximum force transmitted by the damper, F_d/F_{d0} , as predicted by the hybrid frequency/time (Broyden) method, with 9 harmonics used.	60
4.11	Blade frequency response at the tip, normalized by the peak tip amplitude when the damper is totally stuck, for various levels of maximum force transmitted by the damper, F_d/F_{d0} , as predicted by the hybrid frequency/time (Broyden) method, with 9 harmonics.	61
4.12	Blade frequency response at the damper location, at optimal damping, $F_d = F_{d0}$, as predicted by the Runge-Kutta time integration method, and by the hybrid frequency/time (Broyden) method, with 9 harmonics.	62
4.13	Blade frequency response at the tip, at optimal damping, $F_d = F_{d0}$, as predicted by the Runge-Kutta time integration method, and by the hybrid frequency/time (Broyden) method, with 9 harmonics.	63
4.14	Blade assembly with shrouds [Bladh et al., 1998].	66
4.15	36-beam, 36-damper, cyclic, coupled beam assembly.	67
4.16	Beam frequency responses at the damper location (x_1), for beams 13 through 24 from a tuned, 36-beam assembly with engine order two excitation, coupled by a stiffness of $k = 10^5 N/m$, for a force amplitude of $20.313N$, as predicted by the 3-harmonic hybrid frequency/time method.	68

4.17	Beam frequency response at the tip (x_2), for beams 13 through 24 from a tuned, 36-beam assembly with engine order two excitation, coupled by a stiffness of $k = 10^5 N/m$, for a force amplitude of $20.313N$, as predicted by the 3-harmonic hybrid frequency/time method.	69
4.18	Displacement at the damper location (x_1) and damper displacement (x_d), of the first six of 36 tuned beams, coupled at the tip by a stiffness of $k = 10^5 N/m$, for an engine order two excitation and a force amplitude $20.313N$, at frequency $\omega = 220 rad/s$, as predicted by the 7-harmonic hybrid frequency/time method.	70
4.19	Displacement at the damper location, x_1 , and damper displacement, x_d , for the 7% mistuned 36-beam assembly. Beams numbered 8, 11 and 22 are shown, coupled by a stiffness, $k_c = 7.10^3 N/m$, for engine order three excitation and a force amplitude of $20.313N$ at $200 rad/s$, as predicted by (a) the 1-harmonic Broyden method and (b) 9-harmonic Broyden method, and numerical time integration.	73
4.20	Frequency response of beams 1 through 12, at the damper locations, x_1 , for the 7% mistuned 36-beam assembly, coupled by a stiffness, (a) $k_c = 10^3 N/m$, (b) $3.10^3 N/m$, and (c) $5.10^3 N/m$, for engine order three excitation and a force amplitude of $20.313N$, as predicted by the 3-harmonic Broyden method.	74
4.21	Frequency response of beams 1 through 12, at the damper locations, x_1 , for the 7% mistuned 36-beam assembly, coupled by a stiffness, (d) $6.10^3 N/m$, (e) $1.2.10^4 N/m$, and (f) $10^5 N/m$, for engine order three excitation and a force amplitude of $20.313N$, as predicted by the 3-harmonic Broyden method.	75
4.22	Magnification factor, \mathcal{M} , at the damper locations, x_1 , and the tips of the beams, x_2 , for the 7%-mistuned, 36-beam assembly, as a function of the coupling stiffness, k_c , for engine order 3 excitation and a force amplitude of $20.313N$, as predicted by the Broyden method for 1 and 3 harmonics.	76
5.1	Displacement amplitude of the mass (x), as a function of the negative viscous damping ratio, r , as predicted by the single-harmonic balance method. There is no stable motion for $r > r_{max}$	81
5.2	Frequency of motion of the mass, as a function of the negative viscous damping ratio, r , as predicted by the single-harmonic balance method. There is no stable motion for $r > r_{max}$	82

5.3	Mass displacement amplitude, as predicted by the Broyden method, with 1 and 31 harmonics used, as a function of the negative viscous damping ratio.	86
5.4	Amplitude of the displacement of a single-DOF friction damped system, as a function of the negative viscous damping ratio, as predicted by the 5-harmonic hybrid frequency/time method, and time integration.	87
5.5	Amplitude of the displacement of a single-DOF friction damped system, as a function of the negative viscous damping ratio, as predicted by the 5-harmonic hybrid frequency/time method, and time integration (sticking branch only).	88
5.6	Frequency of the displacement of a single-DOF friction damped system, as a function of the negative viscous damping ratio, as predicted by the 5-harmonic hybrid frequency/time method, and time integration.	89
5.7	Frequency of the displacement of a single-DOF friction damped system, as a function of the negative viscous damping ratio, as predicted by the 5-harmonic hybrid frequency/time method, and time integration (sticking branch only).	90
5.8	Amplitude of the displacement of a single-DOF friction damped system, as a function of the ratio of friction damper stiffness, v , as predicted by the multi-harmonic free-response method.	93
5.9	Fundamental frequency of the displacement of a single-DOF friction damped system, as a function of the ratio of friction damper stiffness, v , as predicted by the hybrid frequency/time method.	94
5.10	Time history of displacement of the three DOF's of the SNECMA beam and of the friction damper, for the first case listed in Table 5.2 (the time origin is shifted). The steady-state reached corresponds to the first mode of vibration of the beam.	98
5.11	Time history of displacement of the three DOF's of the SNECMA beam and of the friction damper, for the second case listed in Table 5.2 (the time origin is shifted). The steady-state reached corresponds to the second mode of vibration of the beam.	99

5.12	Time history of displacement of the three DOF's of the SNECMA beam and of the friction damper, for the third case listed in Table 5.2 (the time origin is shifted). The steady-state reached corresponds to the third mode of vibration of the beam.	100
5.13	Amplitude of displacement of the first DOF of the SNECMA beam, for the three possible modes, as a function of the negative viscous damping ratio, as predicted by the hybrid frequency/time method, with 3 harmonics used.	102
5.14	Amplitude of displacement of the second DOF of the SNECMA beam, for the three possible modes, as a function of the negative viscous damping ratio, as predicted by the hybrid frequency/time method, with 3 harmonics used.	103
5.15	Amplitude of displacement of the third DOF of the SNECMA beam, for the three possible modes, as a function of the negative viscous damping ratio, as predicted by the hybrid frequency/time method, with 3 harmonics used.	104
5.16	Frequency of free motion of the SNECMA beam, for the three possible modes of vibration, as a function of the negative viscous damping ratio, as predicted by the hybrid frequency/time method, with 3 harmonics used.	105
5.17	Amplitude of the first DOF displacement for the sticking branch of the three modes of vibration of the SNECMA beam, as predicted by the hybrid frequency/time method, with 3 harmonics used, and by forward numerical time integration with initial conditions near mode 3, as a function of the negative viscous damping ratio. When time integration fails to converge or is unstable the amplitude is shown as zero.	110
5.18	Amplitude of the second DOF displacement for the sticking branch of the three modes of vibration of the SNECMA beam, as predicted by the hybrid frequency/time method, with 3 harmonics used, and by forward numerical time integration with initial conditions near mode 3, as a function of the negative viscous damping ratio.	111
5.19	Amplitude of the third DOF displacement for the sticking branch of the three modes of vibration of the SNECMA beam, as predicted by the hybrid frequency/time method, with 3 harmonics used, and by forward numerical time integration with initial conditions near mode 3, as a function of the negative viscous damping ratio.	112

5.20	Frequency of free motion for the sticking branch of the three modes of vibration of the SNECMA beam, as predicted by the hybrid frequency/time method, with 3 harmonics used, and by forward numerical time integration with initial conditions near mode 3, as a function of the negative viscous damping ratio.	113
5.21	Time history of the first DOF of the SNECMA beam, as predicted by hybrid frequency/time method (sticking branch of mode 1), and by time integration (initial conditions 2% below the slipping branch of mode 3). The negative viscous damping ratio is 0.361.	114
5.22	Time history of the second DOF of the SNECMA beam, as predicted by hybrid frequency/time method (sticking branch of mode 1), and by time integration (initial conditions 2% below the slipping branch of mode 3). The negative viscous damping ratio is 0.361.	115
5.23	Time history of the third DOF of the SNECMA beam, as predicted by hybrid frequency/time method (sticking branch of mode 1), and by time integration (initial conditions 2% below the slipping branch of mode 3). The negative viscous damping ratio is 0.361.	116
5.24	Power spectral density of the time history of the third DOF displacement, as predicted by time integration. Same initial conditions as in Fig. 5.23.	118
5.25	Amplitude of displacement of the first DOF of the SNECMA beam, with only the third mode negatively damped, as a function of the negative viscous damping ratio, as predicted by the hybrid frequency/time free response method, with 9 harmonics used.	121
5.26	Amplitude of displacement of the second DOF of the SNECMA beam, with only the third mode negatively damped, as a function of the negative viscous damping ratio, as predicted by the hybrid frequency/time free response method, with 9 harmonics used.	122
5.27	Amplitude of displacement of the third DOF of the SNECMA beam, with only the third mode negatively damped, as a function of the negative viscous damping ratio, as predicted by the hybrid frequency/time free response method, with 9 harmonics used.	123

5.28	Frequency of displacement of the SNECMA beam, with only the third mode negatively damped, as a function of the negative viscous damping ratio, as predicted by the hybrid frequency/time free response method, with 9 harmonics used.	124
6.1	Model of the elementary friction damper.	128
6.2	Model of an advanced, structure-like friction damper.	130
6.3	4-DOF damper element connected to two SNECMA beams.	141
6.4	Time histories of the four friction forces, of the sticking linear forces at the damper locations, and of the sum of the forces transmitted by the friction element, when no damper is slipping, for $\omega = 250rad/s$ and $F_{ex} = 15N$	143
6.5	Time histories of the four friction forces, of the sticking linear forces at the damper locations, and of the sum of the forces transmitted by the damper element, when only damper 1 is slipping, for $\omega = 550rad/s$ and $F_{ex} = 35N$	144
6.6	Time histories of the four friction forces, of the sticking linear forces at the damper locations, and of the sum of the forces transmitted by the damper element, when only two dampers are slipping at the same time, for $\omega = 550rad/s$ and $F_{ex} = 140N$	146
6.7	Time histories of the four friction forces, of the sticking linear forces at the damper locations, and of the sum of the forces transmitted by the damper element, when at most three dampers are slipping at the same time, for $\omega = 550rad/s$ and $F_{ex} = 550N$	147
6.8	Beam displacement amplitude at dampers 1 and 2, as a function of the frequency, for different force amplitudes: $F_{ex} = 20, 30, 40, 50, 55,$ and $60N$ (from left to right, top to bottom).	148
6.9	Beam displacement amplitude at dampers 1 and 2, as a function of the frequency, for different force amplitudes: $F_{ex} = 70, 80, 90, 100, 110,$ and $120N$ (from left to right, top to bottom).	149
6.10	Beam displacement amplitude at dampers 3 and 4, as a function of the frequency, for different force amplitudes: $F_{ex} = 20, 30, 40, 50, 55,$ and $60N$ (from left to right, top to bottom).	151

6.11 Beam displacement amplitude at dampers 3 and 4, as a function of the frequency, for different force amplitudes: $F_{ex} = 70, 80, 90, 100, 110,$ and $120N$ (from left to right, top to bottom). 152

LIST OF TABLES

Table

2.1	Improved update of the damper displacement z	15
2.2	Numerical values of the single-DOF system used to compare the results of the time integration procedure and the results of the improved single-harmonic approximation.	20
2.3	Comparison of peak displacement amplitude predicted by the time integration procedure and the improved single-harmonic approximation, for different force amplitudes at the tip of the beam and at the damper location.	27
3.1	Update for the nonlinear force transmitted by the i -th friction damper.	37
4.1	Computational time needed by the multi-harmonic frequency/time method and numerical time integration for the determination of the frequency response of the SNECMA beam presented in Section 4.2.1 and of the blade presented in Section 4.3.	64
5.1	Values of the parameters for the single-DOF case.	83
5.2	Three sets of initial conditions, used for the numerical time integration of the free response of the 3-DOF SNECMA beam. All initial velocities are taken to be zero.	97
5.3	Slipping and sticking natural frequencies of the SNECMA beam. . .	106
6.1	Update for the nonlinear force transmitted by the elementary friction damper in Fig. 6.1.	128
6.2	Update for the nonlinear force transmitted by the elementary friction damper in Fig. 6.1 using increments.	131
6.3	Maximum forces transmitted by the structure-like friction element. .	141

6.4	First three natural resonance frequencies of the two-beam/damper system in various slip/stick damper configurations (in <i>rad/s</i>). . . .	150
-----	---	-----

CHAPTER I

INTRODUCTION

1.1 Foreword

Safety and reliability are two foremost concerns in the design of high-speed rotating equipment. In order to reduce vibrations-induced wear and probability of failure, dry friction damping is widely used. In bladed disk assemblies, like the ones used in jet engines, friction damping may occur between two adjacent blades, between the blades and the disk, and between the blades and friction dampers inserted for that purpose below the platform of the blades. Figure 1.1 depicts a typical, industrial 29-blade assembly [Kruse and Pierre, 1996]. Figure 1.2 shows a finite-element blade model, provided by the Société Nationale D'Étude et de Construction de Moteurs d'Aviation (SNECMA) [Berthillier et al., 1998a], along with the disk section to which the blade is attached. Manufacturers of such equipment are interested in predicting the vibrations the rotating parts undergo. Many works have focused on the study of the steady-state response of friction damped structural systems and some of them are listed in the next section.

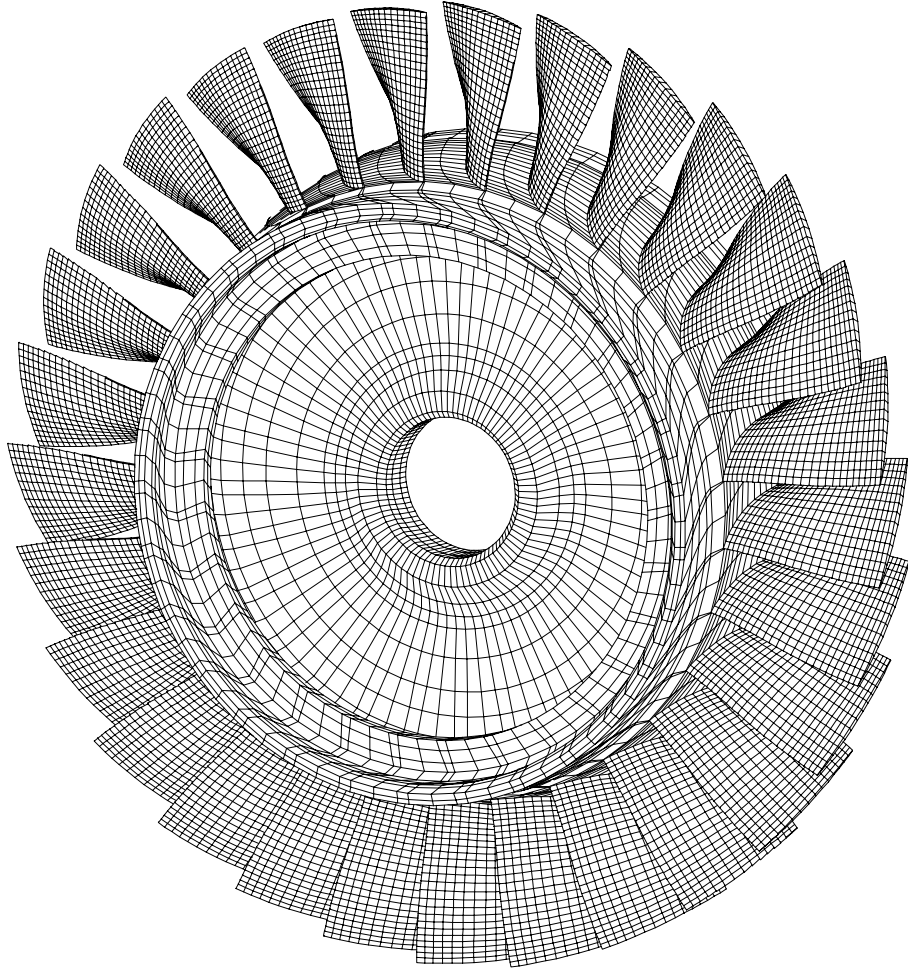


Figure 1.1: Blade assembly model [Kruse and Pierre, 1996].

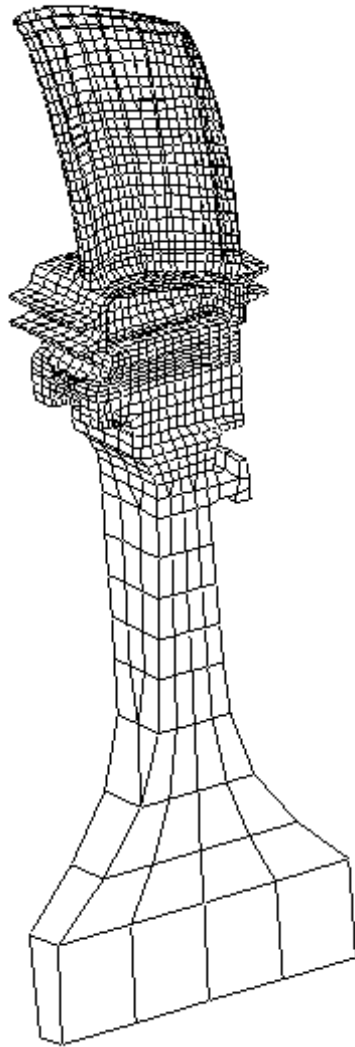


Figure 1.2: Blade model [Berthillier et al., 1998a].

1.2 Literature review

In this section, previous works on the dynamics of friction damped systems are presented. Some parts of this literature review are repeated throughout the dissertation to introduce the different chapters. Hopefully, this will put the present dissertation into perspective and not confuse the reader.

Numerical time integration procedures, such as fourth-order Runge-Kutta, provide an easy way to calculate the dynamic response of friction damped systems. Given the low level of viscous damping present in turbomachinery elements, the time integration procedure has to be performed over a large number of periods in order to reach the steady-state response, and the time step of the time integration procedure has to be small enough to prevent numerical instabilities. Both the large number of computation cycles and the small size of the time step required make numerical time integration methods computationally very expensive. Thus they are not suited to design and parametric analyses for which structural and friction parameters must be varied to achieve optimal damper performance.

The steady-state response of friction damped systems can be found in a semi-analytical way in some particular cases. Wang proposed an analytic solution when a single-degree-of-freedom (DOF) system with an elastic friction damper attached is considered [Wang, 1996], but the method cannot be readily extended to large-scale systems with many friction dampers. Most analytical solutions for friction damped systems are based on matching the solutions found for phases of the motion when the damper is stuck and when it is slipping [Natsiavas and Gonzalez, 1992]. The procedure implies knowing *a priori* how many slipping and sticking phases there are during each cycle, something not readily available [Natsiavas, 1998]. Moreover, if

several friction dampers were to be considered, the analytical method would result in complex systems of non-linear equations, for which no analytical solutions can be found. Wang also presented a finite element in time (FET) approach: the friction force is approximated by simple interpolation functions [Wang, 1997]. This approximation may lead to numerical problems when large-scale systems are considered.

The dynamics of friction damped systems are often studied using methods derived from the Harmonic Balance (HB) procedure [Nayfeh and Mook, 1979], with a single temporal harmonic retained in the solution. Early works [Griffin, 1980, Sinha and Griffin, 1983] used the single-harmonic approximation for single degree-of-freedom (DOF) systems. The approximation was used to obtain both the forced and free responses of friction damped blade systems [Sinha and Griffin, 1984, 1985], hollow blades [Griffin et al., 1998], and tuned and mistuned blade assemblies [Muszýnska and Jones, 1983, Griffin and Sinha, 1985, Sinha et al., 1986]. The single-harmonic method was also used on equations obtained by component mode analysis [Ferri and Dowell, 1985], on bi-dimensional friction dampers [Sanliturk and Ewins, 1996, Yang et al., 1998], and on dampers undergoing microslip [Menq et al., 1986, Sanliturk et al., 1997]. Provided that a number of conditions are met [Mickens, 1984], the HB method used with a single temporal harmonic is a fast and accurate way to study the dynamics of friction damped systems. Although the method cannot predict stick/slip motion, it can provide an acceptable approximation of the response amplitude, provided the first harmonic dominates the response of the system. Most single-harmonic studies have been limited to small- or medium-size models [Wei and Pierre, 1989, Sanliturk and Ewins, 1996].

Including several temporal harmonics of the response allows for the approximation of stick/slip motions, not permitted by single-harmonics studies. When

several temporal harmonics are considered, analytic approximations of the friction force are often used [Ferri and Dowell, 1988, Berthillier et al., 1998b], and/or structural models with a single friction damper are considered [Wang and Chen, 1993, Shiau and Yu, 1996, Shiau et al., 1998]. Two significant outgrowths of the HB method are the Incremental Harmonic Balance (IHB) [Lau et al., 1983, Pierre et al., 1985, Lau and Zhang, 1992] and the Alternating Frequency Time (AFT) method [Cameron and Griffin, 1989]. Both methods are based on iterative algorithms that yield a multi-harmonic, frequency-domain representation of the response. While they can produce good results (particularly for systems with polynomial nonlinearities), the IHB method can be numerically cumbersome, and the AFT one can suffer slow convergence. These methods are known to have significantly limiting convergence problems when applied to non-analytic friction damping. Other multi-harmonic works may involve determining the sticking and slipping transition times [Wang and Chen, 1993] –a rather difficult task that cannot be easily generalized to multi-DOF systems. Receptance-based methods for friction damped systems are sometimes used [Ren and Beards, 1994]: the method makes use of experimental data to determine the linear part of the response and of perturbation methods to obtain the steady-state response in non-linear cases. The receptance-based method requires about the same computational time as direct time integration, and therefore it is not suited for parametric studies. To alleviate the numerical difficulties of IHB methods, schemes involving Toeplitz Jacobian Matrices have been proposed [Leung and Ge, 1995], but they have only been successfully applied to polynomial nonlinearities.

In the studies of friction damped structural systems, friction damper elements may be described as rigid friction dampers [Pierre et al., 1985]. In bladed-disk assem-

blies, the damper interfaces undergo small motion prior to any slipping [Ferri, 1995]. Flexible friction dampers are needed to model this characteristic. The simplest model of a flexible friction damper is the hysteretic spring friction model, which is studied in this dissertation. By considering several flexible friction dampers in parallel, this model can take into account microslip [Menq et al., 1986]. The model can also be extended to some particular, elliptical, planar motion, provided that only one temporal harmonic is retained in the solution [Sanliturk and Ewins, 1996].

1.3 Dissertation outline

The goal of this dissertation is to present a new, efficient technique to predict the steady-state dynamics –both forced and free responses– of dry-friction damped structural systems.

In Chapter II, a single-harmonic approximation is presented. The traditional single-harmonic method is enhanced to allow a more accurate computation of the friction forces. The method is applied to multi-degree-of-freedom (DOF) systems in an efficient manner: complex, reduced dynamic and force matrices are introduced to reduce the number of equations. Results are presented for various structural parameters.

In Chapter III, a multi-harmonic, hybrid frequency/time method is developed for the forced response analysis of friction damped structural systems. With this method, the friction force transmitted by the dampers to the structure is evaluated in the time domain. The equations of motion are transformed in the frequency domain by the Harmonic Balance (HB) procedure and are solved using a robust, efficient algorithm derived from the Broyden method. The Broyden method is presented and compared to the more traditional Newton-Raphson scheme.

In Chapter IV, the multi-harmonic method presented in Chapter III is applied to several systems for a variety of structural and friction parameters. Large-scale systems with many friction dampers attached are considered. In particular, tuned and mistuned blade assembly configurations subject to various traveling wave “engine order” excitations are studied. Complex features of the non-linear response are revealed, including subresonances and localization.

In Chapter V, the method presented in Chapter III is modified to study the free response and stability of friction-damped structural systems. The procedure is developed for multi-DOF systems with a single friction damper attached, and subject to negative viscous damping. Results are presented for various structural and friction parameters. When several modes of vibration are negatively damped, the HB method predicts multiple solutions and the stability analysis is often not conclusive. When a single mode of vibration is negatively damped, which is usually the case in turbomachinery applications, the method is able to predict in an efficient and reliable manner the steady-state response of the system and its stability.

In Chapter VI, a new friction damper model is introduced: the damper element is treated as a general, massless structure with its own stiffness matrix. Slip is possible at several points of the interface between the damper and its adjacent structure (e.g., blade). Configurations where a damper is connected to two adjacent blades can be considered with this model. A new formulation is presented to compute the force transmitted by the damper element to the structure at the various contact points. Results are presented for an example system and reveal the rich dynamics of such general friction damper models.

CHAPTER II

SINGLE-HARMONIC BASED METHODS

2.1 Introduction

The dynamics of friction damped systems are often studied using methods derived from the Harmonic Balance (HB) procedure [Nayfeh and Mook, 1979], with a single temporal harmonic retained in the solution. Early works [Griffin, 1980, Sinha and Griffin, 1983] used the single-harmonic approximation for single degree-of-freedom (DOF) systems. The approximation was used to obtain both the forced and free responses of friction damped blade systems [Sinha and Griffin, 1984, 1985], hollow blades [Griffin et al., 1998], and tuned and mistuned blade assemblies [Muszyńska and Jones, 1983, Griffin and Sinha, 1985, Sinha et al., 1986]. The single harmonic method was also used on equations obtained by component mode analysis [Ferri and Dowell, 1985], on bi-dimensional friction dampers [Sanliturk and Ewins, 1996, Yang et al., 1998], and on dampers undergoing microslip [Menq et al., 1986, Sanliturk et al., 1997]. Provided that a number of conditions are met [Mickens, 1984], the HB method used with a single temporal harmonic is a fast and accurate way to study the dynamics of friction damped systems. Although the method cannot predict stick/slip motion, it can provide an acceptable approximation of the response amplitude, provided the first harmonic dominates the response of the system.

This chapter is organized as follows. First, the single-harmonic method [Griffin, 1980] is applied to single-DOF systems. The procedure is improved so that the friction force is computed more accurately than in the traditional single harmonic approximation. Then, the method is extended to several-DOF, several-damper systems.

2.2 Single-Degree of Freedom Systems

2.2.1 System Model

A spring-mass-dashpot, single-DOF system with a flexible friction damper attached is considered, see Fig. 2.1. Only the forced response is studied in this chapter. The equation of motion for this system can be written as:

$$m\ddot{x} + c\dot{x} + kx + f_{nl}(x, \dot{x}) = P \cos(\omega t) \quad (2.1)$$

where m is the mass of the single-DOF system, c the viscous damping coefficient, k the stiffness of the single-DOF system, x the displacement of the mass, and $f_{nl}(x, \dot{x})$ the force transmitted by the friction damper, and where an overdot represents a time derivative. The system is subject to a harmonic excitation, $P \cos(\omega t)$. The force transmitted by the non-linear damper is expressed as:

$$f_{nl}(x, \dot{x}) = \begin{cases} k_d z & \text{when } |z| \leq F_d/k_d \text{ (sticking)} \\ F_d \text{sign}(\dot{x}) & \text{when } |z| = F_d/k_d \text{ (slipping)} \end{cases} \quad (2.2)$$

where k_d is the stiffness of the damper, z is the damper displacement, and F_d is the maximum force sustained by the damper.

2.2.2 Force-displacement relation

A coulomb-type dry-friction law is assumed, and no further assumption is made on the nature of the force at the damper. Namely, the relative velocity at the frictional

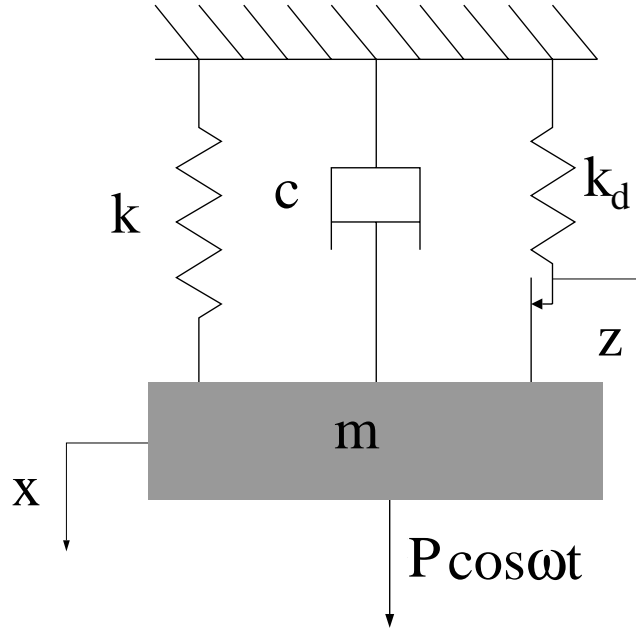


Figure 2.1: Single-DOF system with attached flexible dry-friction damper

interface is taken to vanish when the damper is stuck. Therefore, an elastic/perfectly plastic friction element is being considered.

Assuming that the motion of mass DOF is harmonic, the force transmitted by the damper follows the hysteresis cycle depicted in Fig. 2.2. When the friction damper is slipping, the force transmitted by the damper is constant and equal to its maximum or minimum value, $\pm F_d$. When the damper is sticking, it can be viewed as a mere spring of stiffness k_d . In this sticking case, the force transmitted by the damper can be written as $f_{nl}(x, \dot{x}) = k_d z = k_d x + Q$, where Q is a constant corresponding to the initial value at the beginning of the sticking phase.

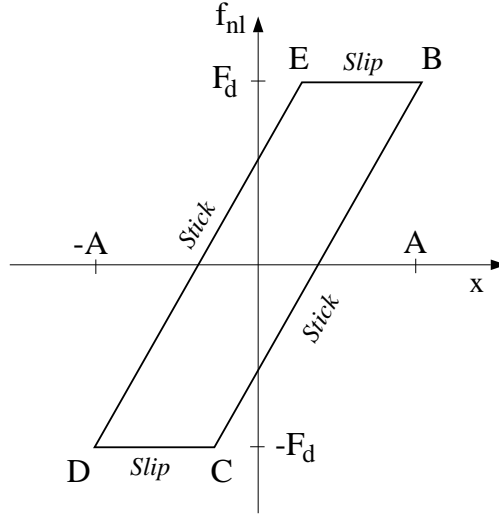


Figure 2.2: Force transmitted by the damper as a function of the mass DOF displacement

2.2.3 Single-harmonic approximation

The mass DOF displacement x and the damper displacement z are assumed to be harmonic. Therefore they can be written as

$$x = A \cos(\omega t + \phi) \quad (2.3)$$

$$z = a \cos(\omega t + \phi) + b \sin(\omega t + \phi) \quad (2.4)$$

where ϕ is the phase angle between the external force $P \cos(\omega t)$ and the mass DOF displacement x , and A , a and b are the amplitudes of the first harmonic of x and z . Substituting the expansions Eqs. (2.3) and (2.4) in the equation of motion Eq. (2.1) leads to

$$[(-\omega^2 m + k)A + k_d a] \cos(\omega t + \phi) + (-c\omega A + k_d b) \sin(\omega t + \phi) = P \cos(\omega t) \quad (2.5)$$

Balancing the harmonics in Eq. (2.5) leads to the following single nonlinear equation:

$$[(-\omega^2 m + k)A + k_d a]^2 + (-c\omega A + k_d b)^2 = P^2 \quad (2.6)$$

Since it is assumed that the motion of the mass DOF displacement, x , is harmonic, the damper displacement amplitudes, a and b , may be computed as a function of the mass displacement amplitude, A . Thus, a and b are given by

$$a = \frac{2}{\pi} \int_{\theta_B}^{\theta_D} z(\theta) \cos(\theta) d\theta \quad (2.7)$$

$$b = \frac{2}{\pi} \int_{\theta_B}^{\theta_D} z(\theta) \sin(\theta) d\theta \quad (2.8)$$

where $\theta = \omega t$, is a non-dimensionalized time, with $\theta \in [0, 2\pi]$. The times, θ_B, θ_C , and θ_D , refers to the times at points B, C, and D in Fig. 2.2. In order to evaluate these expressions, the damper displacement must be determined from the state of the damper (sticking or slipping):

$$z(\theta) = \begin{cases} x(\theta) - x(\theta_B) + z(\theta_B) = x(\theta) - A + F_d/k_d, & \theta_B \leq \theta \leq \theta_C \\ -F_d/k_d, & \theta_C \leq \theta \leq \theta_D \end{cases} \quad (2.9)$$

At point C in Fig. 2.2, the damper switches from slipping to sticking. Therefore

$$f_{nl}(x_C, \dot{x}_C) = -F_d \quad (\text{slipping}) \quad (2.10)$$

$$= k_d z(\theta_C) \quad (\text{sticking})$$

$$= k_d (x(\theta_C) - x(\theta_B) + z(\theta_B))$$

$$= k_d (A \cos(\theta_C) - A + F_d/k_d) \quad (2.11)$$

Hence, θ_C can be deduced:

$$\theta_C = \arccos\left(1 - \frac{2F_d}{Ak_d}\right) \quad (2.12)$$

Using Eqs. (2.9) and (2.12) in Eqs. (2.7) and (2.8), it can be shown that

$$a = \frac{A}{\pi} \left(\theta_C + \frac{1}{2} \sin 2\theta_C \right) \quad (2.13)$$

$$b = \left(\frac{F_d}{k_d A} - 1 \right) \frac{4F_d}{k_d \pi} \quad (2.14)$$

Substituting Eqs. (2.13) and (2.14) in Eq. (2.6) leads to a single nonlinear equation whose unique unknown is the amplitude, A , of the single-harmonic approximation of the mass DOF displacement, x . This non-linear equation is solved by a standard Newton procedure. Once the amplitude, A , is found, the sine and cosine terms, a and b , in the expansion of the damper displacement, z , can be determined using Eqs. (2.13) and (2.14), and the phase angle, ϕ , can be computed from Eq. (2.5) as:

$$\cos \phi = [(k - \omega^2 m)A + k_d a]P/det \quad (2.15)$$

$$\sin \phi = (-c\omega A + k_d b)P/det \quad (2.16)$$

where $det = [(k - \omega^2 m)A + k_d a]^2 + (-c\omega A + k_d b)^2$.

2.2.4 Improvement to the single-harmonic approximation

The procedure described in section 2.2.3 [Griffin, 1980] gives a single-harmonic approximation of the mass DOF displacement, x , and the damper displacement, z . The damper undergoes periods of sticking motion when its velocity is equal to that of the mass DOF, and periods of slipping motion when its velocity vanishes. The velocity discontinuities cannot be reproduced accurately using a single-harmonic approximation, since a combination of a single sine and a single cosine function cannot precisely describe a function whose derivative is not continuous.

The results predicted by the single-harmonic method can be greatly improved by performing a simple time-marching procedure (similar to a numerical time integration) over one period of the motion. When the damper is slipping, the damper displacement is constant and equal to its maximum value $\pm F_d/k_d$, the sign being the same as that of the velocity of the mass. When the damper is sticking, the value of the damper displacement is deduced from the value of the mass DOF displacement,

since the velocities of the mass and the damper are equal:

$$\dot{z} = \dot{x} \Rightarrow z(\theta) = x(\theta) - x(\theta_B) + z(\theta_B) \quad (2.17)$$

The procedure is summarized in Table 2.1. The slipping and sticking phases of the

<i>State of the damper</i>	<i>Damper displacement</i>
Slipping	$z(\theta) = \begin{cases} F_d/k_d & \text{if } \dot{x}(\theta) > 0 \\ -F_d/k_d & \text{if } \dot{x}(\theta) < 0 \end{cases}$
Sticking	$z(\theta) = \begin{cases} x(\theta) - x(\theta_B) + z(\theta_B) & \text{if } \theta \in [\theta_B, \theta_C] \\ x(\theta) - x(\theta_D) + z(\theta_D) & \text{if } \theta \in [\theta_D, \theta_E] \end{cases}$

Table 2.1: Improved update of the damper displacement z .

motion are determined from the instants of time when the damper starts slipping, referred to as slipping time, θ_C , and when the damper starts sticking, referred to as sticking time, $\theta_B = \phi$ (see Fig. 2.2). Figure 2.3 shows the damper displacement as predicted by the fourth-order Runge-Kutta numerical time integration procedure, by the standard single-harmonic solution [Griffin, 1980], and the improved single-harmonic approximation. The standard single-harmonic solution gives a rather poor approximation of the damper displacement z , because it is unable to capture the non-differentiable motion associated with the transition between sticking and slipping phases. On the other hand, the agreement between the numerical time integration and the improved single-harmonic approximation is excellent.

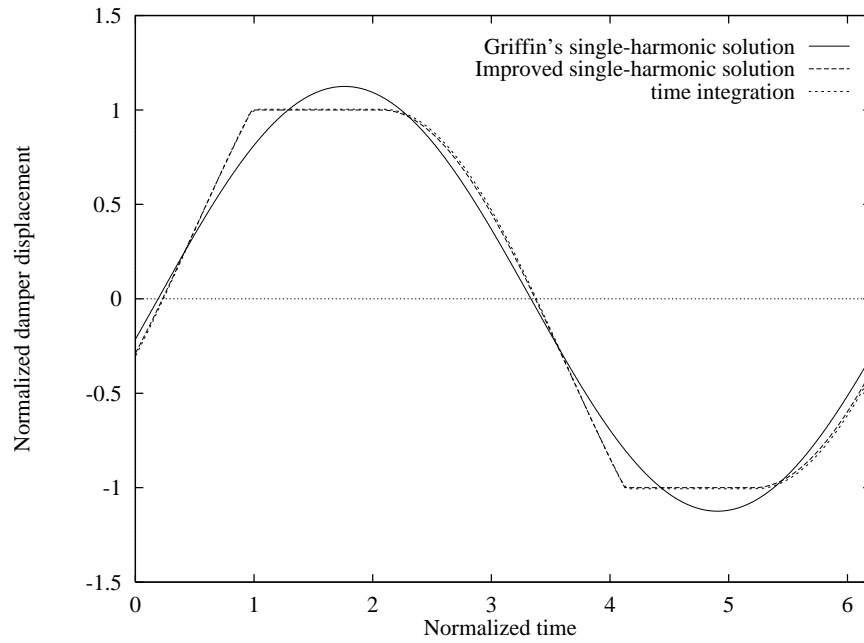


Figure 2.3: Damper displacement predicted by Griffin's single-harmonic solution [Griffin, 1980], by the improved single-harmonic approximation and by full time integration, $P = 0.5F_d$, $\omega = 225 \text{ rad/s}$.

2.2.5 Results

The improved single-harmonic approximation is applied to a specific model whose parameter values are given in Table 2.2. In Figs. 2.4 and 2.5, the forced response of the system is shown as a function of the excitation frequency for various force amplitudes, ranging from a low level ($P = 0.5F_d$) for which the damper is mostly sticking during one period of the motion, to a high level ($P = 2F_d$) for which the damper is mostly slipping during one period of the motion. The numerical time integration scheme used in this study is a fourth-order Runge-Kutta procedure. The agreement between the numerical time integration procedure and the improved single-harmonic approximation is of high quality. As could be expected, the single-harmonic approximation is not able to reproduce the subresonances (Fig. 2.5) of the frequency response curves, since these are due to higher harmonic content of the forced response of the system. The damper displacement amplitude cannot exceed its maximum value F_d/k_d , reached when the friction damper is slipping. Therefore, over the frequency ranges where the friction damper slips, the amplitude of the damper displacement is equal to its maximum value.

Figure 2.6 presents the forced response amplitude of the system normalized by the force amplitude for various excitation amplitudes. There is a level of optimum friction damping for which the peak response amplitude is minimum. Here, the optimum is reached for values of the ratio of external force to maximum friction force, P/F_d , ranging from 0.5 to 1. It is within this range that the friction damper is the most effective at reducing the overall amplitude of vibrations of the system.

Since the viscous damping affecting the system is rather low, numerical time integration procedures have to be carried out over several hundred cycles in order to reach steady-state. The single-harmonic approximation is therefore orders of mag-

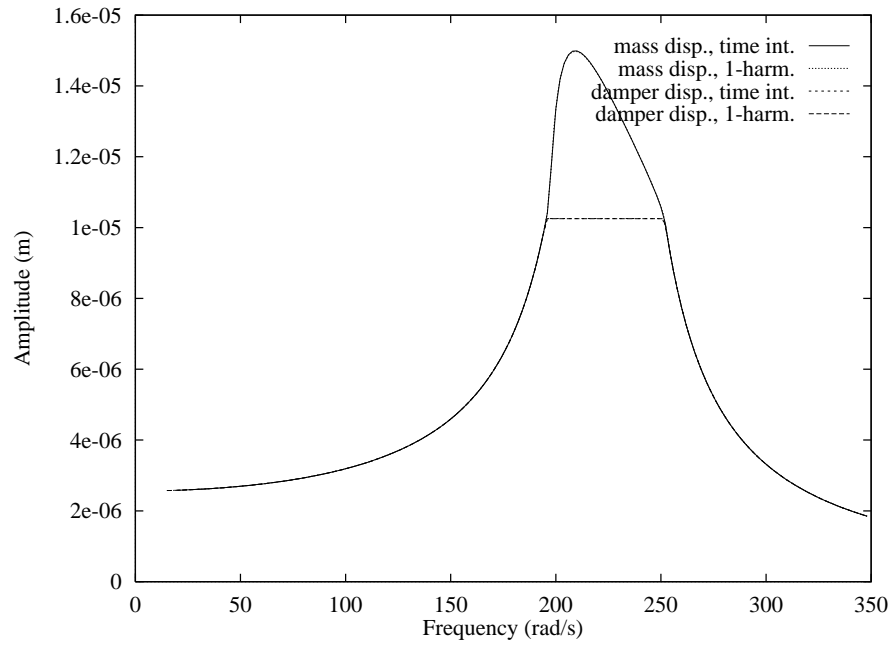


Figure 2.4: Mass displacement and damper displacement for a single-DOF system using numerical time integration and improved single-harmonic approximation. External force $P = 0.5F_d$.

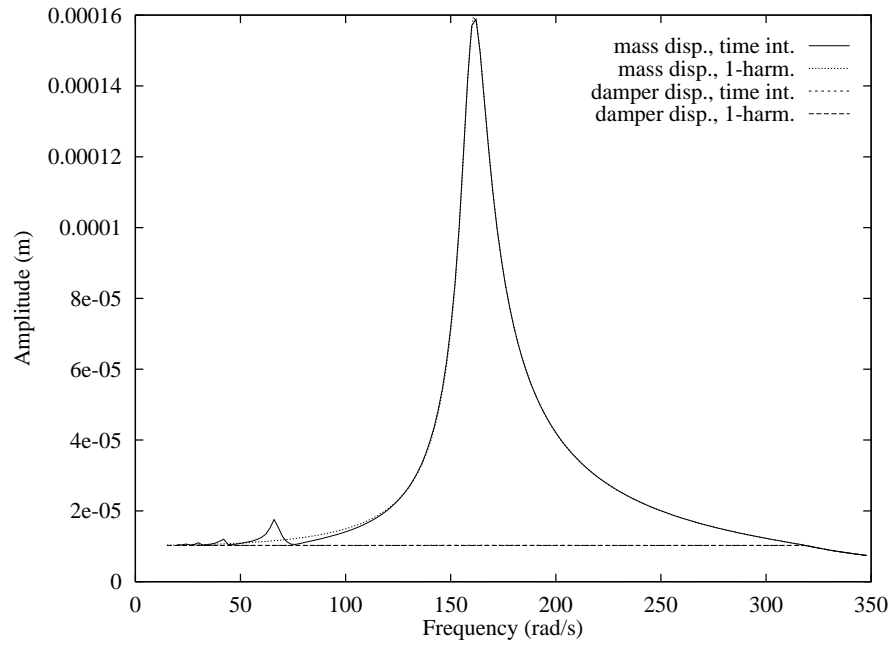


Figure 2.5: Mass displacement and damper displacement for a single-DOF system using numerical time integration and improved single-harmonic approximation. External force $P = 2F_d$.

nitide faster than the numerical time integration. The speed of the single-harmonic approximation makes it useful, even if some precision is lost with respect to the time-based methods.

$m = 944.6 \text{ kg}$	$c = 7700 \text{ kg/s}$
$k = 2.4 \cdot 10^7 \text{ N/m}$	$k_d = 2.4 \cdot 10^7 \text{ N/m}$
$F_d = 246.048 \text{ N}$	$\omega \in [20, 350](\text{rad/s})$

Table 2.2: Numerical values of the single-DOF system used to compare the results of the time integration procedure and the results of the improved single-harmonic approximation.

2.3 Multi-DOF systems with a single friction damper

2.3.1 System model

A multi-DOF linear structure with one flexible dry friction damper attached between any of the structure DOF's and the ground is considered. This model can represent, for example, a single sector of a friction damped bladed-disk assembly. The equations of motion for the N DOF's of the structure can be written as

$$\underline{\mathbf{M}}\ddot{\mathbf{x}} + \underline{\mathbf{C}}\dot{\mathbf{x}} + \underline{\mathbf{K}}\mathbf{x} + \mathbf{f}_{\text{nl}}(\mathbf{x}, \dot{\mathbf{x}}) = \mathbf{P} \cos(\omega t) \quad (2.18)$$

where $\underline{\mathbf{M}}$ is the mass matrix of the linear structure, $\underline{\mathbf{K}}$ is its stiffness matrix, $\underline{\mathbf{C}}$ is its viscous damping matrix, \mathbf{x} is the vector made of the displacements of the DOF's of the structure, \mathbf{P} is the vector of the external forces applied to the DOF's of the linear structure, and $\mathbf{f}_{\text{nl}}(\mathbf{x}, \dot{\mathbf{x}})$ is the vector of the nonlinear forces due to the friction damper. Since only one friction damper is considered here, all components of $\mathbf{f}_{\text{nl}}(\mathbf{x}, \dot{\mathbf{x}})$ are equal to zero except the one corresponding to the DOF of the structure to which the friction damper is attached. All bold quantities refer to vectors, all underlined quantities refer to matrices.

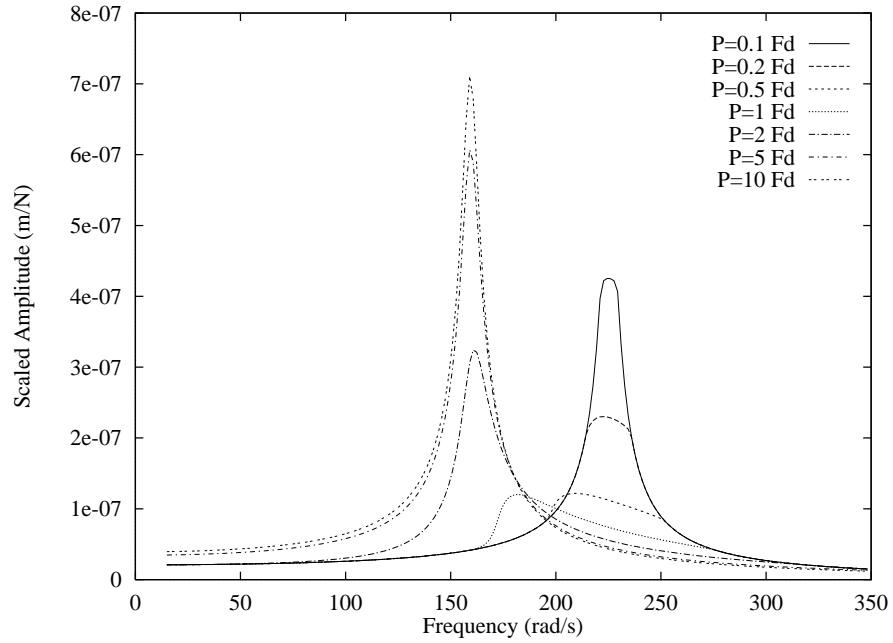


Figure 2.6: Mass displacement for a single-DOF system using the improved single-harmonic approximation. The frequency responses are scaled by the force amplitude.

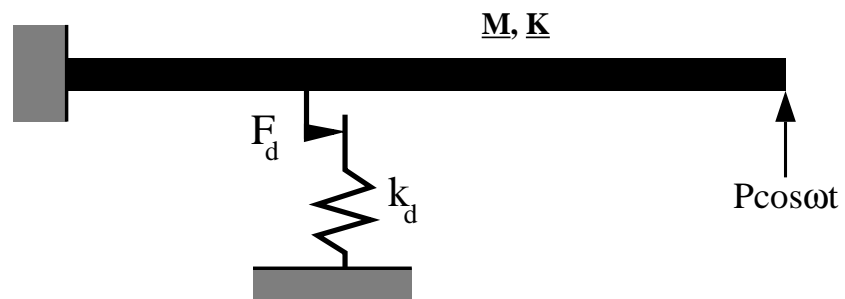


Figure 2.7: Three-DOF beam of length L , with an attached flexible friction damper at $0.239L$.

2.3.2 Reduction of the number of equations

Equation (2.18) is a set of $(N - 1)$ linear equations coupled to a single non-linear equation. These N equations can be reduced to a single nonlinear equation whose only unknown is the amplitude of motion of the structure DOF attached to the friction damper. Without loss of generality, the friction damper is assumed to be attached to the first DOF of the system, x_1 . All displacement are assumed to be mono-harmonic and the complex notation is used:

$$\mathbf{x} = \Re(\mathbf{X}e^{i\omega t}) \quad (2.19)$$

where \mathbf{X} is a vector whose components are complex. Substituting Eq. (2.19) into Eq.(2.18) leads to

$$\left(-\omega^2 \underline{\mathbf{M}} + i\omega \underline{\mathbf{C}} + \underline{\mathbf{K}}\right) \mathbf{X} = \mathbf{P} - \mathbf{f}_{\text{nl}}^* = \mathbf{R} \quad (2.20)$$

where $\mathbf{f}_{\text{nl}} = \Re(\mathbf{f}_{\text{nl}}^* e^{i\omega t})$. Let us introduce the following notations:

$$\mathbf{X} = \begin{bmatrix} X_1 \\ \mathbf{X}_2 \end{bmatrix}, \quad \mathbf{R} = \begin{bmatrix} R_1 \\ \mathbf{R}_2 \end{bmatrix}, \quad (2.21)$$

$$\left(-\omega^2 \underline{\mathbf{M}} + i\omega \underline{\mathbf{C}} + \underline{\mathbf{K}}\right) = \underline{\mathbf{M}}^*, \quad \underline{\mathbf{M}}^* = \begin{bmatrix} M_{11} & \mathbf{M}_{12} \\ \mathbf{M}_{21} & \underline{\mathbf{M}}_{22} \end{bmatrix} \quad (2.22)$$

where the index 1 refers to the first, nonlinear equation governing the displacement of the structure DOF connected to the friction damper, and the index 2 refers to all linear DOF's. The $(N - 1)$ equations for the linear DOF's are separated from the first, nonlinear equation. Substituting Eqs.(2.21) and (2.22) into Eq. (2.20) leads to

$$\mathbf{X}_2 = \underline{\mathbf{M}}_{22}^{-1}(\mathbf{R}_2 - \mathbf{M}_{21}X_1) \quad (2.23)$$

$$(M_{11} - \mathbf{M}_{12}\underline{\mathbf{M}}_{22}^{-1}\mathbf{M}_{21})X_1 = R_1 - \mathbf{M}_{12}\underline{\mathbf{M}}_{22}^{-1}\mathbf{R}_2 \quad (2.24)$$

Equation (2.24) is a single nonlinear equation whose only unknown is X_1 , the amplitude of the displacement of the structure DOF connected to the friction damper. Once Eq. (2.24) is solved, Eq. (2.23) can be used to obtain the amplitude, \mathbf{X}_2 , of the linear DOF's of the structure.

2.3.3 Single-harmonic approximation

The procedure for predicting the motion of a multi-DOF system with a single friction damper attached is similar to the one for a single-DOF system, as developed in Section 2.2.3. Let us denote $X_1 = Ae^{i\phi}$ with A a real number, and f_{nl} the only non-zero component of $\mathbf{f}_{nl}(\mathbf{x}, \dot{\mathbf{x}})$. The non-linear force is equal to $f_{nl} = k_d z$, with z being the damper displacement. The single-harmonic expansion of z can be written as

$$z = \Re(ae^{i(\omega t + \phi)} - ibe^{i(\omega t + \phi)}) \quad (2.25)$$

where a and b are real, harmonic components given by Eqs. (2.7) and (2.8). The force/displacement relationship depicted in Fig. 2.2 is still valid. Consequently, a and b are still given by Eqs. (2.13) and (2.14). Let us introduce the complex, dynamic and force quantities, m_{red} and r_{red} :

$$m_{red} = M_{11} - \mathbf{M}_{12}\mathbf{M}_{22}^{-1}\mathbf{M}_{21}, \quad \text{and} \quad r_{red} = P_1 - \mathbf{M}_{12}\mathbf{M}_{22}^{-1}\mathbf{R}_2 \quad (2.26)$$

Substituting Eqs. (2.25) and (2.26) into Eq. (2.24), leads to

$$(m_{red}A + k_d(a - ib))e^{i\phi} = r_{red} \quad (2.27)$$

which can be re-written as

$$([\Re(m_{red})A + k_d a] + i[-k_d b + \Im(m_{red})A])e^{i\phi} = r_{red} \quad (2.28)$$

Taking the modulus of these expressions leads to the non-linear equation in the amplitude displacement of the structure DOF connected to the damper, A :

$$[\Re(m_{red})A + k_da]^2 + [-k_db + \Im(m_{red})A]^2 = \Re(r_{red})^2 + \Im(r_{red})^2 \quad (2.29)$$

Equation (2.29) can be solved by a standard Newton procedure, and \mathbf{X}_2 , the amplitude of the DOF's of the structure not connected to the friction damper, can be deduced from Eq. (2.23). The phase angle ϕ between the external force and the structure displacement at the damper is given by:

$$\cos \phi = [(-k_db + \Im(m_{red})A)\Im(r_{red}) + (\Re(m_{red})A + k_da)\Re(r_{red})]/det \quad (2.30)$$

$$\sin \phi = [(\Re(m_{red})A + k_da)\Im(r_{red}) + (-k_db + \Im(m_{red})A)\Re(r_{red})]/det \quad (2.31)$$

where $det = (-k_db + \Im(m_{red})A)^2 + (\Re(m_{red})A + k_da)^2$.

2.3.4 Results

The forced response in the transverse direction of a fixed-free beam with a flexible friction damper attached is obtained under a wide range of levels of external forces. The beam is $1.33m$ long and the damper is attached at $0.318m$ from the clamped end. The beam-damper system is depicted in Fig. 2.7. A three-DOF component mode synthesis model was developed by the Société Nationale d'Étude et de Construction de Moteurs d'Aviation (SNECMA), and the numerical parameters of the system are the following:

$$\underline{\mathbf{M}} = \begin{bmatrix} 6.67959 & 1.02115 & 0.6343 \\ 1.02115 & 1.22168 & 0.232108 \\ 0.6343 & 0.232108 & 0.121809 \end{bmatrix}$$

$$\underline{\mathbf{K}} = \begin{bmatrix} 4.43203 \cdot 10^6 & -3.77514 \cdot 10^5 & 0 \\ -3.77514 \cdot 10^5 & 6.9626 \cdot 10^4 & 0 \\ 0 & 0 & 1.85323 \cdot 10^5 \end{bmatrix}$$

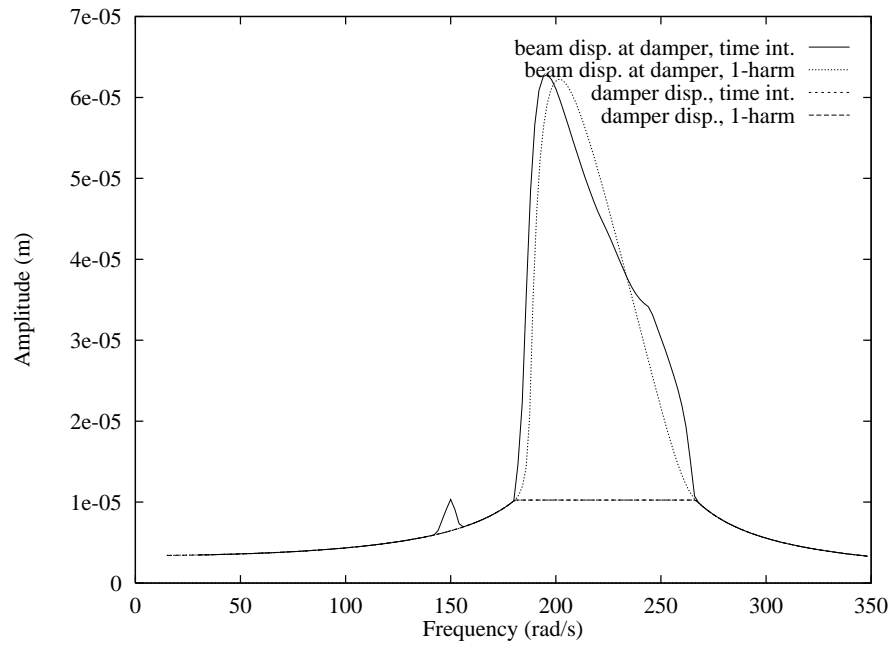


Figure 2.8: Beam displacement amplitude at the damper location and damper displacement for a 3-DOF system using numerical time integration and improved single-harmonic approximation. External force $P = 16.563N$.

$$\underline{\mathbf{C}} = \alpha \underline{\mathbf{K}} + \beta \underline{\mathbf{M}}, \quad \alpha = 2.6 \cdot 10^{-5} s, \quad \beta = 7.49 s^{-1}$$

$$F_d = 246.048 N, \quad k_d = 2.4 \cdot 10^7 N/m \quad (2.32)$$

Here $N = 3$, and the first coordinate corresponds to the beam transverse displacement at the damper location, while the second coordinate corresponds to the beam tip displacement, where the external force is applied. The third coordinate corresponds to a normal mode of vibration, for which the beam is fixed at the tip and at the damper location. The complete system is presented in Berthillier *et al.* (1998), where the 3-DOF model is validated by comparisons with experimental results. The beam is referred to below as the SNECMA beam.

Figure 2.8 and 2.9 show, respectively, the beam displacement at the damper location and the damper displacement, and the beam tip displacement, using the fourth-order Runge-Kutta time integration procedure and the improved single-harmonic approximation, for one particular level of external force. As was the case for the single-DOF system in Section 2.2.5, the single-harmonic approximation is not able to reproduce the subresonances, which are due to higher harmonic content of the forced response, as depicted in Fig. 2.8. The agreement between the time integration procedure and the improved single-harmonic approximation is not as good for the displacement at the tip of the beam as it is for the displacement at the damper location. Since the damper is located at about one third of the beam span, the differences between the results from time integration and single-harmonic approximation are probably amplified along the beam. The difference between the peak tip displacement amplitude predicted by the time integration and the single-harmonic approximation is less than 17.2%, but it is less than 6.2% for all the cases near optimal damping, i.e., the cases where the most accuracy is needed, as shown in Table 2.3.

Forcing (N)	0.94	2.19	6.56	16.56	20.31	25.	31.47	38.44
Peak tip ampl. (time int.) $\times 10^3$	0.37	0.68	0.72	1.22	1.45	1.82	2.98	5.99
Peak tip ampl. (1-harm) $\times 10^3$	0.37	0.71	0.87	1.18	1.36	1.73	2.82	5.22
Error (%)	0	4.1	17.2	3.2	6.5	4.9	5.6	14.7
Peak ampl. at damp. (time int.) $\times 10^5$	0.57	1.12	2.12	6.22	8.74	13.03	24.80	50.68
Peak ampl. at damp. (1-harm) $\times 10^5$	0.57	1.11	2.25	6.22	8.52	12.77	24.12	47.72
Error (%)	0	0.9	6.1	0.	2.6	2.0	2.8	6.2

Table 2.3: Comparison of peak displacement amplitude predicted by the time integration procedure and the improved single-harmonic approximation, for different force amplitudes at the tip of the beam and at the damper location.

Figure 2.10 depicts the forced response amplitude of the beam at the damper location for various force amplitudes, normalized by the force amplitude. It can be seen that for $P = 6.563N$ or $P = 16.653N$, the peak response is approximately minimum. Therefore, these cases correspond to the optimum dry-friction damping of the structure, considering the displacement at the damper location. Similarly, Fig. 2.11 shows the forced response amplitude of the tip of the beam under several force amplitudes. Here again, there are some levels of excitation for which the peak tip displacement is approximately minimum: from $P = 16.563N$ to $P = 25N$. The optimum damping is reached for levels of force amplitude slightly different from the ones in the case of the displacement at the damper location. Therefore, when the forced response of a structure is studied, it is important to determine where the maximum stresses are likely to occur, in order to know where to minimize the peak displacements.

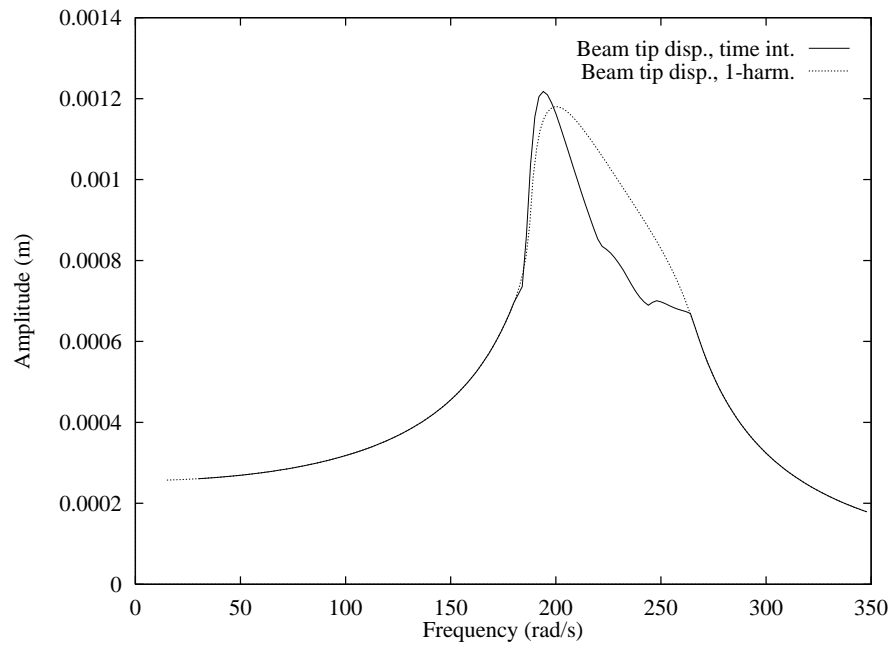


Figure 2.9: Tip beam displacement amplitude for a 3-DOF system using numerical time integration and improved single-harmonic approximation. External force $P = 16.563N$.

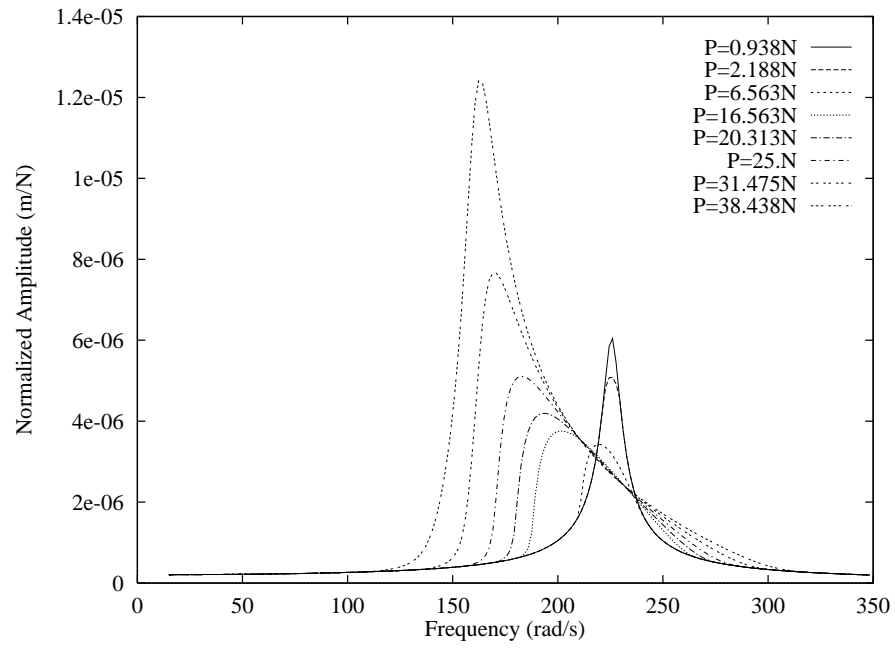


Figure 2.10: Beam displacement amplitude at the damper location for a 3-DOF system using the improved single-harmonic approximation. The frequency responses are normalized by the force amplitudes.

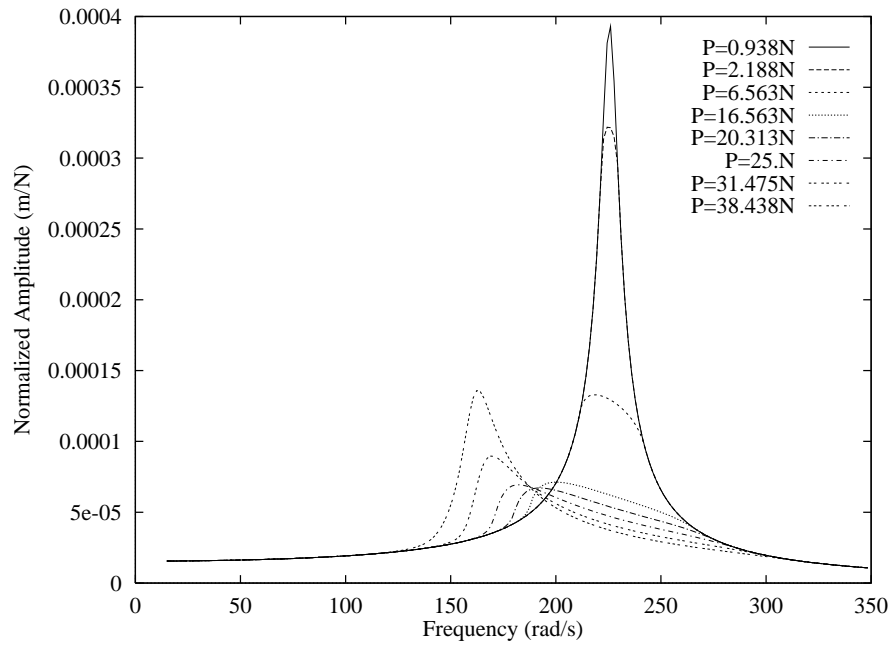


Figure 2.11: Tip beam displacement for a 3-DOF system using the improved single-harmonic approximation. The frequency responses are normalized by the force amplitudes.

2.4 Multi-DOF systems with multiple friction dampers

The method presented in Section 2.3 can be extended to systems with several friction dampers. The equation of motion, Eq. 2.18, is still valid. However, the term $\mathbf{f}_{nl}(\mathbf{x}, \dot{\mathbf{x}})$ has as many non-zero components as there are friction dampers attached to the structure. For the sake of clarity, it is assumed that the first N_d coordinates correspond to the DOF's connected to dry-friction dampers. Therefore, the first N_d coordinates of $\mathbf{f}_{nl}(\mathbf{x}, \dot{\mathbf{x}})$ are different from zero. Equations (2.19) and (2.20) are still valid. The following notations are introduced:

$$\mathbf{X} = \begin{bmatrix} \mathbf{X}_1 \\ \mathbf{X}_2 \end{bmatrix}, \quad \mathbf{R} = \begin{bmatrix} \mathbf{R}_1 \\ \mathbf{R}_2 \end{bmatrix}, \quad (2.33)$$

$$(-\omega^2 \underline{\mathbf{M}} + i\omega \underline{\mathbf{C}} + \underline{\mathbf{K}}) = \underline{\mathbf{M}}^*, \quad \underline{\mathbf{M}}^* = \begin{bmatrix} \underline{\mathbf{M}}_{11} & \underline{\mathbf{M}}_{12} \\ \underline{\mathbf{M}}_{21} & \underline{\mathbf{M}}_{22} \end{bmatrix} \quad (2.34)$$

where the index 1 refers to the N_d nonlinear equations governing the displacement of the structure DOF's connected to the friction dampers, and the index 2 refers to all linear DOF's. Substituting Eqs. (2.33) and (2.34) into Eq. (2.20) leads to:

$$\mathbf{X}_2 = \underline{\mathbf{M}}_{22}^{-1}(\mathbf{R}_2 - \underline{\mathbf{M}}_{21}\mathbf{X}_1) \quad (2.35)$$

$$(\underline{\mathbf{M}}_{11} - \underline{\mathbf{M}}_{12}\underline{\mathbf{M}}_{22}^{-1}\underline{\mathbf{M}}_{21})\mathbf{X}_1 = \mathbf{R}_1 - \underline{\mathbf{M}}_{12}\underline{\mathbf{M}}_{22}^{-1}\mathbf{R}_2 \quad (2.36)$$

Equation (2.36) is a set of N_d coupled, non-linear equations, whose unknowns are the N_d components of \mathbf{X}_1 , that is, the displacement amplitudes of the structure DOF's connected to the friction dampers.

The single-harmonic method followed for this multi-damper, multi-DOF system is very similar to the one described in Section 2.3. When several dampers are considered, each component of the non-linear force can be written as $f_{nl,j} = k_{d,j}z_j$, where

j refers to the damper considered, $j = 1, \dots, N_d$. The complex notation is adopted for the amplitudes of the DOF's attached to friction dampers:

$$X_j = A_j e^{i\phi_j} \quad 1 \leq j \leq N_d \quad (2.37)$$

The single-harmonic expansion of any component z_j of \mathbf{z} can be written as

$$z_j = \Re(a_j e^{i(\omega t + \phi_j)} - i b_j e^{i(\omega t + \phi_j)}) \quad 1 \leq j \leq N_d \quad (2.38)$$

where a_j and b_j are still given by Eqs. (2.13) and (2.14), since the same assumptions on the nature of the friction force are made as in Section 2.3. Let us introduce the complex, reduced dynamic and force matrices, $\underline{\mathbf{m}}_{\text{red}}$ and \mathbf{r}_{red} :

$$\underline{\mathbf{m}}_{\text{red}} = \underline{\mathbf{M}}_{11} - \underline{\mathbf{M}}_{12} \underline{\mathbf{M}}_{22}^{-1} \underline{\mathbf{M}}_{21}, \quad \text{and} \quad \mathbf{r}_{\text{red}} = \mathbf{P}_1 - \underline{\mathbf{M}}_{12} \underline{\mathbf{M}}_{22}^{-1} \mathbf{R}_2 \quad (2.39)$$

Substituting Eqs. (2.38) and (2.39) into Eq. (2.36) leads to

$$\left(\sum_{j=1}^{N_d} m_{\text{red},ij} A_j + k_{d,i} (a_i - i b_i) \right) e^{i\phi_i} i = r_{\text{red},i}, \quad 1 \leq i \leq N_d \quad (2.40)$$

The following set of non-linear equations is deduced:

$$\begin{aligned} & \left[\sum_{j=1}^{N_d} \Re(m_{\text{red},ij}) A_j + k_{d,i} a_i \right]^2 + \left[-k_{d,i} b_i + \sum_{j=1}^{N_d} \Im(m_{\text{red},ij}) A_j \right]^2 \\ & = \Re(r_{\text{red},i})^2 + \Im(r_{\text{red},i})^2 \quad 1 \leq i \leq N_d \end{aligned} \quad (2.41)$$

The system (2.41) can be solved using a non-linear solver. A multidimensional secant method, based on the Broyden method has been implemented, which gives fast results.

The displacements \mathbf{X}_2 of the linear DOF's can be obtained by using Eq. (2.35). The phase angle ϕ_i between the external forcing and the structure displacement at the i th damper is given by:

$$\cos \phi_i = \left[(-k_{d,i} b_i + \sum_{j=1}^{N_d} \Im(m_{\text{red},ij}) A_j) \Im(r_{\text{red},i}) \right]$$

$$\left. + \left(\sum_{j=1}^{N_d} \Re(m_{red,ij})A_j + k_{d,i}a_i \right) \Re(r_{red,i}) \right] / det \quad (2.42)$$

$$\sin \phi_i = \left[\left(\sum_{j=1}^{N_d} \Re(m_{red,ij})A_j + k_{d,i}a_i \right) \Im(r_{red,i}) \right. \\ \left. + \left(-k_{d,i}b_i + \sum_{j=1}^{N_d} \Im(m_{red,ij})A_j \right) \Re(r_{red,i}) \right] / det \quad (2.43)$$

where $det = (-k_{d,i}b_i + \sum_{j=1}^{N_d} \Im(m_{red,ij})A_j)^2 + (\sum_{j=1}^{N_d} \Re(m_{red,ij})A_j + k_{d,i}a_i)^2$.

Results for multi-DOF systems with multiple friction dampers are presented in Fig. 4.19a.

2.5 Conclusion

An improved single-harmonic approximation was developed for the response of a single-DOF mass-dashpot-spring system connected to a flexible friction damper. The forced response of the system under a wide range of force amplitudes has been obtained. The agreement between the results given by this single-harmonic method and a fourth-order Runge-Kutta numerical time integration procedure is virtually perfect.

The method has been expanded to multi-DOF structures connected to a single flexible friction damper. Frequency response curves have been obtained for an example beam system, for a wide range of force amplitudes. It was shown that the agreement between the improved single-harmonic approximation and the numerical time integration is acceptable for the displacement of the structure at the damper location. This agreement is not as good for the displacement of the tip of the beam considered in the present study. However, in general, errors are not too large (less than 7%) in the range of external forcing levels which correspond to optimal damping, i.e., levels which correspond in practice to desired damper configurations.

The contributions of this work are along three lines. *First*, the single-harmonic approximation was improved so that the force transmitted by the friction dampers is much more accurately represented than in standard single-harmonic methods -see Fig. 2.3. *Second*, the single-harmonic approximation was extended to systems with several dampers and several DOF's. *Third*, the reduction of the number of equations to solve to the number of nonlinear DOF's was made in a systematic way, using reduced, complex dynamic and force matrices.

The single-harmonic approximation is an efficient, reliable method that is able to predict in an economical fashion the forced response of a friction damped structural system. It can also be used as an initial guess for the multi-harmonic method which is presented in the next chapter.

CHAPTER III

MULTI-HARMONIC, HYBRID FREQUENCY/TIME METHOD

3.1 Introduction

Many works on dry friction-damped structural systems are based on the harmonic balance (HB) method [Nayfeh and Mook, 1979], which provides an efficient alternative to the costly time integration procedure. Most studies have been limited to single-harmonic approximations for small- or medium-size models [Wei and Pierre, 1989, Sanliturk and Ewins, 1996]. When several temporal harmonics are considered, analytic approximations of the friction force are used [Berthillier et al., 1998b], and/or models with a single friction damper are considered [Shiau et al., 1998, Shiau and Yu, 1996, Wang and Chen, 1993]. Convergence problems and robustness are often cited as severe limitations of these methods.

In this chapter, the frequency-time method originally introduced in Guillen and Pierre (1996) and Guillen and Pierre (1998) is presented and further developed. The method allows for many flexible friction dampers, a multi-harmonic representation of the response, and large structural systems. A frequency-time algorithm is proposed, derived from the HB method. The force transmitted by the friction damper is evaluated solely in the time domain at each iteration, and transformed back into

the frequency domain by Fast Fourier Transform (FFT). The resulting non-linear equations are solved using a modified Broyden's method, which greatly enhances the robustness, convergence, and efficiency of the procedure.

This chapter is organized as follows. First, the treatment of the non-linear force transmitted by the damper is described. Then, the multi-harmonic hybrid frequency/time method is presented. Finally, the Broyden method is explained.

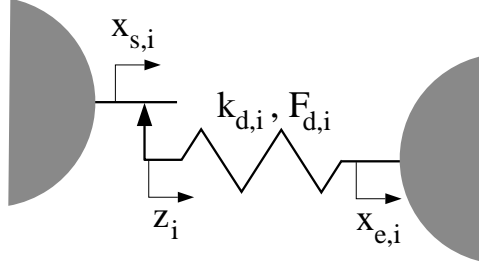
3.2 Friction force treatment

A multi-DOF linear structure is considered, with several flexible friction dampers attached between any two of the structure DOF's, or between one of the structure's DOF and the ground. This model can represent, for example, a dry-friction damped bladed disk assembly with several blade-to-blade or blade-to-ground dampers. For such a N -DOF structure, the equations of motion are:

$$\underline{\mathbf{M}}\ddot{\mathbf{x}} + \underline{\mathbf{C}}\dot{\mathbf{x}} + \underline{\mathbf{K}}\mathbf{x} + \mathbf{f}_{\text{nl}}(\mathbf{x}, \dot{\mathbf{x}}) = \mathbf{P} \cos(\omega t) \quad (3.1)$$

where $\underline{\mathbf{M}}$ is the mass matrix of the linear structure, $\underline{\mathbf{K}}$ is its stiffness matrix, $\underline{\mathbf{C}}$ is its viscous damping matrix, \mathbf{x} is the vector of the displacements (physical or modal) of the structure, \mathbf{P} is the vector of the external forces, and $\mathbf{f}_{\text{nl}}(\mathbf{x}, \dot{\mathbf{x}})$ is the vector of the nonlinear forces due to the friction dampers. The external forcing is harmonic and can be applied to any DOF's of the structure.

A model of the i -th friction damper is shown in Fig. 3.1. Denote by $x_{s,i}$ the displacement of the structure at one end of the i -th damper, $x_{e,i}$ the displacement of the structure at the other end, $f_{s,i}$ the force transmitted by the i -th damper to the s -th DOF of the structure, $F_{d,i}$ the maximum force transmitted by the i -th damper, and $k_{d,i}$ the i -th damper stiffness. The value of the non-linear force depends on the state of the friction damper, sticking or slipping. According to the macroslip

Figure 3.1: Model of the i -th friction damper.

Damper state	Update	Test for next time step
Sticking	$f_{s,i}(j) = f_{s,i}(j-1) + k_{d,i}(x_{s,i}(j) - x_{e,i}(j) - x_{s,i}(j-1) + x_{e,i}(j-1))$	$ f_{s,i}(j) > F_{d,i}?$
Slipping	$f_{s,i}(j) = f_{s,i}(j-1)$	$v_{r,i}(j)v_{r,i}(j-1) < 0?$

Table 3.1: Update for the nonlinear force transmitted by the i -th friction damper.

approach, the friction force, $f_{s,i}$, can be expressed as:

$$f_{s,i} = \begin{cases} k_{d,i}(z_i - x_{e,i}) & \text{when } k_d|x_{s,i} - z_i| \leq F_{d,i} \text{ (sticking)} \\ F_{d,i} \text{sign}(\dot{x}_{e,i} - \dot{x}_{s,i}) & \text{when } k_d|x_{s,i} - z_i| = F_{d,i} \text{ (slipping)} \end{cases} \quad (3.2)$$

The force transmitted by the i -th friction damper is computed in the time domain by performing a time-marching procedure (similar to numerical time integration) over one period of the motion. The force is fully determined from the displacements and velocities of the structure DOF's to which the i -th friction damper is attached. The time-marching procedure is presented in Table 3.1. This approach relies only on the nature of the dry-friction force, and no other assumption than the Coulomb-type friction law is made. The damper displacements are not treated as unknowns of the system.

3.3 Frequency domain treatment

When a high level of accuracy is desired for the forced response, several temporal harmonics must be considered in the periodic solution. Practically, a few harmonics will give a good approximation of the solution, and in all cases a couple dozens of harmonics will predict virtually the same answer as the numerical time integration. Assume that N_h harmonics are retained in the solution. The harmonic expansions of the periodic displacement, \mathbf{x} , and nonlinear force, \mathbf{f}_{nl} , are:

$$\mathbf{x}(t) = \sum_{k=0}^{N_h} \mathbf{X}_k^c \cos(k\omega t) + \sum_{k=1}^{N_h} \mathbf{X}_k^s \sin(k\omega t) \quad (3.3)$$

$$\mathbf{f}_{nl}(t) = \sum_{k=0}^{N_h} \mathbf{F}_{nl,k}^c \cos(k\omega t) + \sum_{k=1}^{N_h} \mathbf{F}_{nl,k}^s \sin(k\omega t) \quad (3.4)$$

The harmonic expansions of the periodic displacement, \mathbf{x} , and nonlinear force, \mathbf{f}_{nl} , Eqs. (3.3) and (3.4), are substituted into Eq. (3.1):

$$\begin{aligned} & -\underline{\mathbf{M}} \left(\sum_{k=1}^{N_h} \mathbf{X}_k^c (k\omega)^2 \cos(k\omega t) + \sum_{k=1}^{N_h} \mathbf{X}_k^s (k\omega)^2 \sin(k\omega t) \right) \\ & + \underline{\mathbf{C}} \left(\sum_{k=1}^{N_h} \mathbf{X}_k^c (-k\omega) \sin(k\omega t) + \sum_{k=1}^{N_h} \mathbf{X}_k^s (k\omega) \cos(k\omega t) \right) \\ & + \underline{\mathbf{K}} \left(\sum_{k=0}^{N_h} \mathbf{X}_k^c \cos(k\omega t) + \sum_{k=1}^{N_h} \mathbf{X}_k^s \sin(k\omega t) \right) \\ & + \left(\sum_{k=0}^{N_h} \mathbf{F}_{nl,k}^c \cos(k\omega t) + \sum_{k=1}^{N_h} \mathbf{F}_{nl,k}^s \sin(k\omega t) \right) = \mathbf{P} \cos(\omega t) \end{aligned} \quad (3.5)$$

All $\sin(k\omega t)$ and $\cos(l\omega t)$ functions are orthogonal to each other over one period of the motion:

$$\int_0^T \sin(k\omega t) \cos(l\omega t) dt = 0 \quad 0 \leq k \leq N_h, 0 \leq l \leq N_h \quad (3.6)$$

$$\int_0^T \sin(k\omega t) \sin(l\omega t) dt = \frac{\pi}{\omega} \delta_{kl} \quad 1 \leq k \leq N_h, 1 \leq l \leq N_h \quad (3.7)$$

$$\int_0^T \cos(k\omega t) \cos(l\omega t) dt = \frac{\pi}{\omega} \delta_{kl} \quad 0 \leq k \leq N_h, 0 \leq l \leq N_h \quad (3.8)$$

where $T = 2\pi/\omega$ is the period of the motion and δ is the Kronecker symbol. Let us introduce the notation:

$$\mathbf{X} = \begin{bmatrix} \mathbf{X}_0^c \\ \mathbf{X}_1^c \\ \mathbf{X}_1^s \\ \vdots \\ \mathbf{X}_{N_h}^c \\ \mathbf{X}_{N_h}^s \end{bmatrix}, \quad \mathbf{F}_{nl} = \begin{bmatrix} \mathbf{F}_{nl,0}^c \\ \mathbf{F}_{nl,1}^c \\ \mathbf{F}_{nl,1}^s \\ \vdots \\ \mathbf{F}_{nl,N_h}^c \\ \mathbf{F}_{nl,N_h}^s \end{bmatrix} \quad (3.9)$$

Using the orthogonality relations, Eqs. (3.6)-(3.8), a HB procedure [Nayfeh and Mook, 1979] is applied to Eq. (3.5). This leads to the following system of equations:

$$\underline{\mathbf{A}}\mathbf{X} + \mathbf{F}_{nl}(\mathbf{X}) = \mathbf{P}^* \quad (3.10)$$

where $\underline{\mathbf{A}}$ is the block-diagonal linear Jacobian matrix whose first block is the stiffness matrix, $\underline{\mathbf{K}}$, and whose $(k+1)$ -th block is defined as:

$$\begin{bmatrix} -(k\omega)^2\underline{\mathbf{M}} + \underline{\mathbf{K}} & k\omega\underline{\mathbf{C}} \\ -k\omega\underline{\mathbf{C}} & -(k\omega)^2\underline{\mathbf{M}} + \underline{\mathbf{K}} \end{bmatrix}, \quad k = 1, \dots, N_h \quad (3.11)$$

The external forcing is also written in vectorial form: $\mathbf{P}^* = [\mathbf{0} \ \mathbf{P} \ \mathbf{0} \ \dots \ \mathbf{0}]^T$. Equation (3.10) is a system of $N(2N_h + 1)$ equations in the frequency domain. The equations corresponding to the nonlinear DOF's, i.e., the DOF's attached to a friction damper, can be uncoupled from the equations corresponding to the linear DOF's, i.e., the DOF's not attached to a friction damper, as follows.

Let us partition the harmonic component vector \mathbf{X} into linear and non-linear parts, as $\mathbf{X} = (\mathbf{X}_{ln}, \mathbf{X}_{nl})^T$ [Guillen and Pierre, 1996, Berthillier et al., 1998b]. Equation (3.10) is thus written as

$$\begin{bmatrix} \underline{\mathbf{A}}_{ln} & \underline{\mathbf{A}}_{ln,nl} \\ \underline{\mathbf{A}}_{nl,ln} & \underline{\mathbf{A}}_{nl} \end{bmatrix} \begin{Bmatrix} \mathbf{X}_{ln} \\ \mathbf{X}_{nl} \end{Bmatrix} + \begin{Bmatrix} \mathbf{0} \\ \mathbf{F}_{nl} \end{Bmatrix} = \begin{Bmatrix} \mathbf{P}_{ln}^* \\ \mathbf{P}_{nl}^* \end{Bmatrix} \quad (3.12)$$

where the index nl refers to the nonlinear DOF's, i.e., the ones connected to a friction damper, and the index ln refers to the linear DOF's, i.e., the ones not connected to a friction damper. Equation (3.12) can be reduced to, and solved for the nonlinear DOF's as

$$(\underline{\mathbf{\Lambda}}_{nl} - \underline{\mathbf{\Lambda}}_{nl,ln}\underline{\mathbf{\Lambda}}_{ln}^{-1}\underline{\mathbf{\Lambda}}_{ln,nl})\mathbf{X}_{nl} + \mathbf{F}_{nl} = \mathbf{P}_{nl}^* - \underline{\mathbf{\Lambda}}_{nl,ln}\underline{\mathbf{\Lambda}}_{ln}^{-1}\mathbf{P}_{ln}^* \quad (3.13)$$

Let us introduce the reduced linear Jacobian matrix, $\underline{\mathbf{\Lambda}}_{red}$, and the reduced external forcing, \mathbf{P}_{red} :

$$\underline{\mathbf{\Lambda}}_{red} = (\underline{\mathbf{\Lambda}}_{nl} - \underline{\mathbf{\Lambda}}_{nl,ln}\underline{\mathbf{\Lambda}}_{ln}^{-1}\underline{\mathbf{\Lambda}}_{ln,nl}) \quad (3.14)$$

$$\mathbf{P}_{red} = \mathbf{P}_{nl}^* - \underline{\mathbf{\Lambda}}_{nl,ln}\underline{\mathbf{\Lambda}}_{ln}^{-1}\mathbf{P}_{ln}^* \quad (3.15)$$

Using Eqs. (3.14) and (3.15), Eq. (3.13) can be rewritten as:

$$\underline{\mathbf{\Lambda}}_{red}\mathbf{X}_{nl} + \mathbf{F}_{nl}(\mathbf{X}_{nl}) = \mathbf{P}_{red} \quad (3.16)$$

which is a set of $N_d(2N_h + 1)$ non-linear equations, where N_d is the number of DOF's of the structure attached to a friction damper. Once the displacement of nonlinear DOF's, \mathbf{X}_{nl} , have been calculated, the linear ones, \mathbf{X}_{ln} , are obtained as

$$\mathbf{X}_{ln} = \underline{\mathbf{\Lambda}}_{ln}^{-1}(\mathbf{P}_{ln}^* - \underline{\mathbf{\Lambda}}_{ln,nl}\mathbf{X}_{nl}) \quad (3.17)$$

The size of the reduced system, Eq. (3.16), may be significantly smaller than the size of the initial system, Eq. (3.10), if many DOF's of the structure are linear, i.e., $N_d \ll N$.

3.4 Solving the nonlinear equations in the frequency domain

Most of the previous HB studies of dry friction-damped systems have used Newton-Raphson (NR) schemes to solve the non-linear equations in the frequency domain

[Pierre et al., 1985, Shiau et al., 1998]. However, significant convergence problems and long computation times were encountered, especially in stick-slip regions. Therefore, a new nonlinear solution algorithm was implemented in order to ensure better numerical stability.

3.4.1 *QR* vs. *LU* decomposition

The Newton-Raphson schemes used in the HB analysis of friction-damped systems are often presented as suffering convergence problems. Oftentimes, these NR procedures rely on a *LU* decomposition of the Jacobian matrix, $\underline{\mathbf{J}}$, as

$$\underline{\mathbf{J}} = \underline{\mathbf{L}}\underline{\mathbf{U}}$$

where $\underline{\mathbf{L}}$ is a lower $N \times N$ triangular matrix, $\underline{\mathbf{U}}$ is an upper $N \times N$ triangular matrix, and $N \times N$ is the size of the Jacobian $\underline{\mathbf{J}}$. Generally, partial pivoting is necessary in order to improve the numerical stability. Therefore, it is assumed that

$$\underline{\mathbf{P}}\underline{\mathbf{J}} = \underline{\mathbf{L}}\underline{\mathbf{U}}$$

where $\underline{\mathbf{P}}$ is a $N \times N$ permutation matrix. Even with partial pivoting, the numerical stability problems of the *LU* method persist. This is probably due to the fact that the amplitudes of the harmonic components of the modes retained to describe the dynamics of the structure are of very different orders of magnitude.

The Jacobian matrix can also be treated by a *QR* decomposition. In this case, the Jacobian can be written as

$$\underline{\mathbf{J}} = \underline{\mathbf{Q}}\underline{\mathbf{R}}$$

where $\underline{\mathbf{Q}}$ is a $N \times N$ orthogonal matrix and $\underline{\mathbf{R}}$ is a $N \times N$, non-singular, upper triangular matrix, i.e., $R[i, j] = 0$ for $i > j$ and $R[i, i] \neq 0$. The *QR* decompositions of

the Jacobian do not require the scaling of the dependent variables and are numerically stable without pivoting [Allgower and Georg, 1990].

LU and QR decompositions are often used to solve linear systems of equations such as

$$\underline{\mathbf{J}} \Delta \mathbf{X} = -\mathbf{F} \quad (3.18)$$

When a LU decomposition of the Jacobian, $\underline{\mathbf{J}}$, is used, Eq. (3.18) can be resolved in two steps. The lower system is first solved

$$\underline{\mathbf{L}} \mathbf{Y} = -\mathbf{F} \quad (3.19)$$

Then the upper one is solved using the results of the first sub-problem:

$$\underline{\mathbf{U}} \Delta \mathbf{X} = -\mathbf{Y} \quad (3.20)$$

Both Eqs. (3.19) and (3.20) are elementary: since $\underline{\mathbf{L}}$ and $\underline{\mathbf{U}}$ are triangular, the system can be solved by back-substitution. When the QR decomposition is used, only one step is needed since Eq. (3.18) is equivalent to

$$\underline{\mathbf{R}} \Delta \mathbf{X} = -\underline{\mathbf{Q}}^T \mathbf{F} \quad (3.21)$$

Eq. (3.21) is straightforward to solve by back-substitution since $\underline{\mathbf{R}}$ is a non-singular triangular matrix.

Although QR decompositions are more numerically stable than LU ones, they require about twice as many operations as LU decompositions. Therefore, it is important to examine algorithms which allow one not to compute $\underline{\mathbf{Q}}$ and $\underline{\mathbf{R}}$ at each iteration. These methods are briefly discussed in the next section.

3.4.2 Broyden method

Newton and Newton-Chord methods

Denote by \mathbf{F} the function whose zeros the method needs to find. In the case of friction damped structural systems, \mathbf{F} is deduced from Eq. (3.16):

$$\mathbf{F}(\mathbf{X}) = \underline{\mathbf{A}}_{red}\mathbf{X} + \mathbf{F}_{nl}(\mathbf{X}) - \mathbf{P}_{red} \quad (3.22)$$

When a Newton method is used to solve Eq. (3.22), the n -th iterative step is

$$\mathbf{X}_{n+1} = \mathbf{X}_n - \underline{\mathbf{J}}^{-1}(\mathbf{X}_n)\mathbf{F}(\mathbf{X}_n) \quad (3.23)$$

where $\underline{\mathbf{J}}$ is the Jacobian matrix of Eq. (3.22):

$$\underline{\mathbf{J}}(\mathbf{X}_n) = \left. \frac{\partial \mathbf{F}}{\partial \mathbf{X}} \right|_{\mathbf{x}_n} \quad (3.24)$$

The Newton procedure, as presented in Eq. (3.23), is locally quadratically convergent and requires the computation and the inversion of the Jacobian matrix, $\underline{\mathbf{J}}$, after each iteration. This is computationally very demanding and a Newton-Chord method is often used. In the Newton-Chord method, the Jacobian is fixed:

$$\underline{\mathbf{A}} = \underline{\mathbf{J}}(\mathbf{X}_0) \quad (3.25)$$

and the iterative step, Eq. (3.23), is substituted by

$$\mathbf{X}_{n+1} = \mathbf{X}_n - \underline{\mathbf{A}}^{-1}\mathbf{F}(\mathbf{X}_n) \quad (3.26)$$

The iterative Newton-Chord method has only locally linear convergence. The Broyden and the other quasi-Newton, multidimensional secant methods involve the use of the previously calculated data in order to improve the quality of the approximated Jacobian $\underline{\mathbf{A}}$ via successive rank-one updates. The quasi-Newton step substituting Eq. (3.23) is

$$\mathbf{X}_{n+1} = \mathbf{X}_n - \underline{\mathbf{A}}_n^{-1}\mathbf{F}(\mathbf{X}_n) \quad (3.27)$$

where $\underline{\mathbf{A}}_n$ is the approximate Jacobian at the n -th iteration.

Secant condition and Broyden's update

A first-order Taylor expansion of the function $\mathbf{F}(\mathbf{X})$ leads to the following relation:

$$\mathbf{F}(\mathbf{X}_{n+1}) - \mathbf{F}(\mathbf{X}_n) = \underline{\mathbf{J}}(\mathbf{X}_n) (\mathbf{X}_{n+1} - \mathbf{X}_n) \quad (3.28)$$

which is called the secant condition and is naturally verified by the Newton method, as defined in Eq. (3.24):

$$\underline{\mathbf{J}}_{Newton} (\mathbf{X}_{n+1} - \mathbf{X}_n) = \mathbf{F}(\mathbf{X}_{n+1}) - \mathbf{F}(\mathbf{X}_n) \quad (3.29)$$

where $\underline{\mathbf{J}}_{Newton}$ is the Newton Jacobian. When Newton-type steps are used, it is natural to require that the next approximate Jacobian, $\underline{\mathbf{A}}_{n+1}$, satisfies the secant condition:

$$\underline{\mathbf{A}}_{n+1} (\mathbf{X}_{n+1} - \mathbf{X}_n) = \mathbf{F}(\mathbf{X}_{n+1}) - \mathbf{F}(\mathbf{X}_n) \quad (3.30)$$

Equation (3.30) provides N_d relations, which are not sufficient to determine the $N_d \times N_d$ components of the new approximate Jacobian $\underline{\mathbf{A}}_{n+1}$. Since it is assumed that the approximate Jacobian at the previous iteration, $\underline{\mathbf{A}}_n$, is a good approximation of the real Jacobian, the new approximation is determined from the old one by the least change principle. Therefore, among all matrices $\underline{\mathbf{A}}$ which satisfy the secant condition, Eq. (3.30), the new approximate Jacobian will be chosen to be the one with the smallest distance from $\underline{\mathbf{A}}_n$.

The Broyden method uses the Frobenius norm, $\|\cdot\|_F$, in order to find the approximate Jacobian, $\underline{\mathbf{A}}_{n+1}$, as the matrix satisfying the secant equation with the smallest distance from the approximate Jacobian of the previous iteration:

$$\underline{\mathbf{A}}_{n+1} = \min_{\underline{\mathbf{A}}} \left\{ \|\underline{\mathbf{A}} - \underline{\mathbf{A}}_n\|_F ; \underline{\mathbf{A}} (\mathbf{X}_{n+1} - \mathbf{X}_n) = \mathbf{F}(\mathbf{X}_{n+1}) - \mathbf{F}(\mathbf{X}_n) \right\} \quad (3.31)$$

where the Frobenius norm is defined as:

$$\|\underline{\mathbf{A}}\|_F = \left(\sum_{i,j=1}^{N_d} (A[i,j])^2 \right)^{\frac{1}{2}} \quad (3.32)$$

The solution of Eq. (3.31) can be found analytically, and is given by:

$$\underline{\mathbf{A}}_{n+1} = \underline{\mathbf{A}}_n + \frac{\mathbf{F}(\mathbf{X}_{n+1}) - \mathbf{F}(\mathbf{X}_n) - \underline{\mathbf{A}}_n (\mathbf{X}_{n+1} - \mathbf{X}_n)}{\|\mathbf{X}_{n+1} - \mathbf{X}_n\|} (\mathbf{X}_{n+1} - \mathbf{X}_n)^T \quad (3.33)$$

The Broyden update, Eq. (3.33), leads to superlinear convergence of the Broyden method. The interested reader is referred to Allgower and Georg (1990) for more details on the Broyden algorithm.

Given the particular form of the update, Eq. (3.33), the QR decomposition of $\underline{\mathbf{A}}_{n+1}$ can be updated from the QR decomposition of $\underline{\mathbf{A}}_n$ in $O(N^2)$ operations. All that is needed is the initial guess $\underline{\mathbf{A}}_0$, which is computed as a finite-difference approximation of the Jacobian. Therefore, because of the improved updates of $\underline{\mathbf{Q}}$ and $\underline{\mathbf{R}}$, the Broyden iteration is faster than the Newton step, Eq. (3.23).

For the friction-damped systems considered in this study, the Broyden method seems to have better stability than NR schemes [Ling and Wu, 1987]. The Broyden algorithm needs more iterations to converge, but since there are fewer operations involved at each iteration, the Broyden method turns out to be faster than the NR algorithm. Moreover, the convergence of the method is nearly always guaranteed, even with a poor initial guess. Bobilev *et al.* (1994) presents a proof of the convergence of HB in the case of some nonlinearities.

3.5 Overview of the multi-harmonic, hybrid frequency/time method

The multi-harmonic, hybrid frequency/time method can be summarized as follows:

Procedure 1 *Multi-harmonic, hybrid frequency/time method.*

1. *At a given frequency, the number of equations is reduced to the number of nonlinear DOF's [Guillen and Pierre, 1996, Berthillier et al., 1998b], using a reduced Jacobian matrix and external forcing.*
2. *An initial guess is obtained by, e.g., improved single-harmonic approximation, see Chapter II.*
3. *The Broyden method is used iteratively until convergence criteria are met and Eq. (3.16) is solved:*
 - *From the harmonic components of the displacement, \mathbf{X}_{nl} , the periodic nonlinear displacement, \mathbf{x}_{nl} , is computed in the time domain by FFT.*
 - *From the nonlinear displacement, \mathbf{x}_{nl} , the non-linear force transmitted by the friction dampers, \mathbf{f}_{nl} , is computed in the time domain, following the procedure presented in Section 3.2.*
 - *From the non-linear friction forces in the time domain, \mathbf{f}_{nl} , the harmonic component of the friction forces in the frequency domain, $\mathbf{F}_{\text{nl}}(\mathbf{X})$ are computed by FFT.*
 - *The objective function, $\mathbf{F}(\mathbf{X})$, is computed according to Eq. (3.22).*
 - *A new estimate of the harmonic components, \mathbf{X} is obtained by solving Eq. (3.27).*
 - *The new approximate Jacobian is computed using the Broyden update, Eq. (3.33).*
4. *Move to the next frequency.*

3.6 Conclusion

A new multi-harmonic method was developed for the forced response analysis of multi-DOF systems connected to several ground-to-ground or ground-to-blade flexible friction dampers. The main contributions of this work are as follows. *First*, the force transmitted by the friction dampers is evaluated in the time domain only, and no approximation other than Coulomb's law of friction is made. *Second*, the equations of motion are transformed into the frequency domain in an efficient way, while retaining only the non-linear terms. *Third*, the Broyden method is implemented for friction-damped systems.

The results of the method are presented in the next chapter.

CHAPTER IV

SELECTED FORCED RESPONSE RESULTS

4.1 Introduction

The method presented in Chapter III for the analysis of the forced response of friction damped structural systems is applied in this chapter to several structures. First, a simple beam attached to a flexible friction damper is considered. Second, a model of a blade used in a jet engine turbine stage, and attached to a flexible friction damper, is studied. Time histories and frequency responses are presented for both systems. Complex features of the non-linear response are revealed such as: motions for several stick-slip phases per period, subresonances, effects of higher harmonics, optimal damping. Finally, large-scale models of dry-friction damped bladed disks used in turbomachinery applications are examined. Both tuned configurations (with all blades identical) and mistuned ones (with slightly different blades) are considered. Results obtained for mistuned systems evidence the occurrence of localized responses, which are characterized by mostly sticking motion at most blades and mostly slipping motion at a few blades.

4.2 Forced response of beam system

4.2.1 System model and influence of force amplitude

The first system considered is a beam undergoing transverse vibrations, fixed at one end, excited at the other end, and attached to an elastic friction damper. The system is the same as the one presented in Section 2.3.4 and whose characteristics were provided by SNECMA [Berthillier et al., 1998b]. The system model is depicted in Fig. 2.7. Three component modes are retained to describe the dynamics of the beam: two constraint modes corresponding to the static shape of the beam with unit displacement at the damper location and at the tip, respectively, and a normal vibration mode, for which the beam is fixed at the tip and at the damper location.

Figures 4.1 and 4.2 present sample time histories of the displacement of the 3-DOF SNECMA beam, as predicted by the hybrid frequency/time method (labeled as “Broyden” on the figures) and by numerical time integration. In Fig. 4.1, the damper displacement and the displacement at the damper location have almost the same amplitude, with the damper slipping only during a small portion of each period. It can be observed that the occurrence of slipping introduces a small phase shift between the damper displacement and the displacement at the damper location. Here a large number of harmonics ($N_h = 19$) are considered in the solution, and the hybrid frequency/time method is able to match almost perfectly the results predicted by time integration. Figure 4.2 presents a case of near optimal damping. It is interesting to notice that there are in this case more than two slipping phases during one period of the motion. The hybrid frequency/time method is able to handle these cases and, when 19 harmonics are accounted for, the results are almost identical to the ones predicted by time integration.

Figure 4.3 shows the frequency response of the 3-DOF SNECMA beam, at the

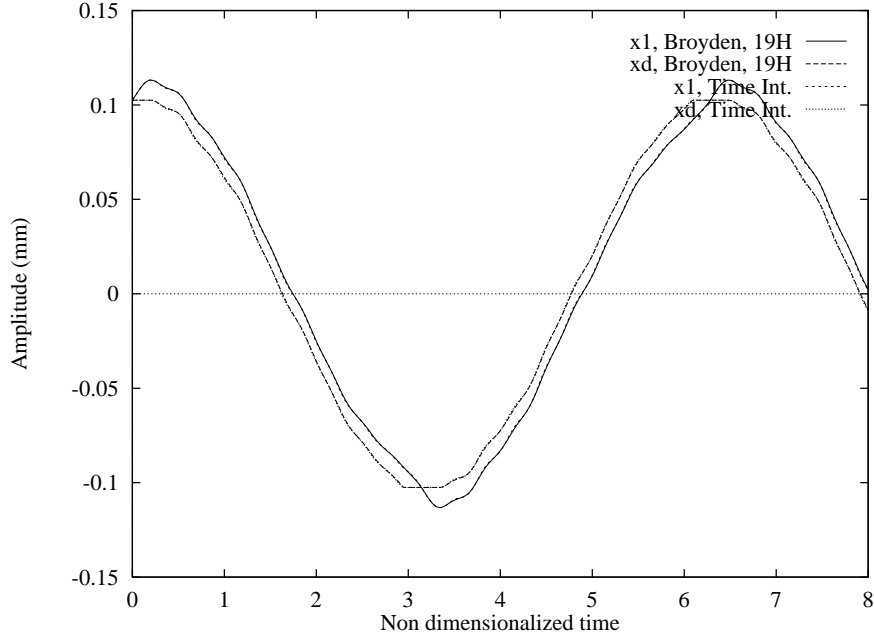


Figure 4.1: Time histories of displacement at the damper location, x_1 , and damper displacement, x_d , for the 3-DOF SNECMA beam, for a force amplitude of $20.313N$, at $170rad/s$, as predicted by the 19-harmonic hybrid frequency/time method (Broyden), and numerical time integration.

damper location, for various force amplitudes, as predicted by the multi-harmonic hybrid frequency/time method. The amplitudes have been normalized by the external force amplitude. Three sets of curves can be identified: the *first* one corresponds to cases where the damper is slipping most of the time. This is the case for high force amplitudes, namely for $P = 31.475N$ and $P = 38.438N$. As the force amplitude increases, the resonance frequency of these response curves tends to the so-called *slipping resonance frequency*, equal to the natural frequency of the beam without any friction damper attached to it. The *second* group of curves corresponds to cases where the damper is sticking during most of the motion. This is the case for low levels of force amplitude, from $P = 0.938N$ to $P = 6.563N$. As the force amplitude

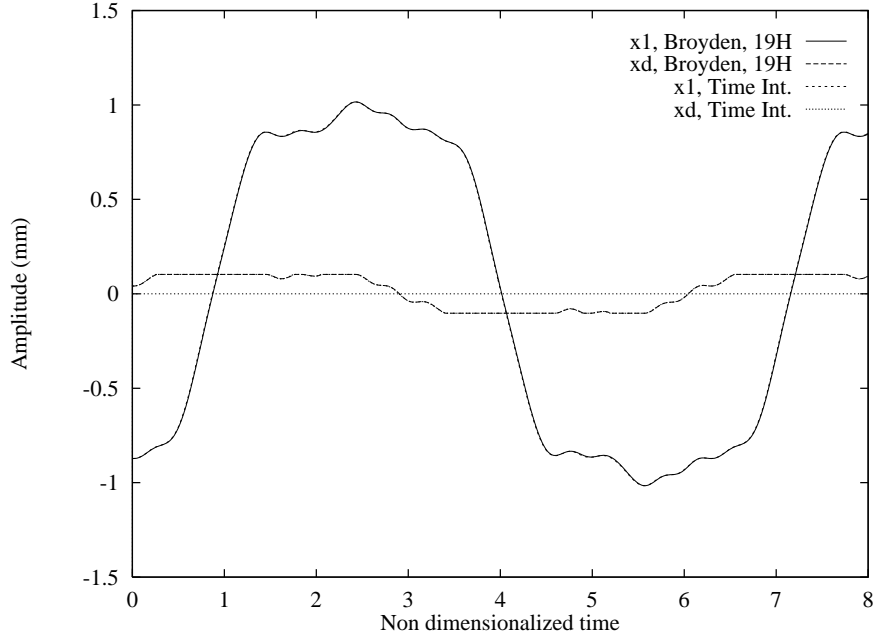


Figure 4.2: Time histories of displacement at the damper location, x_1 , and damper displacement, x_d , for the 3-DOF SNECMA beam, for a force amplitude of $25.0N$, at $200rad/s$, as predicted by the 19-harmonic hybrid frequency/time method (Broyden), and numerical time integration.

decreases, the resonance frequency of these response curves tends to the so-called *sticking resonance frequency*, equal to the natural frequency of the beam with an attached stiffness connected to ground at the damper location, equal to the stiffness of the flexible friction damper. Finally, the *third* group of curves corresponds to cases where the damper undergoes both significant slipping and sticking phases during each period of the motion. These cases correspond to intermediate levels of force amplitude, from $P = 6.563N$ to $P = 16.563N$, and it can be seen that they also correspond to the optimal friction damper effect. Since the ratio of maximum amplitude over force amplitude is minimum for the curves of the third group, the damper is most effective at reducing the response amplitude in these regions.

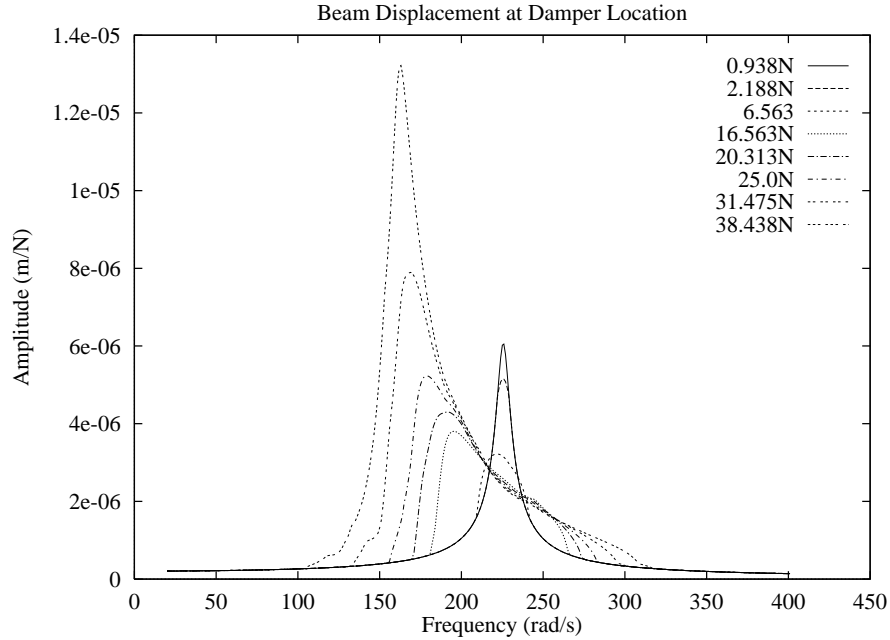


Figure 4.3: Frequency responses at the damper location, for the 3-DOF SNECMA beam, for various force amplitudes, as predicted by the 15-harmonic hybrid frequency/time method.

Figure 4.4 also shows the frequency response of the beam system, but at the tip of the 3-DOF SNECMA beam. Several levels of external force are considered and results are obtained by the multi-harmonic hybrid frequency/time method with 15 harmonics. As in Fig. 4.3, there are three groups of curves which correspond to the cases described above. It is interesting to notice that the force amplitude that corresponds to optimal damping for the beam's tip response is not the same as the one yielding optimal damping for the response at the damper location. For the beam tip response, $P = 20.313N$ for optimal damping, while $P = 6.563N$ for minimum peak response at the damper location. Therefore, when a system is designed, the maximum stress location must be first determined so that the proper friction damper will minimize the vibrations at this location.

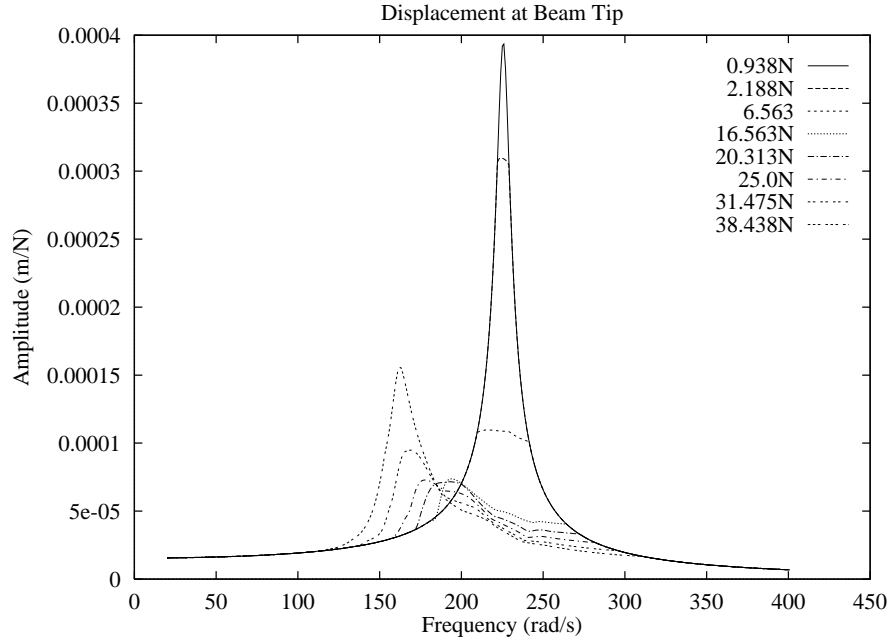


Figure 4.4: Frequency responses at the tip of the beam, for the 3-DOF SNECMA beam, for various force amplitudes, as predicted by the 15-harmonic hybrid frequency/time method.

4.2.2 Influence of the damper stiffness

The damper stiffness is an important characteristic of friction damped systems. Its influence on the response of the 3-DOF beam attached to a single friction damper presented in Section 4.2.1 is investigated here. The amplitude of the external force is held constant to $P = 20.313N$, which is the value corresponding to optimal damping at the beam's tip, and the damper stiffness is varied. Figures 4.5 and 4.6 depict the beam's frequency responses at the damper location and at the tip, respectively, for various damper stiffnesses. For low values of the damper stiffness, $k_d \leq 2.4 \times 10^5 N/m$, the damper is hardly slipping because the force in the damper cannot build up to the slipping value. With the damper hardly slipping and the damper stiffness small, the response of the system is very similar to the response of the beam without an

attached friction damper, and the frequency of the motion approaches the natural frequency of the cantilevered beam, $\omega_{beam} = 159.39 \text{ rad/s}$.

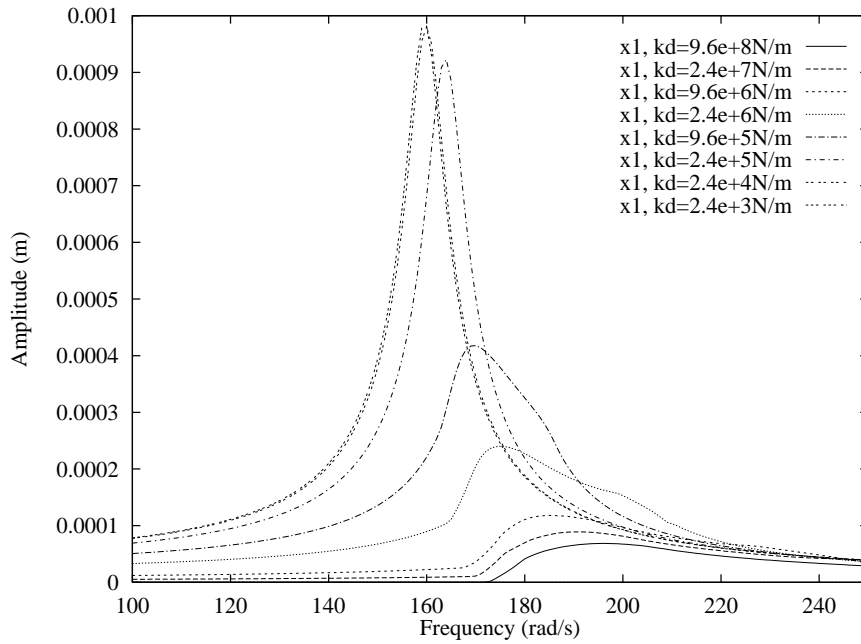


Figure 4.5: Beam frequency response at the damper location, x_1 , for the 3-DOF SNECMA beam, for various damper stiffnesses, k_d , as predicted by the 15-harmonic hybrid frequency/time method, and for force amplitude $P = 20.313N$.

As the damper becomes stiffer, there is more slipping and thus more friction during each cycle of the motion and more energy is dissipated. Therefore, as seen in Figs. 4.5 and 4.6, the overall amplitude of the motion decreases when the damper stiffness increases, all other parameters remaining constant, and the amplitude versus frequency trend is the same for the tip displacement, x_2 , and the displacement at the damper location, x_1 .

Figures 4.7 and 4.8 show the beam's frequency responses at the damper location and at the tip, respectively, for various, large values of the damper stiffness. Observe that, as the damper stiffness becomes large, the frequency response of the system

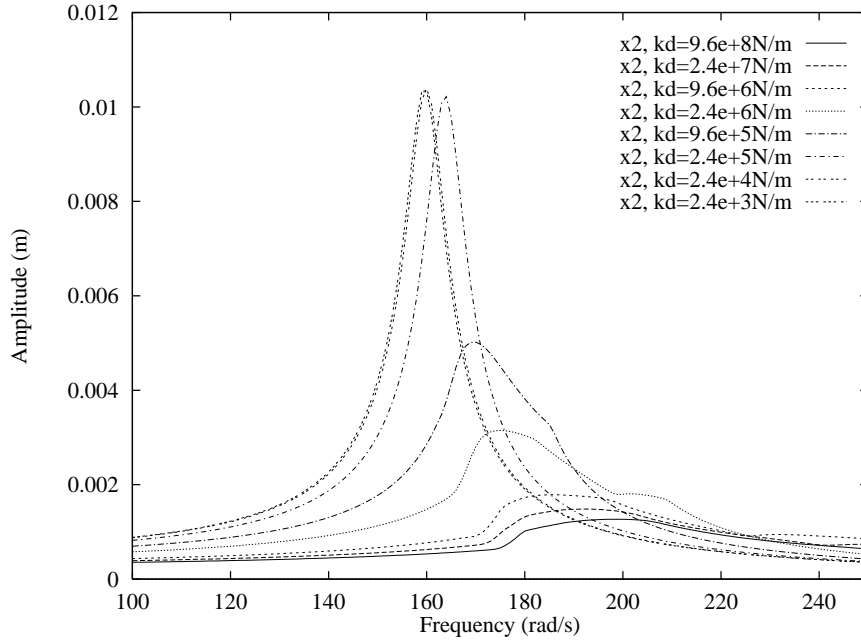


Figure 4.6: Beam frequency response at the tip, x_2 , for the 3-DOF SNECMA beam, for various damper stiffnesses, k_d , as predicted by the 15-harmonic hybrid frequency/time method, and for force amplitude $P = 20.313N$.

converges toward the response of the beam attached to a rigid damper, that is, a damper with an infinite stiffness. The proof of this convergence is not presented here, but the interested reader is referred to Section 5.2.3 for a similar study in the free response case. Therefore, using the method presented in Chapter III, it is possible to study the dynamics of structural systems attached to rigid friction dampers: the dampers must be modeled as flexible dampers with stiffnesses large enough to represent correctly the dynamics of rigid dampers.

4.3 Forced response of turbine blade system

A model of a turbine blade of a jet engine provided by SNECMA is considered in this section and is depicted in Fig. 4.9 [Berthillier et al., 1998a]. The blade is shown

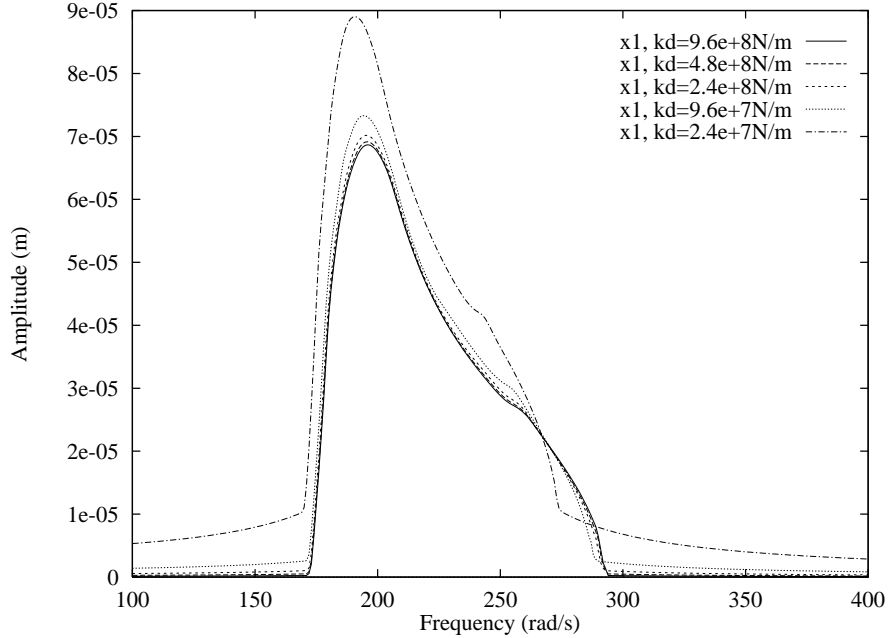


Figure 4.7: Beam frequency response at the damper location, x_1 , for the 3-DOF SNECMA beam, for various damper stiffnesses, k_d , as predicted by the 15-harmonic hybrid frequency/time method, and for force amplitude $P = 20.313N$.

with the disk section to which it is attached and the location of the dampers, i.e., cavities underneath the blade platform, is indicated. The blade properties, including the natural resonance frequencies, are proprietary. The finite element model of the blade contains more than 50000 DOF's, but a reduced order modeling technique is performed to reduce the size of the model to 18 modes of vibration. Of those 18 component modes, 2 are constraint modes corresponding to the static shape of the blade with unit displacement at the damper location and at the tip, respectively, and 16 are normal vibration modes, for which the blade is fixed at the tip and at the damper location. A single, blade-to-ground flexible friction damper is inserted inside a cavity, underneath the blade platform, as indicated on Fig. 4.9. All DOF's of the blade are externally excited, and the excitation data was computed by SNECMA

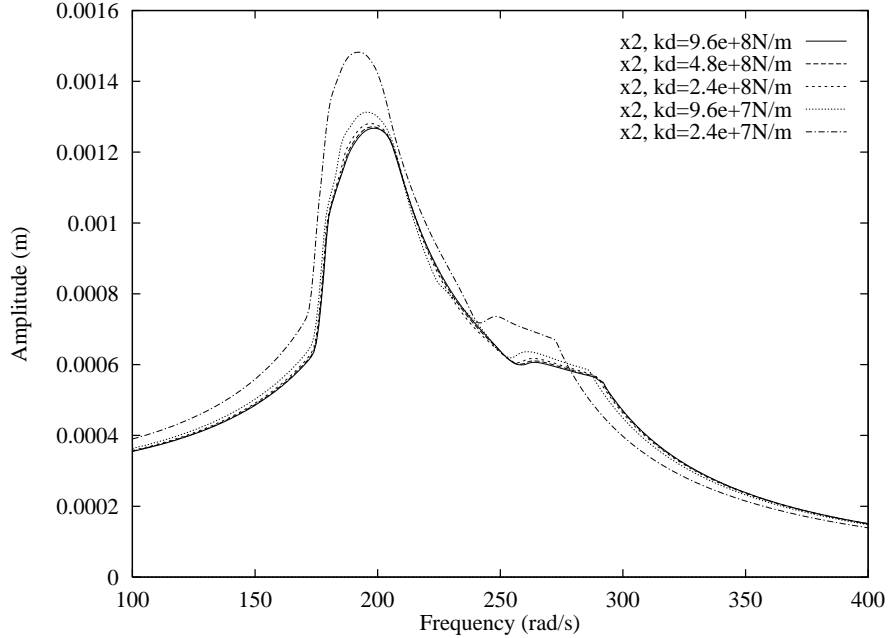


Figure 4.8: Beam frequency response at the tip, for the 3-DOF SNECMA beam, x_2 , for various damper stiffnesses, k_d , as predicted by the 15-harmonic hybrid frequency/time method, and for force amplitude $P = 20.313N$.

using aeroelastic models of the forces exerted on the blade. The equations of motion for the blade are derived from Eq. (3.1):

$$\underline{\mathbf{M}}\ddot{\mathbf{x}} + \underline{\mathbf{C}}\dot{\mathbf{x}} + \underline{\mathbf{K}}\mathbf{x} + \mathbf{f}_{\text{nl}}(\mathbf{x}, \dot{\mathbf{x}}) = \mathbf{P} \cos(\omega t) \quad (4.1)$$

where $N = 18$ and $N_d = 1$. Since there is a single friction damper connecting to a single DOF of the blade, only one of the 18 components of $\mathbf{f}_{\text{nl}}(\mathbf{x}, \dot{\mathbf{x}})$ is different from zero. The viscous damping present in the system is assumed to be proportional:

$$\underline{\mathbf{C}} = \alpha \underline{\mathbf{K}} + \beta \underline{\mathbf{M}} \quad (4.2)$$

The values of the damping coefficients, α and β , are proprietary, but the viscous damping is smaller than 0.1%. Of particular interest here is the fifth mode of vibration, which has been shown to yield a large response amplitude at the tip of

the blade (third DOF). Thus, excitation frequencies near the fifth blade mode are considered in this study. For confidentiality reasons, the amplitude and frequency in Figs. 4.10-4.13 are normalized to the linear values when the damper is fully stuck. The maximum force transmitted by the friction damper, F_d , is normalized to its optimal damping value, F_{d0} .

Frequency responses were obtained for various levels of maximum force transmitted by the friction damper. Figures 4.10 and 4.11 show the response amplitudes at the damper location and at the tip of the blade versus frequency, when nine temporal harmonics are used. As noticed for the beam system in Section 4.2.1, three groups of frequency responses can be observed. The group at the lower frequencies corresponds to motions where the friction damper is mostly slipping during one period of the motion. The group at the higher frequencies corresponds to motions where the friction damper is mostly sticking during one period of the motion. The intermediate group corresponds to cases where the friction damper has a truly stick/slip intermittent motion. The energy dissipation by friction is optimal in these latter cases.

Given the very low level of viscous damping present in the case considered here, the time integration calculations had to be performed over a very large number of cycles (> 10000) in order to reach steady state. Figures 4.12 and 4.13 show the comparison between the results predicted by the hybrid frequency/time Broyden method, and by the time integration procedure, at the damper location and at the tip of the blade, for a value of the maximum force transmitted by the friction damper close to the optimal damping value. The results predicted by the two methods are virtually identical. Therefore, the hybrid frequency/time Broyden method appears to be a robust and efficient design tool, which could be used, for example, to determine the optimal design parameters of the friction damper, so that the peak response

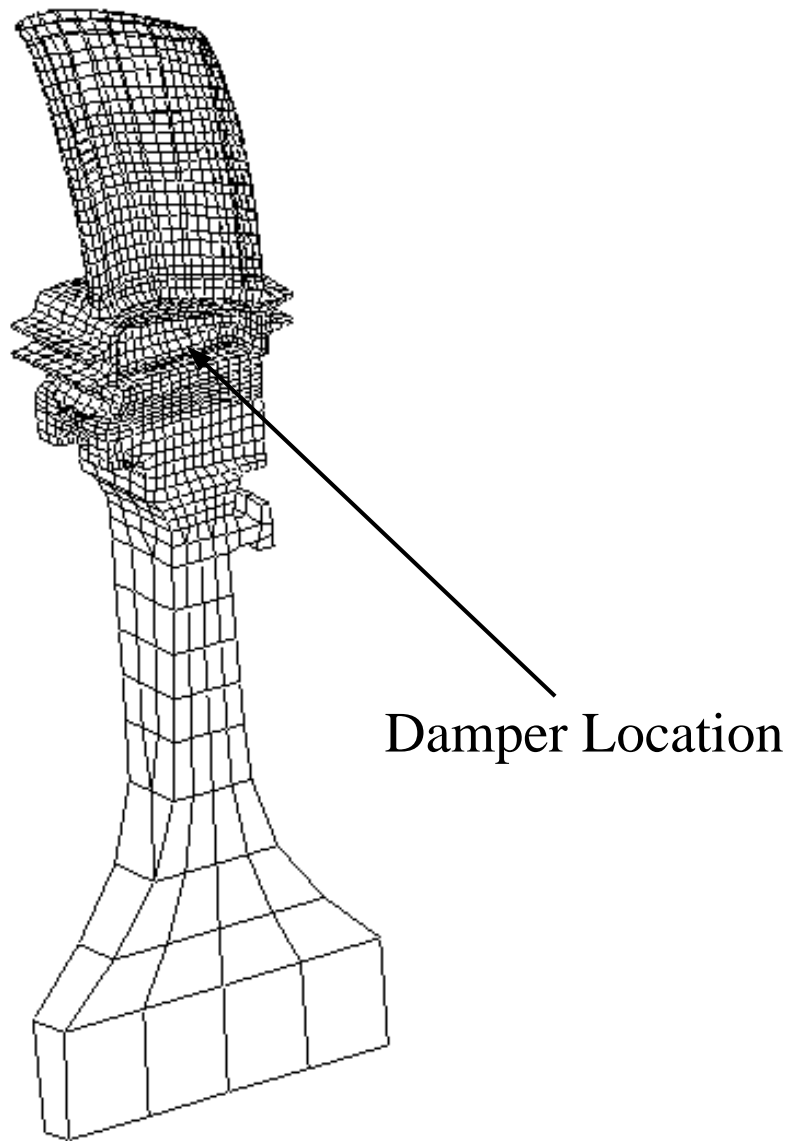


Figure 4.9: 18-mode turbine blade model [Berthillier et al., 1998a]. Friction dampers are inserted between the blade and the platform.

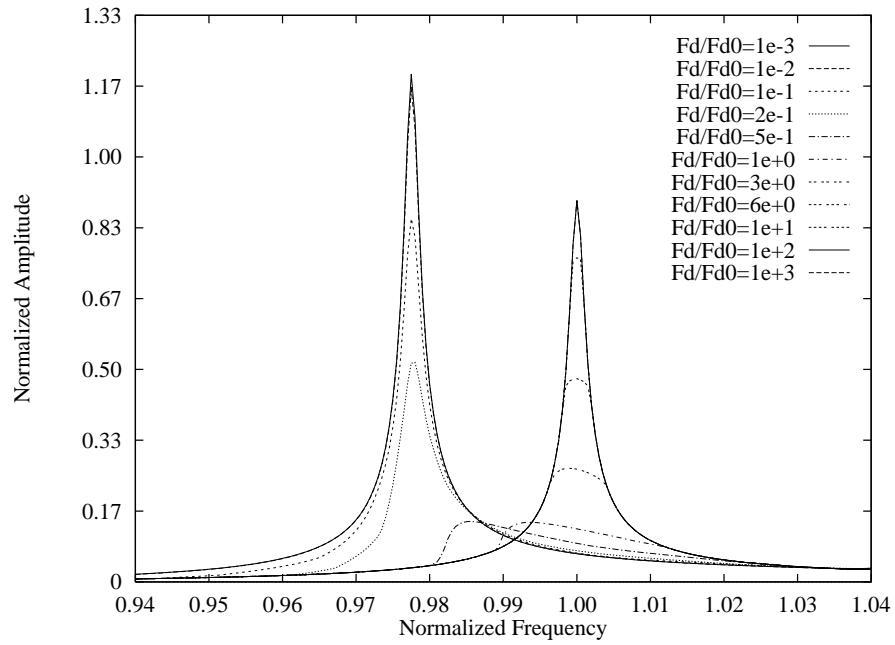


Figure 4.10: Blade frequency response at the damper location, normalized by the peak amplitude when the damper is totally stuck, for various levels of maximum force transmitted by the damper, F_d/F_{d0} , as predicted by the hybrid frequency/time (Broyden) method, with 9 harmonics used.

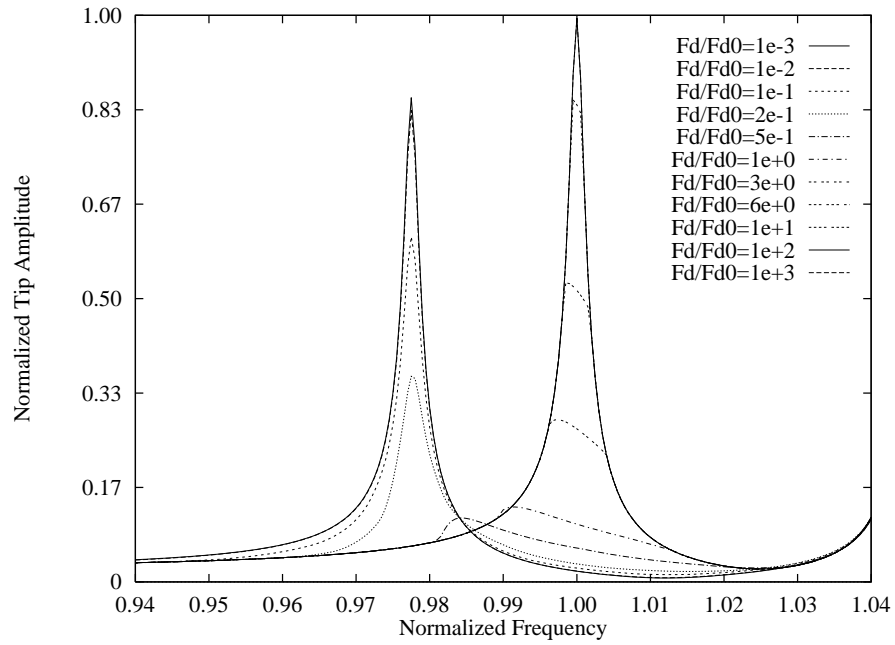


Figure 4.11: Blade frequency response at the tip, normalized by the peak tip amplitude when the damper is totally stuck, for various levels of maximum force transmitted by the damper, F_d/F_{d0} , as predicted by the hybrid frequency/time (Broyden) method, with 9 harmonics.

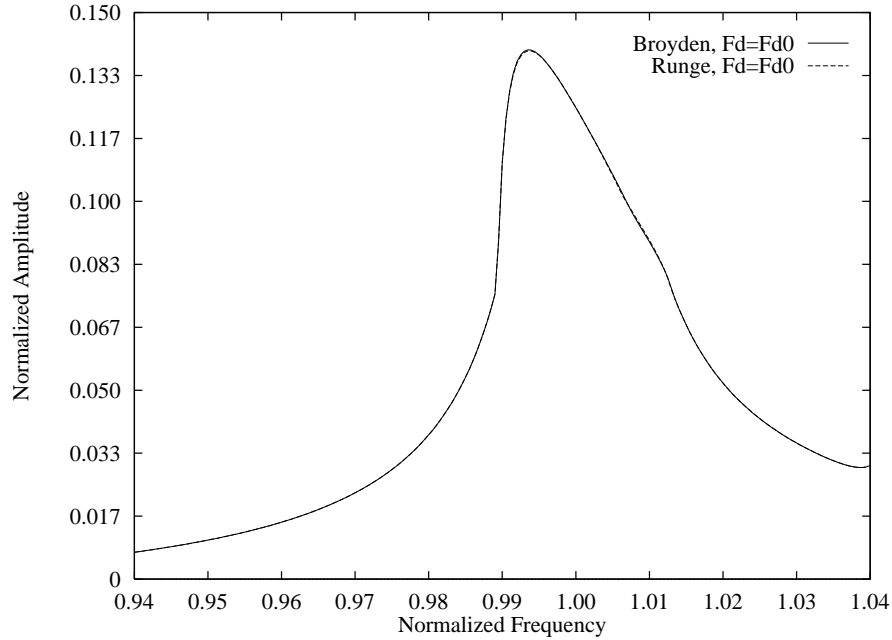


Figure 4.12: Blade frequency response at the damper location, at optimal damping, $F_d = F_{d0}$, as predicted by the Runge-Kutta time integration method, and by the hybrid frequency/time (Broyden) method, with 9 harmonics.

amplitude at the tip of the blade is minimized. Notice that the overall aspect of the frequency response, Figs. 4.10-4.13, is very similar to the one of the frequency response of the beam system presented in Section 4.2.1.

4.4 Performance of the hybrid frequency/time method

In Section 4.2 and 4.3, the results predicted by the hybrid frequency/time method presented in Chapter III are compared with those of the numerical time integration. It was observed that the hybrid frequency/time is able to capture accurately the dynamics of friction-damped structural systems. In this section, the two methods, i.e., the hybrid frequency/time method and the numerical time integration, are compared in terms of computational efficiency. Table 4.1 presents the CPU time needed

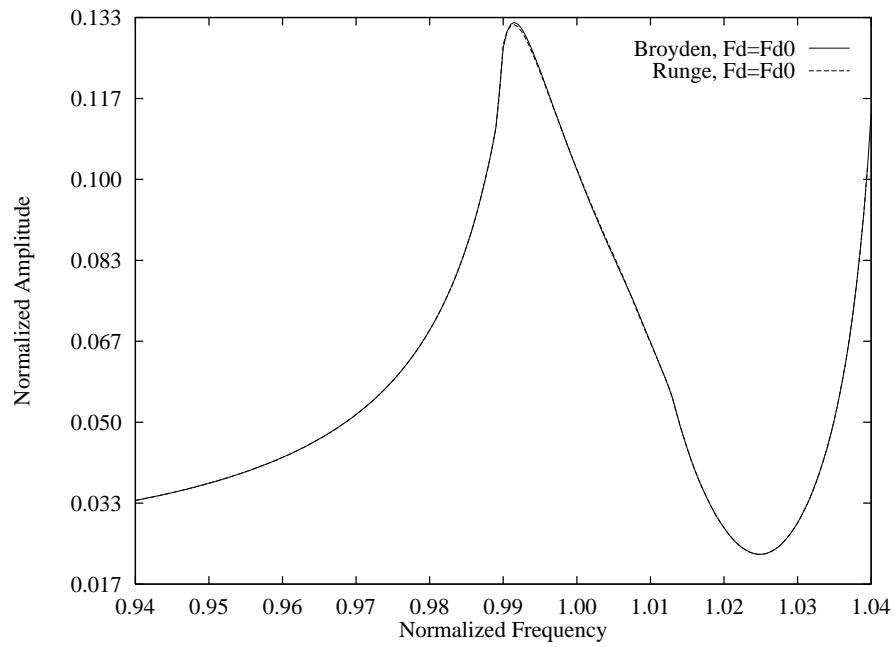


Figure 4.13: Blade frequency response at the tip, at optimal damping, $F_d = F_{d0}$, as predicted by the Runge-Kutta time integration method, and by the hybrid frequency/time (Broyden) method, with 9 harmonics.

Case	3-DOF SNECMA beam	18-DOF blade
Method	CPU time (s)	CPU time (s)
Broyden (1 harm.)	1.87	9.74
Broyden (3 harm.)	4.43	16.69
Broyden (5 harm.)	5.83	25.38
Broyden (7 harm.)	5.04	95.01
Broyden (9 harm.)	7.89	94.72
Broyden (11 harm.)	12.96	405.84
Broyden (13 harm.)	8.02	419.05
Broyden (15 harm.)	18.15	416.25
Broyden (21 harm.)	22.05	407.64
Time integration	3807.6	167685.6

Table 4.1: Computational time needed by the multi-harmonic frequency/time method and numerical time integration for the determination of the frequency response of the SNECMA beam presented in Section 4.2.1 and of the blade presented in Section 4.3.

on a C240 HP workstation to determine the frequency response of the beam and the blade systems presented in Sections 4.2.1 and 4.3, respectively, when the time integration procedure is used and when the multi-harmonic hybrid frequency/method is performed. The level of external force for the beam case, $P = 20.313N$, and the level of maximum slipping force for the blade case, $F_d = F_{d0}$, correspond to a near optimal damping situation where the Broyden method is the slowest. The response is computed at 400 different frequencies.

The hybrid frequency/time method is much faster than the numerical time integration, even when as many as 21 temporal harmonics are retained in the solution. For both systems, the 3-DOF beam and the 18-DOF blade, the time integration requires several hundreds more times computational time than the hybrid frequency/time method.

4.5 Large-scale tuned and mistuned beam assemblies

The multi-harmonic Broyden solution method was applied to large-scale beam assemblies, that may be viewed as simple models of bladed disk assemblies found in turbomachinery rotors. Most of the previous studies on friction damped systems have been limited to structures connected to one, or possibly two friction dampers. In the present study, large-scale structures with many friction dampers are considered.

A cyclic structural system made of 36 SNECMA beams, each attached to a ground-connected friction damper is considered. The characteristics of the beam and the dampers are the same as these in Section 2.3.4, and are given in Eq. (2.32). The beams are elastically coupled at their tips, $k_c = 10^5 N/m$. The 36-th beam is connected to the 35th and to the first, making the beam assembly cyclic. This may represent a friction-damped bladed-disk assembly, where the disk is assumed rigid, and the blades are coupled through shrouds. Figure 4.14 shows a typical blade assembly with shrouds [Bladh et al., 1998] and the coupled beam assembly considered here is depicted in Fig. 4.15.

A harmonic external force is applied at the tip of each beam, and the external force is assumed to be with engine order 2: there are two waves of excitation traveling from blade to blade. Denote by $F_{ex,i}(t)$ the excitations on the i -th blade and by F_{ex} the amplitude of the external force. Assume that the excitation is harmonic at frequency ω and that the engine order is E , we have:

$$F_{ex,i} = F_{ex} \cos\left(\omega t + \frac{2i\pi E}{36}\right) \quad (4.3)$$

where the phase of the 36-th blade is arbitrarily set to zero. In the present case, given that there are 36 beams and that the engine order is 2, the phase difference between two adjacent beams is $\pi/9$ radians, or 20 degrees.

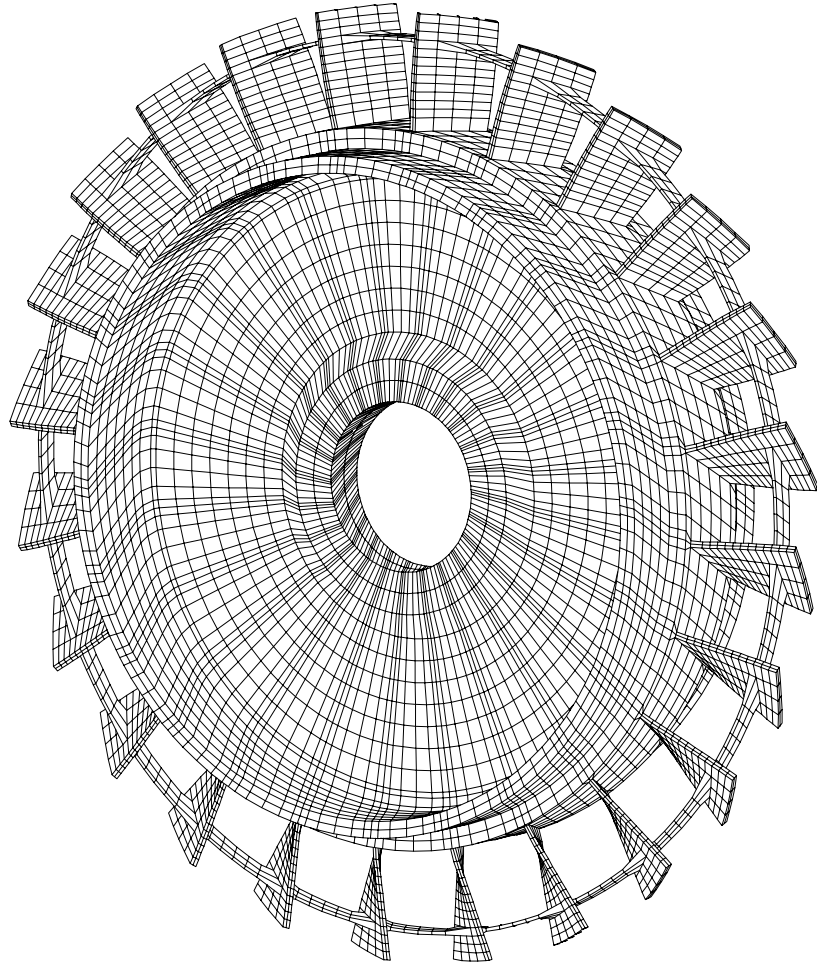


Figure 4.14: Blade assembly with shrouds [Bladh et al., 1998].

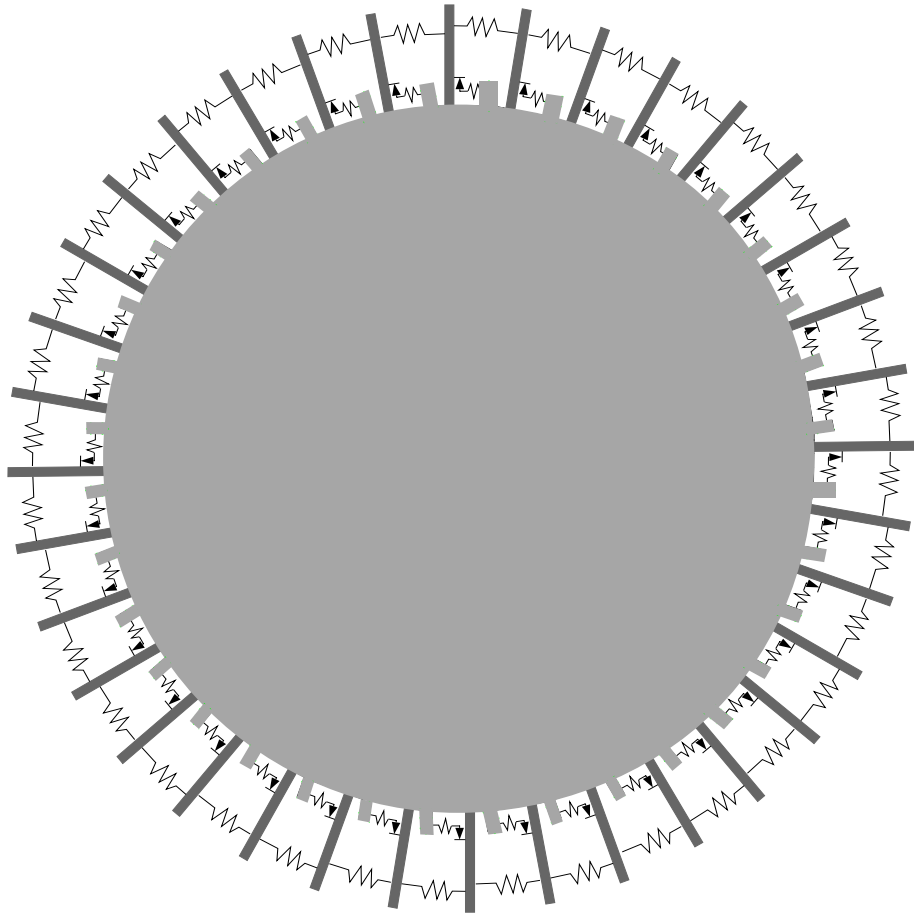


Figure 4.15: 36-beam, 36-damper, cyclic, coupled beam assembly.

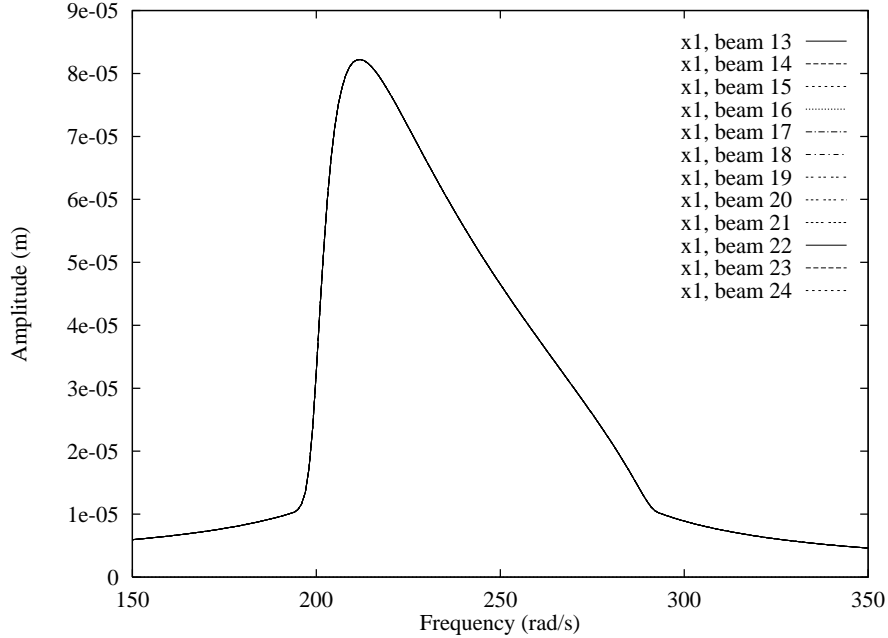


Figure 4.16: Beam frequency responses at the damper location (x_1), for beams 13 through 24 from a tuned, 36-beam assembly with engine order two excitation, coupled by a stiffness of $k = 10^5 N/m$, for a force amplitude of $20.313 N$, as predicted by the 3-harmonic hybrid frequency/time method.

Both tuned and mistuned beam assembly configurations are considered. In the tuned case, all beams are identical with nominal characteristics given in Section 2.3.4. However, in industrial bladed disks, the blades are slightly different from each other, due to manufacturing defects. In order to account for these differences, responsible for the mistuning of the blade assemblies, the Young's modulus of the material is assumed to change from one beam to the other. The introduction of the mistuning is done in the following way. A series of 36 random numbers, $r_i, i = 1, \dots, 36$, of zero-average and unit standard deviation is generated. If a level of $S\%$ mistuning is considered, the Young's modulus E_i of the i -th beam is given by $E_i = (1 + Sr_i)E_0$, where E_0 is the nominal Young's modulus of the beams.

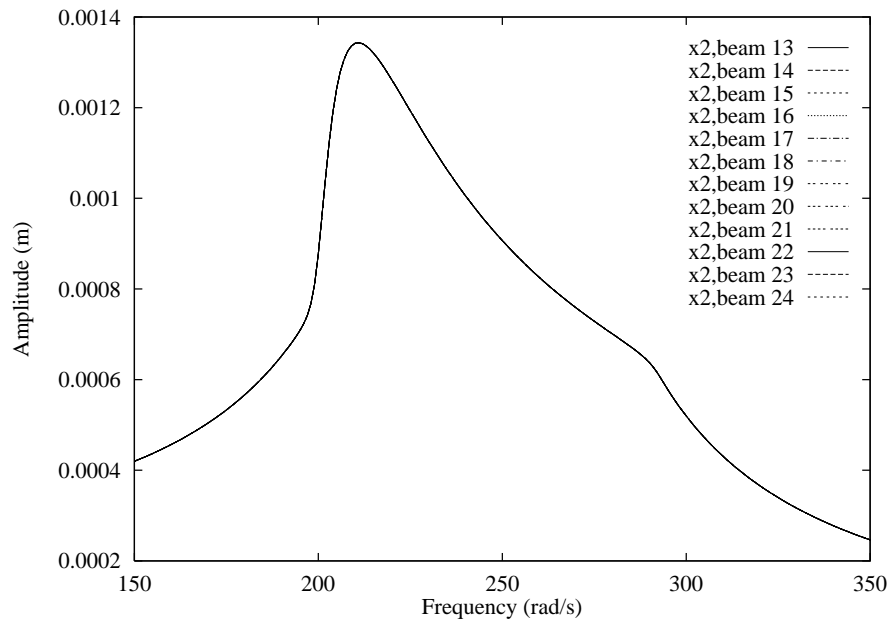


Figure 4.17: Beam frequency response at the tip (x_2), for beams 13 through 24 from a tuned, 36-beam assembly with engine order two excitation, coupled by a stiffness of $k = 10^5 N/m$, for a force amplitude of $20.313 N$, as predicted by the 3-harmonic hybrid frequency/time method.

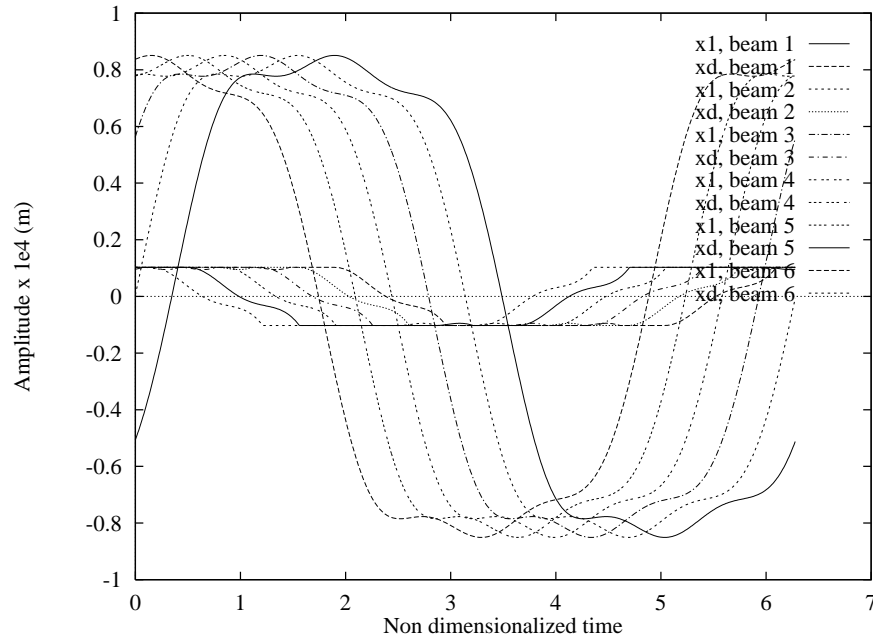


Figure 4.18: Displacement at the damper location (x_1) and damper displacement (x_d), of the first six of 36 tuned beams, coupled at the tip by a stiffness of $k = 10^5 N/m$, for an engine order two excitation and a force amplitude of $20.313N$, at frequency $\omega = 220 rad/s$, as predicted by the 7-harmonic hybrid frequency/time method.

Figures 4.16 and 4.17 show the frequency response of beams number 13 through 24 in the tuned case, at the damper location and at the tip of the beams, respectively. The level of force amplitude considered in this study is near the level, $P = 20.313N$, which corresponds to optimal friction damping for the standard 3-DOF SNECMA beam, as detailed in the Section 4.2.1. As expected, the frequency response is identical for all beams in the tuned case. While the beam response amplitude are the same, there is a 20-degree phase difference in the responses of adjacent beams, as illustrated in Fig. 4.18. The same phase difference characterizes the displacements of adjacent dampers, as seen again in Fig. 4.18.

Figure 4.19 depicts the time histories for selected beams in a mistuned 36-beam assembly (the beam frequencies are generated from a uniform random distribution with 7% standard deviation), for an engine order 3 excitation. The one-harmonic calculation, shown in Fig. 4.19a, provides a fair approximation of the amplitude of the response, but does poorly at describing the complex dynamic response of the system. It is important to notice the results predicted by the one-harmonic calculation are identical to the ones predicted by the improved single-harmonic approximation presented in Section 2.4. On the other hand, results obtained with the hybrid frequency/time method with 9 harmonics, depicted in Fig. 4.19b, describe accurately the truly stick/slip motions or the mostly slipping motions, with several stick/slip phases per cycle. For the results presented in Fig. 4.19b, 2052 equations are solved by the hybrid frequency/time Broyden method, of which 684 are non-linear. No convergence problems were ever encountered, and, even with such a level of accuracy, the Broyden method is still several orders of magnitude faster than the numerical time integration.

Figures 4.20 and 4.21 show the frequency responses of the first 12 beams of the

mistuned system for various values of the coupling stiffness. It can be seen that, for low and high values of the coupling, the beams respond in a similar way. For intermediate values of the coupling, however, the beam assembly exhibits localization, where some beams exhibit a slipping-type resonance, and others exhibit a sticking-type resonance, with large differences in the peak resonant amplitudes of the various beams [Guillen and Pierre, 1998]. Although the system is only 7%-mistuned, there is up to a factor five between the peak response amplitudes of the beams: the localization caused by small mistuning is strong. Beams 13 through 36 are not shown, but would reveal similar behavior. The multi-harmonic method is also able to capture subresonances, as seen in Fig. 4.21f.

The magnification factor, defined as the ratio of the maximum resonant amplitude of the mistuned structure (for any beam) over a frequency range to that of the tuned system, is a measure of the localization taking place due to mistuning. Figure 4.22 presents the influence of the coupling stiffness on the magnification factor, \mathcal{M} . It can be seen that the localization is stronger at the damper locations than at the tip of the beams, where the coupling stiffnesses are attached. Also, the localization factor is stronger for intermediate values of the coupling stiffness, and the number of harmonics has a significant influence on the degree of localization. This is consistent with results published in the literature on localization in nonlinear mistuned assemblies [Wei and Pierre, 1989].

4.6 Conclusion

Results for the forced response of various friction damped structural systems were presented. Small- to large-scale systems were considered for a variety of structural and friction parameters. The multi-harmonic method developed in Chapter III is

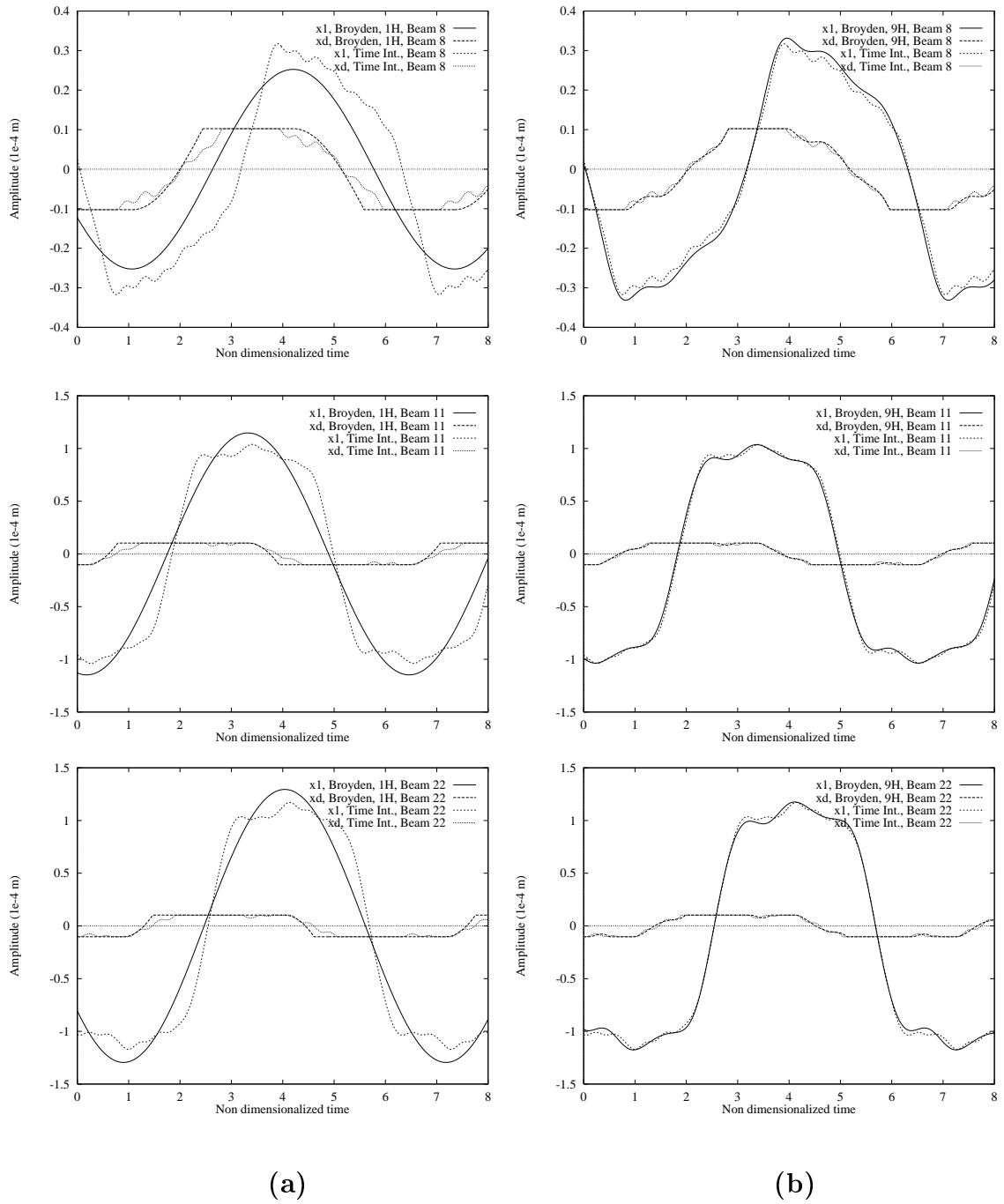


Figure 4.19: Displacement at the damper location, x_1 , and damper displacement, x_d , for the 7% mistuned 36-beam assembly. Beams numbered 8, 11 and 22 are shown, coupled by a stiffness, $k_c = 7.10^3 N/m$, for engine order three excitation and a force amplitude of $20.313 N$ at $200 rad/s$, as predicted by (a) the 1-harmonic Broyden method and (b) 9-harmonic Broyden method, and numerical time integration.

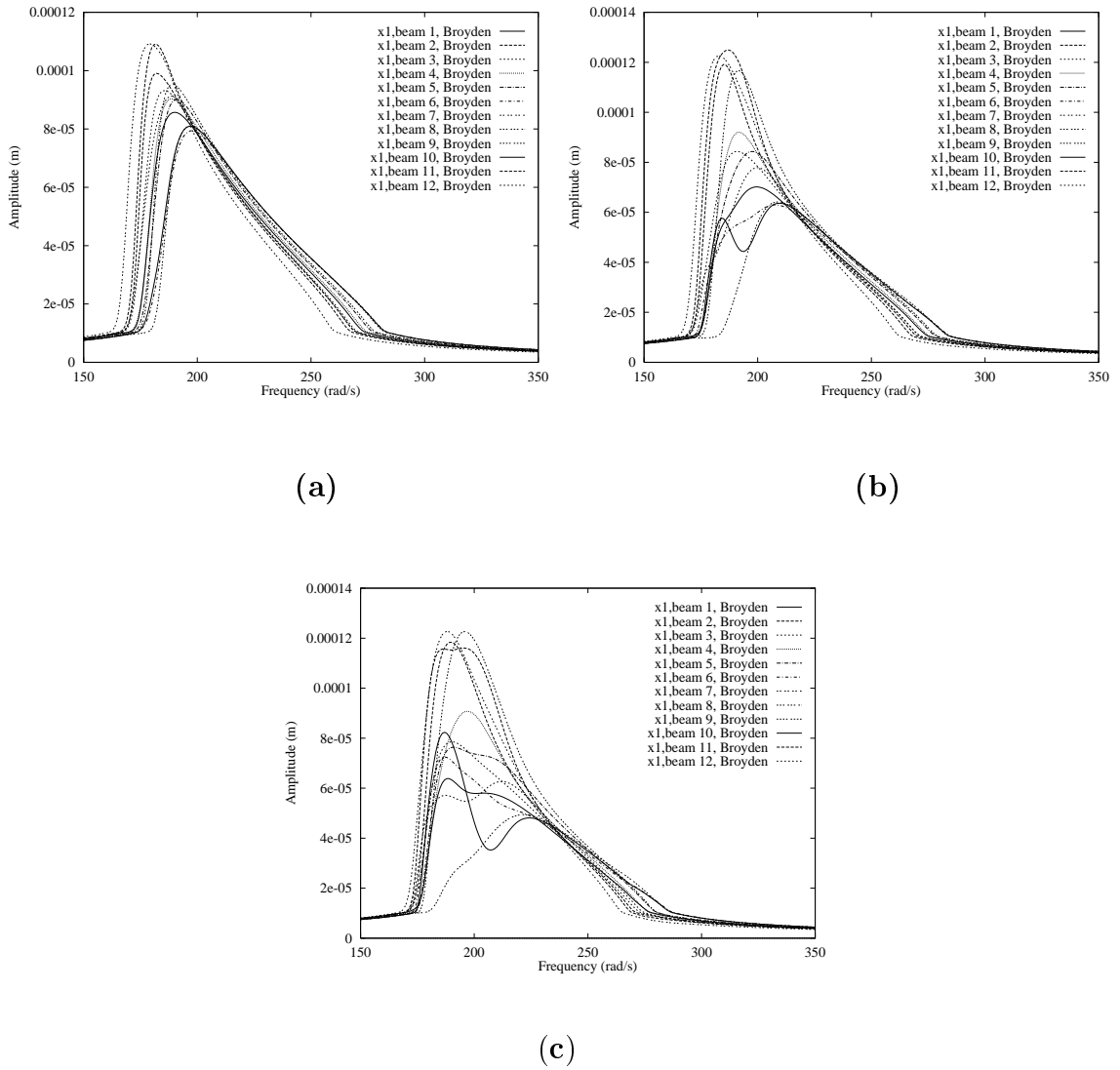
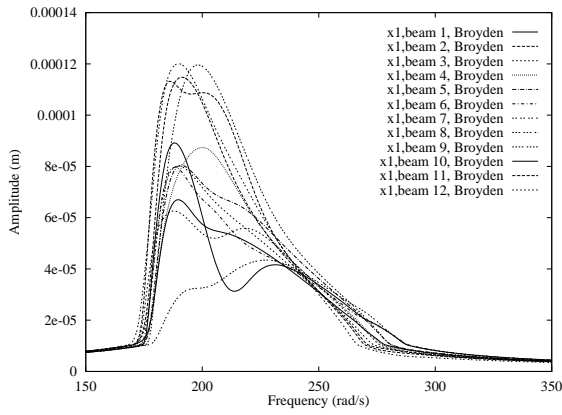
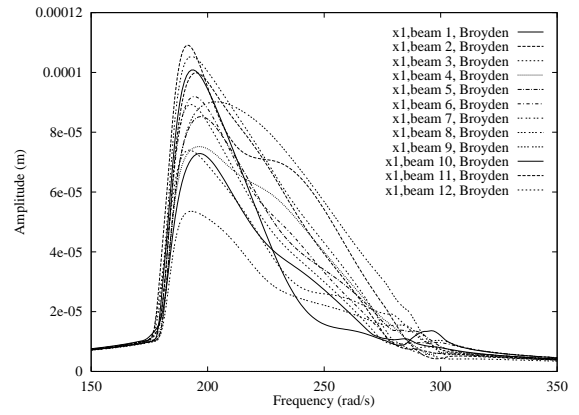


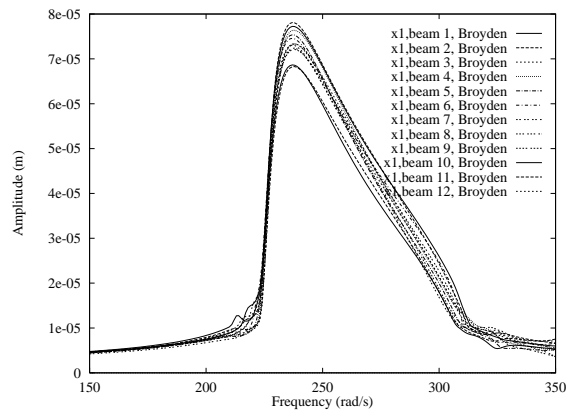
Figure 4.20: Frequency response of beams 1 through 12, at the damper locations, x_1 , for the 7% mistuned 36-beam assembly, coupled by a stiffness, **(a)** $k_c = 10^3 N/m$, **(b)** $3.10^3 N/m$, and **(c)** $5.10^3 N/m$, for engine order three excitation and a force amplitude of $20.313N$, as predicted by the 3-harmonic Broyden method.



(d)



(e)



(f)

Figure 4.21: Frequency response of beams 1 through 12, at the damper locations, x_1 , for the 7% mistuned 36-beam assembly, coupled by a stiffness, (d) $6.10^3 N/m$, (e) $1.2.10^4 N/m$, and (f) $10^5 N/m$, for engine order three excitation and a force amplitude of $20.313N$, as predicted by the 3-harmonic Broyden method.

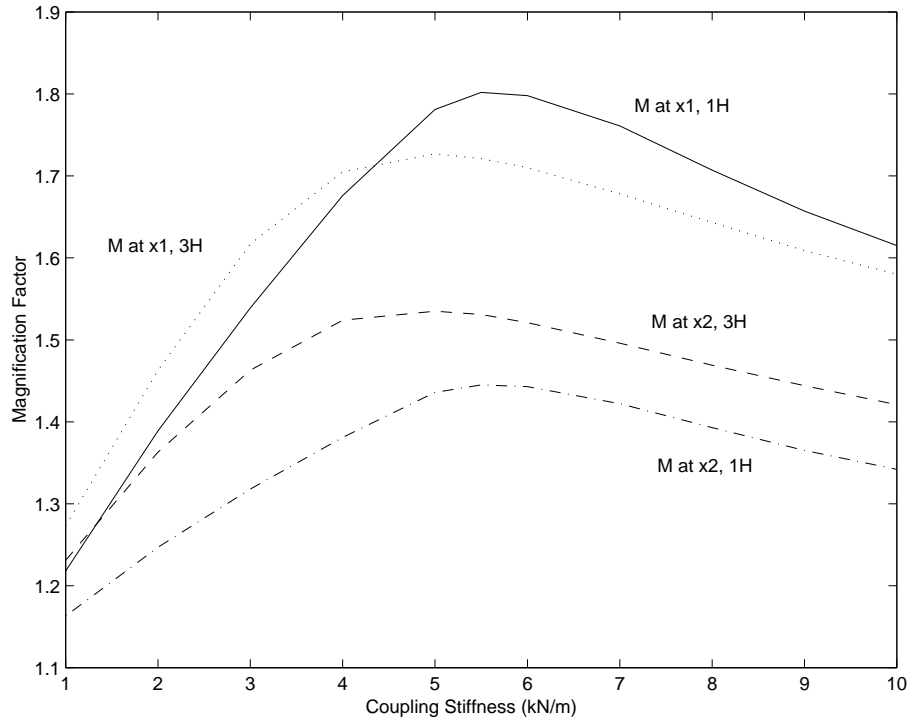


Figure 4.22: Magnification factor, \mathcal{M} , at the damper locations, x_1 , and the tips of the beams, x_2 , for the 7%-mistuned, 36-beam assembly, as a function of the coupling stiffness, k_c , for engine order 3 excitation and a force amplitude of $20.313N$, as predicted by the Broyden method for 1 and 3 harmonics.

efficient and reliable and revealed complex features of the non-linear response, including localization and optimal damping. The method can effortlessly predict the forced response of large-scale models of dry-friction damped bladed disks, and the associated computer code may efficiently be used for the design of such friction-damped systems. The computational time savings provided by the multi-harmonic, hybrid frequency/time method with respect to the numerical time integration make the method attractive to study the influence of structural and friction parameters.

CHAPTER V

FREE RESPONSE AND STABILITY

5.1 Introduction

Chapters II to IV have dealt with the forced response of friction damped structural systems. In some instances, for example for the fan stage of jet engines, free response and stability may become relevant issues of importance. Friction damping is an effective way to reduce vibrations and dissipate the energy brought into the system by, for example, aerodynamic forces, and thus to reduce the occurrence of flutter and enhance stability.

This chapter is organized as follows. First, the free response and stability of a single-DOF friction damped system with negative viscous damping is considered. Then, the method is extended to a multi-DOF system connected to a single friction damper. Finally, some considerations are made on the stability of a multi-DOF friction damped system.

5.2 Free response of single-DOF systems

A single-DOF system, consisting of a spring-mass-dashpot connected to an elastic friction damper is considered, as shown in Fig. 2.1. Negative viscous damping is considered, which may be a model for motion-dependent aerodynamic forces. The

system is autonomous, thus there is no external forcing: the only source of energy is the negative viscous damping, which can induce a flutter instability. Friction damping is the only phenomenon responsible for dissipation of energy. Since the friction damper can dissipate energy only when it is slipping, it is expected that all periodic motions predicted by a harmonic balance analysis will exhibit at least some slipping during each period of the motion, so as to balance the energy brought into the system by the negative viscous damping.

5.2.1 Single-harmonic approximation

The single-DOF system depicted in Fig. 2.1 and considered here has the following equation of motion:

$$m\ddot{x} + c\dot{x} + kx + f_{nl}(x, \dot{x}) = 0 \quad (5.1)$$

where m, c , and k are, respectively, the mass, the (negative) viscous damping coefficient, and the stiffness of the single-DOF system, x represents the amplitude of the mass displacement, $f_{nl}(x, \dot{x})$ is the force transmitted by the friction damper of stiffness k_d and maximum force F_d . The force transmitted by the damper is equal to $f_{nl} = k_d z$, where z denotes the position of the friction damper. The negative viscous damping coefficient is taken as follows:

$$c = -r(\alpha k + \beta m) \quad (5.2)$$

where α and β are constant coefficients, and r is a numerical parameter greater than zero, referred to below as the viscous damping ratio. The single-harmonic procedure is very similar to the one presented in the case of the forced response in Section 2.2.3. It is assumed that x and z can be written as:

$$x = A \cos \omega t \quad (5.3)$$

$$z = a \cos \omega t + b \sin \omega t \quad (5.4)$$

Unlike Eqs. (2.3) and (2.4), Eqs. (5.3) and (5.4) do not need to include a phase difference, since the system is autonomous and the phase of x can be defined arbitrarily. The expressions of a and b are unchanged with respect to the forced response case:

$$\theta_c = \arccos \left(1 - \frac{2F_d}{Ak_d} \right) \quad (5.5)$$

$$a = \frac{A}{\pi} \left(\theta_c + \frac{1}{2} \sin 2\theta_c \right) \quad (5.6)$$

$$b = \left(\frac{F_d}{k_d A} - 1 \right) \frac{4F_d}{k_d \pi} \quad (5.7)$$

Substituting Eqs. (5.3-5.7) into the equation of motion, Eq.(5.1), and balancing the cosine term, leads to the following nonlinear equation for the unknown displacement amplitude, A :

$$-A \left(\frac{k_d b}{cA} \right)^2 m + kA + k_d a = 0 \quad (5.8)$$

where the cosine harmonic component, a , of the damper displacement, z , is a function of the amplitude, A . Balancing the sine term leads to the following equation for the frequency, ω :

$$\omega = \frac{k_d b}{cA} \quad (5.9)$$

Equation (5.8) can be solved by any standard secant Newton method, and the frequency can be deduced from the value of the mass displacement amplitude using Eq. (5.9).

The method was tested on a single-DOF system whose characteristics are listed in Table 5.1. The damper characteristics are the same as the ones of the damper presented in Section 2.3.4. The mass and the stiffness are chosen so that the sticking and slipping resonance frequencies of the single-DOF system are identical to the ones of the 3-DOF beam presented in Section 2.3.4.

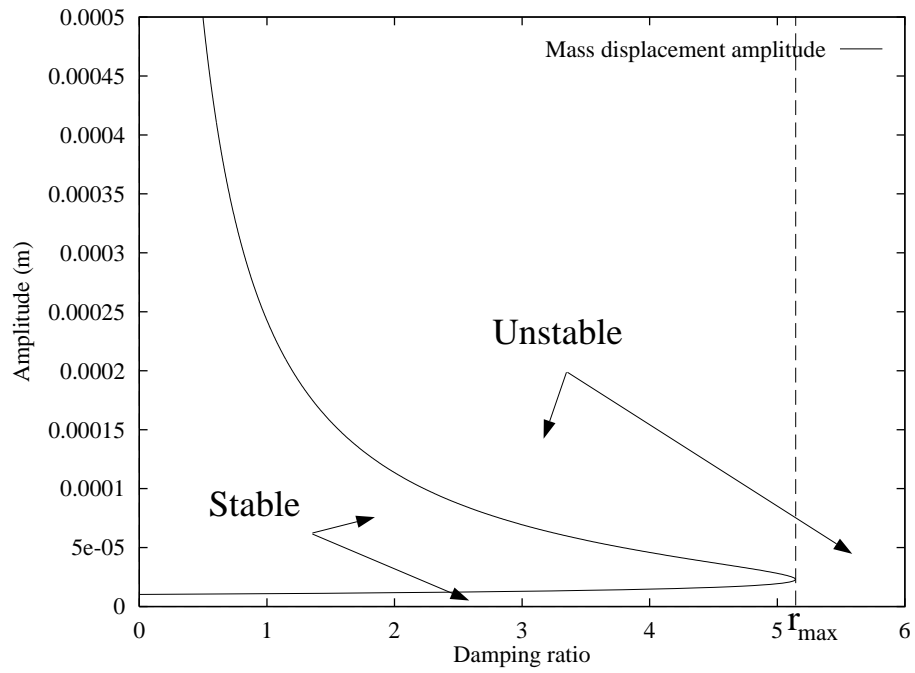


Figure 5.1: Displacement amplitude of the mass (x), as a function of the negative viscous damping ratio, r , as predicted by the single-harmonic balance method. There is no stable motion for $r > r_{max}$.

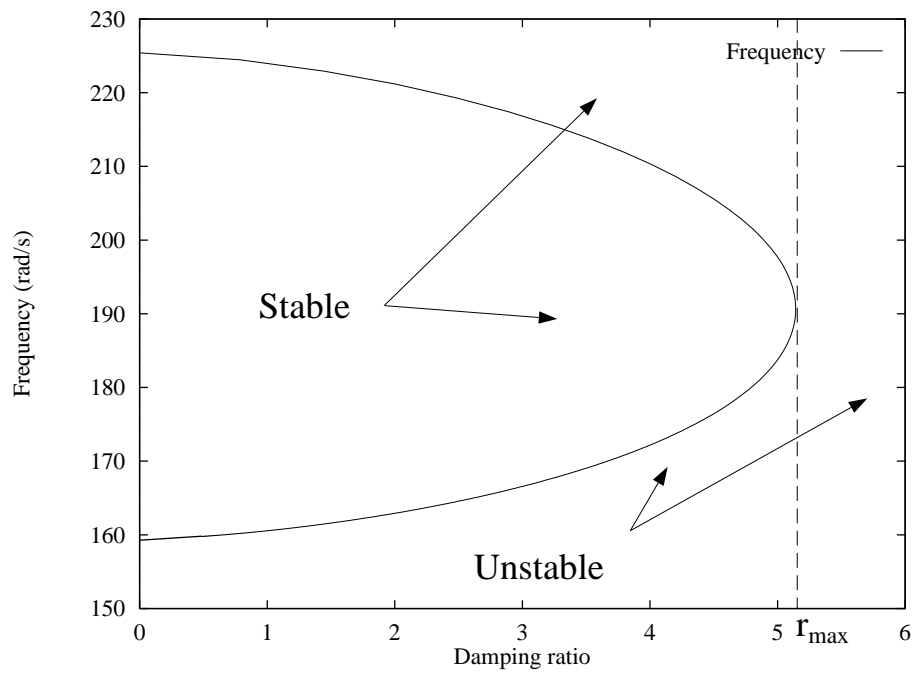


Figure 5.2: Frequency of motion of the mass, as a function of the negative viscous damping ratio, r , as predicted by the single-harmonic balance method. There is no stable motion for $r > r_{max}$.

Parameter (unit)	Value
$m(kg)$	944.6
$k(N/m)$	$2.4 \cdot 10^7$
$k_d(N/m)$	$2.4 \cdot 10^7$
$F_d(N)$	246.048
$\alpha(s)$	$2.6 \cdot 10^{-5}$
$\beta(s^{-1})$	7.49

Table 5.1: Values of the parameters for the single-DOF case.

Figure 5.1 depicts the amplitude of the mass displacement as predicted by the single-harmonic balance method, as a function of the negative viscous damping ratio, r . The results are similar to the ones presented in numerous previous studies [Sinha and Griffin, 1983, Sinha and Griffin, 1985]. For values of the negative viscous damping ratio large enough, $r > r_{max}$, the friction damper is not able to dissipate all the energy brought into the system by negative viscous damping. Therefore, there is a net increase of energy, and no stable motion. For lower values of the damping ratio, there are two amplitudes of harmonic motion predicted by the method. The lower one corresponds to a mostly sticking motion, and the higher one corresponds to a mostly slipping motion. The hybrid frequency/time method is able to find periodic solutions, but it cannot predict their stability. In the case of a single-DOF system, the curves presented in Fig. 5.1 have been studied extensively. The higher amplitude curve depicts unstable equilibrium positions: the system is unstable when the initial displacement is larger than the amplitude of the high branch, and the initial velocity is zero. When the initial displacement is lower than the converged amplitude of the high branch, and the initial velocity is zero, the system is stable, and converges

toward the lower branch.

Figure 5.2 presents the frequency of the mass displacement as predicted by the single-harmonic balance method, as a function of the negative viscous damping ratio r . As seen in the amplitude curve in Fig. 5.1, there can be no stable motion for negative viscous damping ratios larger than a maximum value, $r > r_{max}$, and, when a solution exists, there are two possible frequencies at which the system can oscillate. The higher one is stable and corresponds to the mostly sticking motion, and the lower one is unstable and corresponds to the mostly slipping motion. System oscillations can only take place at a frequency between the slipping natural frequency and the sticking natural frequency, as explained below.

Since friction damping is the only way to dissipate energy in the system, periods of slip alternated with periods of stiction are always present in the steady-state free response. Therefore, the system is less stiff than it would be if it was connected to a stiffness equal to the damper stiffness. However, since the damper is sticking between periods of slip, the system is stiffer than it would be if it was not connected to the damper at all. Consequently, the frequency of the motion has to be lower than the frequency when the friction damper is fully stuck, ω_{max} (sticking natural frequency) and it has to higher to the slipping natural frequency, ω_{min} , where

$$\omega_{min} = \sqrt{\frac{k}{m}} = 159.40 \text{ rad/s} \quad (5.10)$$

$$\omega_{max} = \sqrt{\frac{k+k_d}{m}} = 225.42 \text{ rad/s} \quad (5.11)$$

The values of the limiting resonance frequencies computed in Eqs. (5.10) and (5.11) match the values found by the method as the negative viscous damping tends to zero, as shown in Fig. 5.2. It can also be verified from Fig. 5.2 that the frequency of the motion is indeed bounded by the two limiting values, ω_{min} and ω_{max} .

5.2.2 Multi-harmonic method

In this section, the single-DOF model is now analyzed using a multi-harmonic balance approach. The equation of motion, Eq. (5.1), remains unchanged. However, the harmonic expansion of the mass amplitude, x , and that of the non-linear force, f_{nl} , become:

$$x = A_1 \cos \omega t + \sum_{i=2}^{N_h} (A_i \cos(i\omega t) + B_i \sin(i\omega t)) \quad (5.12)$$

$$f_{nl} = \sum_{i=1}^{N_h} (f_{nl,ci} \cos(i\omega t) + f_{nl,si} \sin(i\omega t)) \quad (5.13)$$

where N_h is the number of temporal harmonics taken into account in the solution. Since an autonomous system is considered, the phase of the mass displacement is arbitrary. Consequently, the coefficient of the fundamental sine term of the expansion of the mass displacement is taken to be zero: $B_1 = 0$. The expressions (5.12) and (5.13) are substituted in the equation of motion, Eq. (5.1). By balancing all sine and cosine terms, the following set of nonlinear equations is obtained:

$$\left\{ \begin{array}{l} (\cos \omega t \text{ term}) \quad -mA_1\omega^2 + kA_1 + f_{nl,c1} = 0 \\ (\sin \omega t \text{ term}) \quad -A_1c\omega + f_{nl,s1} = 0 \\ (\cos i\omega t \text{ term}) \quad -mi^2\omega^2 A_i + ci\omega B_i + kA_i + f_{nl,ci} = 0 \quad i = 2, \dots, N_h \\ (\sin i\omega t \text{ term}) \quad -mi^2\omega^2 B_i - ci\omega A_i + kB_i + f_{nl,si} = 0 \quad i = 2, \dots, N_h \end{array} \right. \quad (5.14)$$

This set of nonlinear equations is solved using a hybrid frequency/time procedure, and the Broyden method, as presented in Chapter III. As in Section 3.2, the coefficients $f_{nl,ci}$ and $f_{nl,si}$ are deduced at each iteration from the values of the mass displacement, x , and the mass velocity, \dot{x} , over one period of the motion. Therefore, there are $2N_h$ equations for $2N_h$ unknowns, which are the $(2N_h - 1)$ harmonic coefficients of the expansion of the mass displacement, x , and the frequency ω .

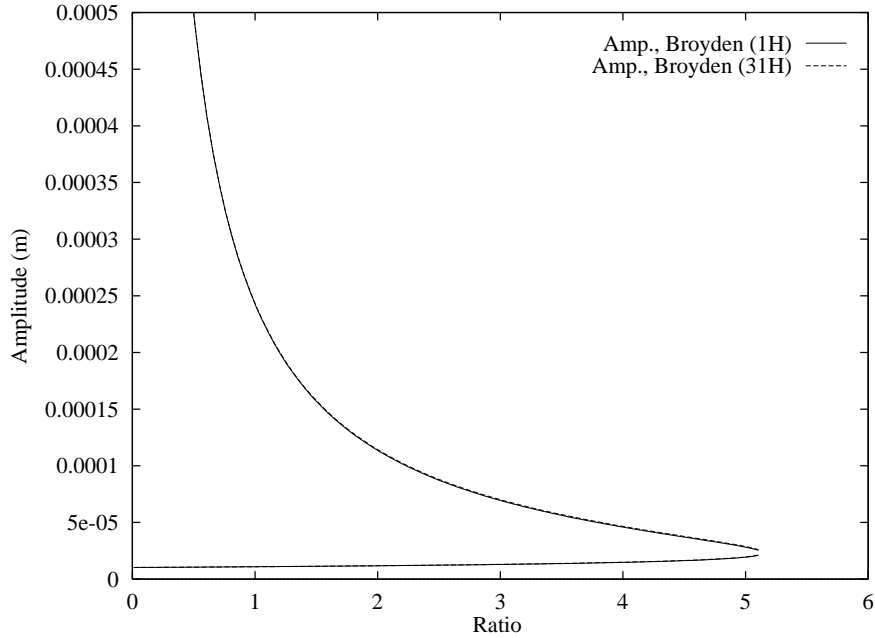


Figure 5.3: Mass displacement amplitude, as predicted by the Broyden method, with 1 and 31 harmonics used, as a function of the negative viscous damping ratio.

Figure 5.3 shows the mass displacement amplitude as a function of the negative viscous damping ratio, as predicted by the hybrid frequency/time Broyden method, using both one and 31 harmonics. Note that the number of harmonics has nearly no effect on the response. The free response of a single-DOF system attached to a flexible friction damper is mostly mono-harmonic, as can be checked by looking at the amplitudes of the different harmonic components retained in the solution.

Figures 5.4-5.7 show the amplitude and the frequency of the single-DOF system, as a function of the negative viscous damping ratio, as predicted by the 5-harmonic hybrid frequency/time Broyden method and by numerical time integration. The agreement between the two methods is very good. Only the stable, mostly sticking motion could be obtained by forward numerical integration.

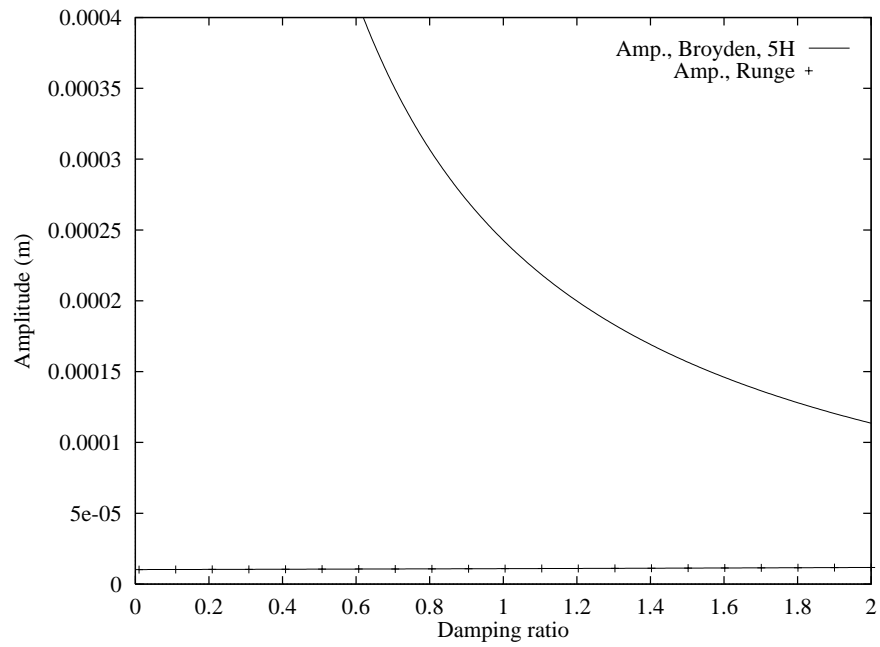


Figure 5.4: Amplitude of the displacement of a single-DOF friction damped system, as a function of the negative viscous damping ratio, as predicted by the 5-harmonic hybrid frequency/time method, and time integration.

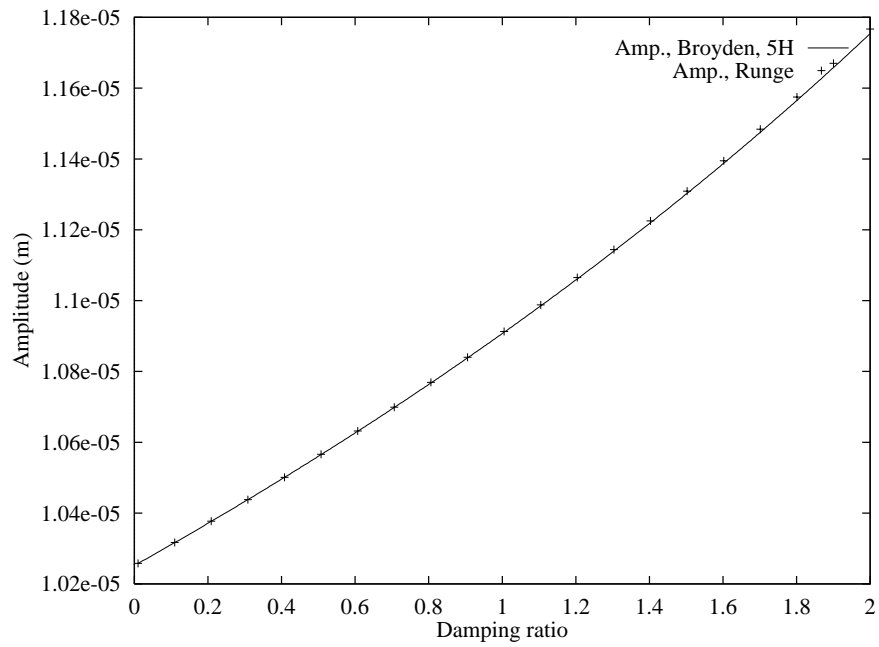


Figure 5.5: Amplitude of the displacement of a single-DOF friction damped system, as a function of the negative viscous damping ratio, as predicted by the 5-harmonic hybrid frequency/time method, and time integration (sticking branch only).

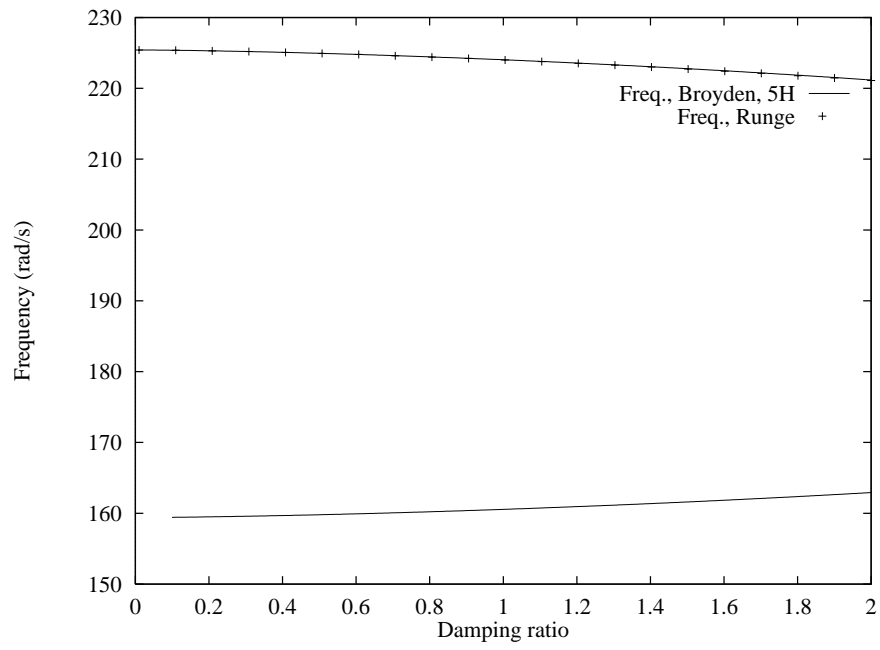


Figure 5.6: Frequency of the displacement of a single-DOF friction damped system, as a function of the negative viscous damping ratio, as predicted by the 5-harmonic hybrid frequency/time method, and time integration.

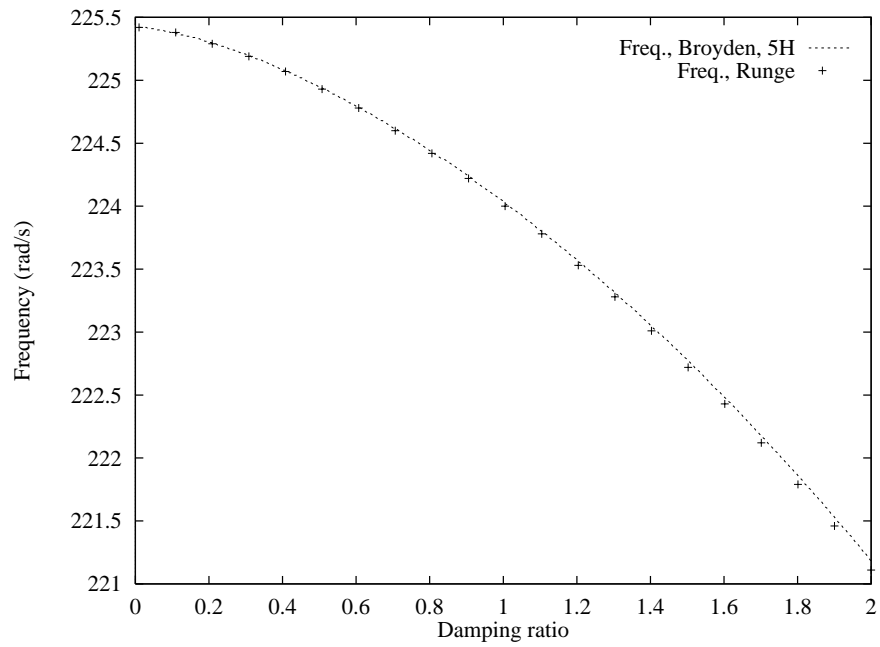


Figure 5.7: Frequency of the displacement of a single-DOF friction damped system, as a function of the negative viscous damping ratio, as predicted by the 5-harmonic hybrid frequency/time method, and time integration (sticking branch only).

5.2.3 Influence of the friction damper stiffness, k_d

The damper stiffness is a parameter critical to the dynamics of friction damped systems. In this section, the influence of the damper stiffness on the free response of the single-DOF system presented in Section 5.2 is considered. Two limiting cases are studied: very large and very small values of the friction damper stiffness.

For small values of the damper stiffness, k_d , large values of the amplitude of motion are required for the damper to slip. Therefore, with all other parameters fixed, the lower the damper stiffness, the less slipping during each cycle of motion. For values of the damper stiffness low enough, no slipping is possible. Since there must be some slipping in order to dissipate the energy brought into the system by negative viscous damping, no periodic motion is possible if the damper stiffness is too small. As stated in Section 5.2.1, the frequency of motion, ω , is bounded as:

$$\omega_{min} \leq \omega \leq \omega_{max} \quad (5.15)$$

Given the expressions of the minimum and maximum frequencies, Eqs. (5.10) and (5.11), the range of possible oscillation frequency decreases as the damper stiffness decreases. Therefore, the mostly sticking and the mostly slipping solutions defined in Section 5.2.1 tend toward a unique solution as the damper stiffness decreases to zero.

For values of the friction damper stiffness large enough, the damper can be considered as rigid. Using the same notations and the same procedure as in Section 5.2.1, the one-harmonic approximation leads to the following values of the cosine and sine coefficients, a and b , of the force transmitted by the friction damper:

$$\begin{aligned} a &= \frac{2}{\pi} \int_0^\pi z(\theta) \cos(\theta) d\theta \\ &= \frac{2}{\pi} \int_0^\pi \frac{F_d}{k_d} \cos(\theta) d\theta = \frac{2F_d}{k_d\pi} \sin \theta \Big|_0^\pi = 0 \end{aligned} \quad (5.16)$$

$$\begin{aligned}
b &= \frac{2}{\pi} \int_0^\pi z(\theta) \sin \theta d\theta \\
&= \frac{2F_d}{\pi k_d} \cos(\theta) \Big|_0^\pi = -\frac{4F_d}{\pi k_d}
\end{aligned} \tag{5.17}$$

Substituting Eqs. (5.16) and (5.17) in Eq. (3.1) leads to the following set of equations for the amplitude, A , and the frequency, ω :

$$\begin{cases} (-m\omega^2 + k)A = 0 & (\text{cosine}) \\ -c\omega A - \frac{4F_d}{\pi} = 0 & (\text{sine}) \end{cases} \tag{5.18}$$

There are two solutions to this system. The first solution is the trivial one: $A = 0$. The second solution corresponds to the following values for the frequency and amplitude of the motion:

$$\omega = \sqrt{k/m} = \omega_{min} \tag{5.19}$$

$$A = \frac{4F_d}{\pi c \omega_{min}} \tag{5.20}$$

Figures 5.8 and 5.9 present, respectively, the amplitude and the frequency of the single-DOF system, as predicted the Broyden method using 3 and 21 harmonics, as a function of the ratio, v , of friction damper stiffness. The ratio, v , is defined such that $k_d = v k_{d0}$, where k_{d0} is the nominal value of the damper stiffness used in Section 5.2.1. As explained above, there is no periodic solution for values of the friction damper stiffness that are small enough, and then the frequency of oscillation tends towards the minimum frequency, ω_{min} . For large values of the friction damper stiffness, the solution predicted by the hybrid frequency/time method tends towards the rigid friction damper solutions: there are two periodic solutions. One solution corresponds to the trivial case: $A = 0$, and the other one has an amplitude and frequency independent of the damper stiffness. According to Eqs. (5.19) and (5.20), the one-harmonic approximation in the rigid friction damper case predicts $\omega_{min} =$

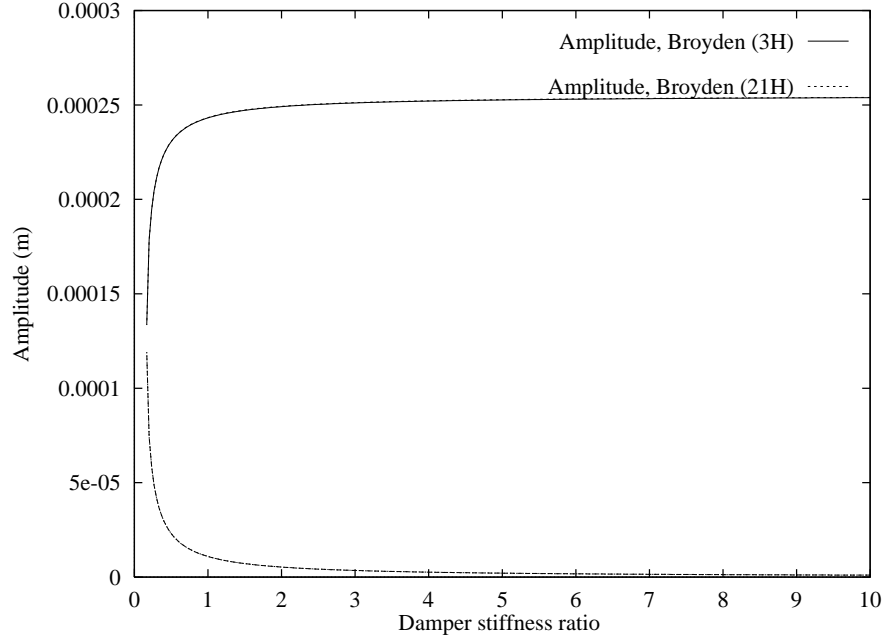


Figure 5.8: Amplitude of the displacement of a single-DOF friction damped system, as a function of the ratio of friction damper stiffness, v , as predicted by the multi-harmonic free-response method.

159.5 rad/s , and $A = 2.65 \cdot 10^{-4} \text{ m}$, and these are the values also found by the multi-harmonic, Broyden method, as shown in Figs. 5.8 and 5.9.

5.3 Free response of multi-DOF system

5.3.1 Equations of motion and multi-harmonic solution method

The method presented in Section 5.2 was further extended to a multi-DOF system, attached to a single friction damper. The equation of motion is:

$$\underline{\mathbf{M}}\ddot{\mathbf{x}} + \underline{\mathbf{C}}\dot{\mathbf{x}} + \underline{\mathbf{K}}\mathbf{x} + \mathbf{f}_{\text{nl}}(\mathbf{x}, \dot{\mathbf{x}}) = \mathbf{0} \quad (5.21)$$

where $\underline{\mathbf{M}}$ and $\underline{\mathbf{K}}$ are the mass and stiffness matrices of the system, and the negative viscous damping matrix $\underline{\mathbf{C}}$ is defined as

$$\underline{\mathbf{C}} = -r(\alpha\underline{\mathbf{K}} + \beta\underline{\mathbf{M}}) \quad (5.22)$$

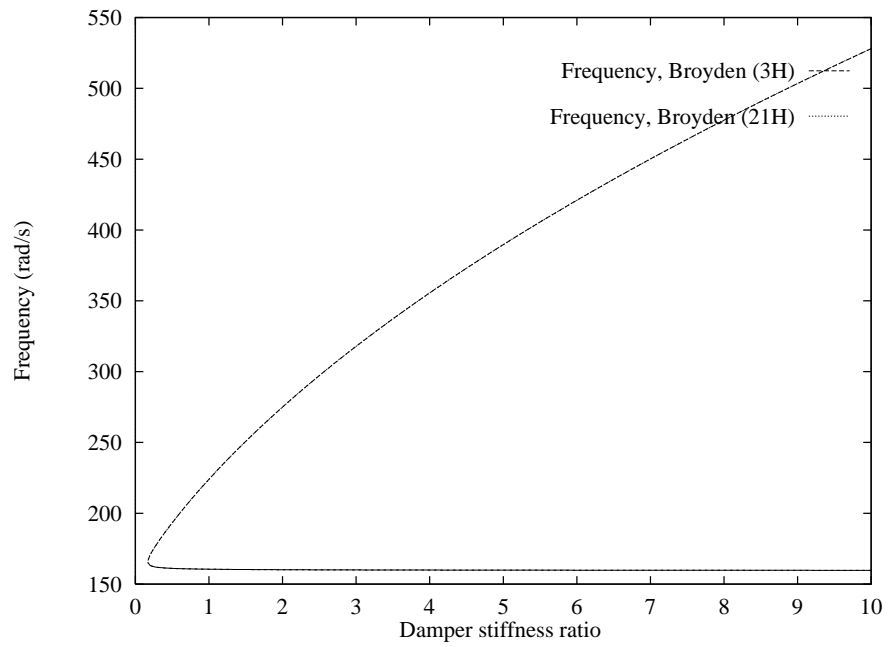


Figure 5.9: Fundamental frequency of the displacement of a single-DOF friction damped system, as a function of the ratio of friction damper stiffness, v , as predicted by the hybrid frequency/time method.

where α and β are constants, defined in Section 2.2.5, r is the viscous damping ratio (positive), and $\mathbf{f}_{nl}(\mathbf{x}, \dot{\mathbf{x}})$ is the vector of the forces exerted by the friction damper. Proportional damping, as defined in Eq. (5.22), makes all three modes of vibration of the beam negatively damped. In this study, only one friction damper is considered, and therefore, all but one of the coordinates of \mathbf{f}_{nl} are equal to zero.

In the forced response case, it is possible to reduce the number of equations in the frequency domain, as presented in Section 3.3. The harmonic components of the linear DOF's, i.e., the DOF's not attached to any friction damper, can be computed from the harmonic components of the nonlinear DOF's, i.e., the DOF's attached to a friction damper. To reduce the number of equations, the mass and stiffness matrices of the system are needed, as well as the frequency of the response [Berthillier et al., 1998b]. Since the frequency of the response is not known a priori when the free response is studied, all equations, the ones corresponding to the nonlinear DOF's as well as the ones corresponding to the linear DOF's, must be solved simultaneously. Thus, the system size cannot be reduced.

Assume that the system has N DOF's, and that N_h harmonics are retained in the solution. The harmonic time expansion of the i -th DOF displacement is defined as:

$$x_i(t) = \sum_{j=1}^{N_h} (A_{i,j} \cos(j\omega t) + B_{i,j} \sin(j\omega t)) \quad i = 1, \dots, N \quad (5.23)$$

As described in Section 5.2, the phase of the free response of the system is arbitrary. Therefore, it can be assumed that $B_{i_0,1} = 0$, where i_0 is the DOF of the structure attached to the friction damper. The friction force is expanded in the same way as the displacement x_i , and is expressed as:

$$f_{nl,i}(t) = \sum_{j=1}^{N_h} (F_{i,j} \cos(j\omega t) + G_{i,j} \sin(j\omega t)) \quad i = 1, \dots, N \quad (5.24)$$

Since only one friction damper is considered in this study, all coefficients $F_{i,j}$ and $G_{i,j}$ are equal to zero, except the ones when $i = i_0$, where i_0 is the DOF attached to the friction damper. Substituting Eqs. (5.23) and (5.24) into (5.21) leads to the following equations, governing the i -th DOF of the system and its l -th harmonic,

$$\begin{aligned}
& -\sum_{j=1}^N M_{i,j} l^2 \omega^2 A_{j,l} + \sum_{j=1}^N K_{i,j} A_{j,l} + \sum_{j=1}^N C_{i,j} l \omega B_{j,l} \\
& \quad + F_{i,l} = 0 \quad i = 1, \dots, N \quad l = 1, \dots, N_h
\end{aligned} \tag{5.25}$$

$$\begin{aligned}
& -\sum_{j=1}^N M_{i,j} l^2 \omega^2 B_{j,l} + \sum_{j=1}^N K_{i,j} B_{j,l} - \sum_{j=1}^N C_{i,j} l \omega A_{j,l} \\
& \quad + G_{i,l} = 0 \quad i = 1, \dots, N \quad l = 1, \dots, N_h
\end{aligned} \tag{5.26}$$

As in Section 5.2, the coefficients $F_{i,l}$ and $G_{i,l}$ are the harmonic components of $f_{nl,i}$, which is deduced at each iteration from the time histories of the displacement and velocity of the i -th DOF. Writing Eqs. (5.25) and (5.26) for all DOF's and all harmonics leads to a set of $2NN_h$ equations for $2NN_h$ unknown variables, the $N(2N_h) - 1$ harmonic components of the displacements, $x_i(t)$, with $i = 1, \dots, N$ (remember that $B_{i0,1} = 0$), and the frequency, ω . This set of equations is solved using a modified Broyden algorithm, as presented in Chapter III.

5.3.2 Multiplicity of solutions

In the free response case, since the frequency of the response is not dictated by the external forcing, the system has the possibility to respond in all its modes of vibration. Numerical time integration reveals that it is indeed the case. Figures 5.10-5.12 depict the time histories of the three DOF's of the SNECMA beam, as predicted by numerical time integration, and for the three sets of initial conditions listed in Table 5.2. Recall that the model parameters for this system are given in Eq. (2.32). All simulation results are after the initial transient has died out, and once a steady-state solution has developed, if there is one.

Case number	$x_1(0) (m)$	$x_2(0) (m)$	$x_3(0) (m)$
1	10^{-5}	10^{-3}	10^{-5}
2	10^{-5}	10^{-5}	$3.0 \cdot 10^{-4}$
3	10^{-6}	10^{-6}	10^{-5}

Table 5.2: Three sets of initial conditions, used for the numerical time integration of the free response of the 3-DOF SNECMA beam. All initial velocities are taken to be zero.

Figure 5.10 shows the time histories of the displacements of all three DOF's, as predicted by numerical time integration, for the first set of initial conditions. For these conditions, the steady state reached by the system corresponds to the first mode of vibration of the beam, because the frequency of the motion belongs to the range defined by the limiting frequencies of the first mode of vibration, as shown in Table 5.3, and because the displacement amplitudes match the ones of the first mode of vibration, as shown in Figs. 5.13-5.15. Similarly, Fig. 5.11 shows that the system motion converges towards the second mode of vibration with the initial conditions of case 2. Figure 5.12 demonstrates that, with the initial conditions of case 3, the system can reach the steady-state of the third mode of vibration. The time scales are different for each mode of vibration: the shorter periods correspond to the higher modes of vibration.

The steady-state response in all three modes of vibrations was computed using the multi-harmonic, hybrid frequency/time method presented in Section 5.3.1. Figure 5.13 depicts the amplitude of displacement of the first DOF of the SNECMA beam, for the three modes of vibration, as a function of the negative viscous damping ratio,

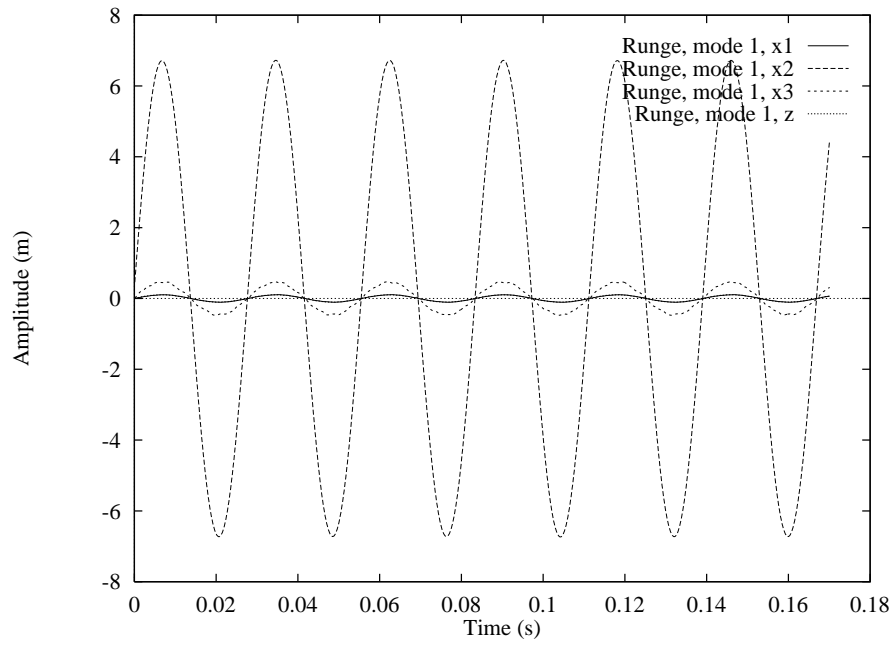


Figure 5.10: Time history of displacement of the three DOF's of the SNECMA beam and of the friction damper, for the first case listed in Table 5.2 (the time origin is shifted). The steady-state reached corresponds to the first mode of vibration of the beam.

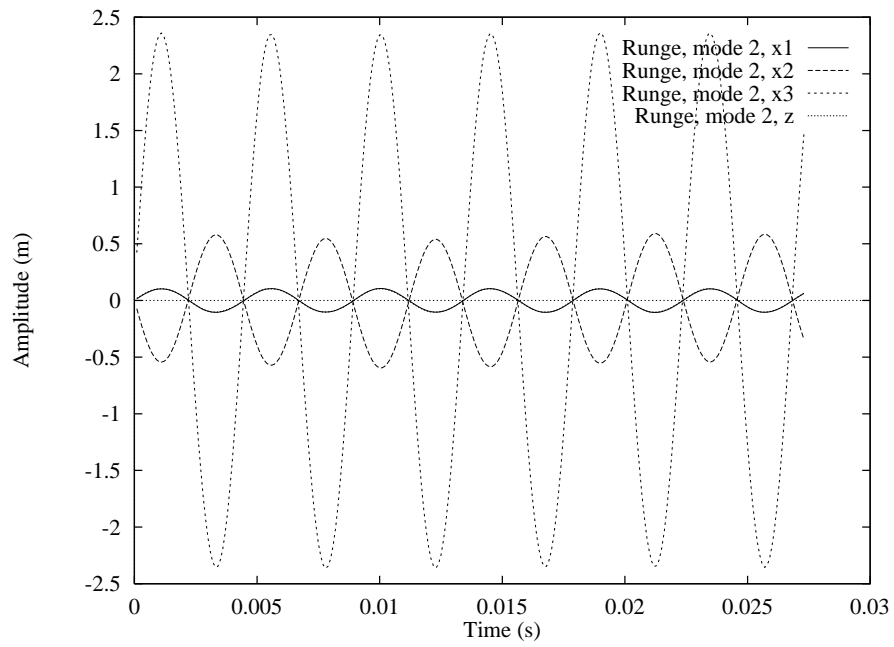


Figure 5.11: Time history of displacement of the three DOF's of the SNECMA beam and of the friction damper, for the second case listed in Table 5.2 (the time origin is shifted). The steady-state reached corresponds to the second mode of vibration of the beam.

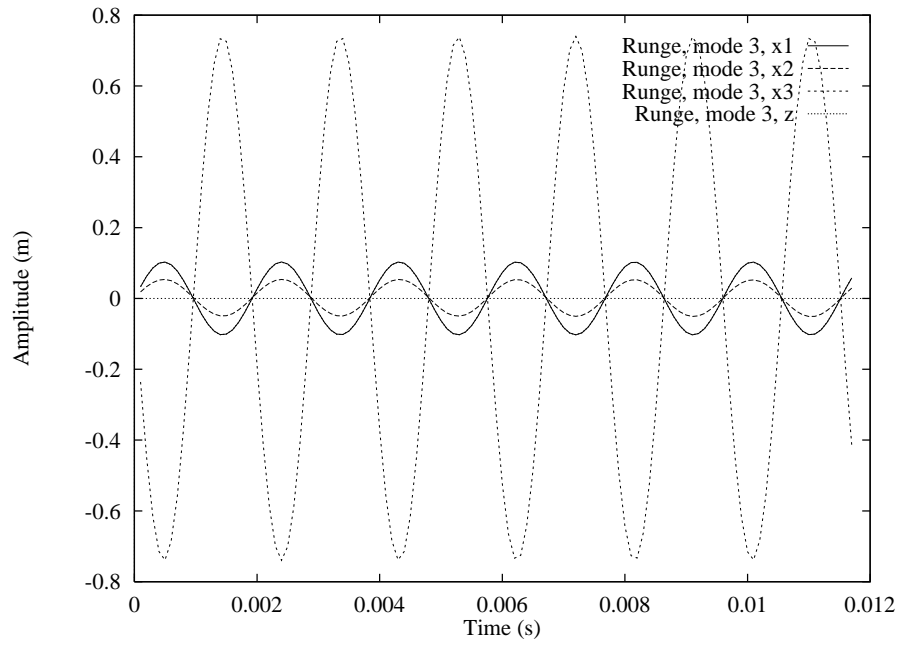


Figure 5.12: Time history of displacement of the three DOF's of the SNECMA beam and of the friction damper, for the third case listed in Table 5.2 (the time origin is shifted). The steady-state reached corresponds to the third mode of vibration of the beam.

as predicted by the hybrid frequency/time method. The results for the three modes of vibration are somehow similar: for each mode, there is a higher branch, which corresponds to a mostly slipping motion, and a lower branch, which corresponds to a mostly sticking motion. For each mode, there is a different maximum negative viscous damping ratio beyond which no periodic solution can be found by the hybrid frequency/time method. In the same way, Figs. 5.14 and 5.15 depict, respectively, the amplitude of displacement of the second and the third DOF of the system, as a function of the negative viscous damping ratio, and as predicted by the hybrid frequency/time method. The general aspects of the curves are similar: there is a higher branch and a lower one for each mode of vibration, as in Fig. 5.1. Figure 5.16 shows the frequencies of the motion in the three modes, as a function of the negative viscous damping ratio, as predicted by the hybrid frequency/time method. The frequencies for the first mode are the lowest ones: the lower part of the curve corresponds to the mostly slipping motion, and the upper part corresponds to the mostly sticking motion. The curve with the intermediate frequencies depicts the second mode of vibration, and the curve with the highest frequency depicts the third one.

As the negative viscous damping tends toward zero, the motion of the system becomes almost linear: it tends either towards the linear, totally stuck case, in which the friction damper is stuck during all the motion, or towards the piecewise linear, totally slipping case, when the force transmitted by the friction damper is negligible compared to other forces acting on the system. The frequencies of motion in these two limiting cases can be computed analytically and are listed in Table 5.3. These computed frequencies match well with the frequencies of the motion of the beam as the negative viscous damping ratio tends towards zero, as shown in Fig. 5.16.

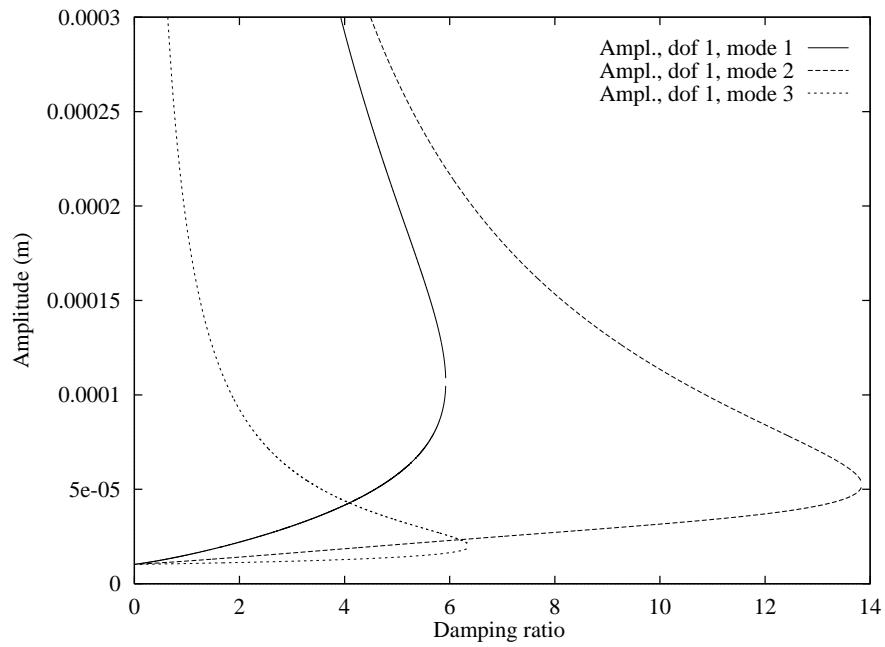


Figure 5.13: Amplitude of displacement of the first DOF of the SNECMA beam, for the three possible modes, as a function of the negative viscous damping ratio, as predicted by the hybrid frequency/time method, with 3 harmonics used.

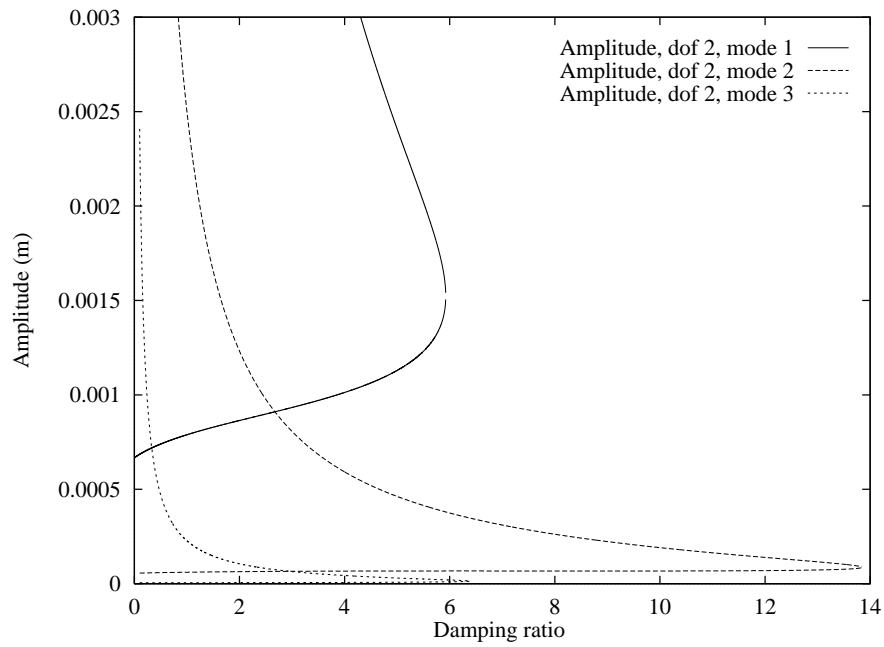


Figure 5.14: Amplitude of displacement of the second DOF of the SNECMA beam, for the three possible modes, as a function of the negative viscous damping ratio, as predicted by the hybrid frequency/time method, with 3 harmonics used.

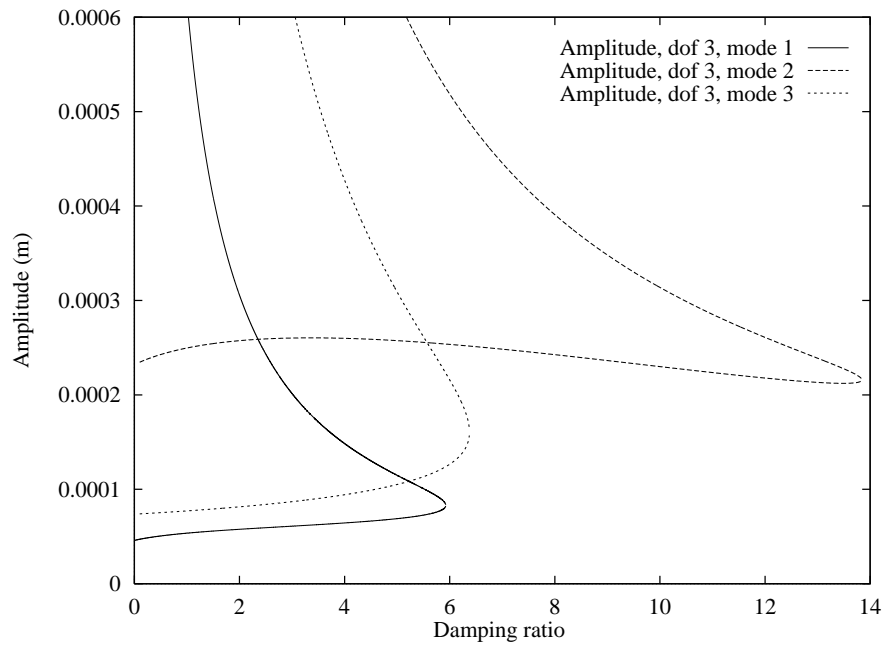


Figure 5.15: Amplitude of displacement of the third DOF of the SNECMA beam, for the three possible modes, as a function of the negative viscous damping ratio, as predicted by the hybrid frequency/time method, with 3 harmonics used.

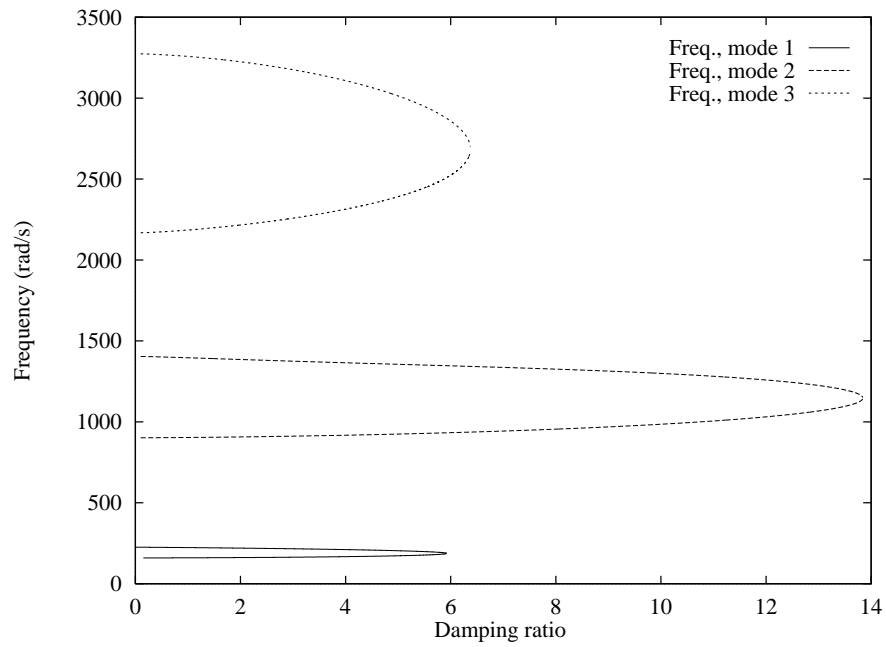


Figure 5.16: Frequency of free motion of the SNECMA beam, for the three possible modes of vibration, as a function of the negative viscous damping ratio, as predicted by the hybrid frequency/time method, with 3 harmonics used.

Mode number	Sticking frequency (rad/s)	Slipping frequency (rad/s)
1	225.42	159.40
2	1404.38	901.76
3	3273.79	2167.54

Table 5.3: Slipping and sticking natural frequencies of the SNECMA beam.

5.4 Stability considerations for multi-DOF systems

5.4.1 Stability of SNECMA beam with all three modes negatively damped

The hybrid frequency/time method presented in Section 5.3.1 predicts the harmonic free response of a system with an attached flexible friction damper, but the method is unable to predict aperiodic solutions, or solutions with multiple mode contents. Moreover, the hybrid frequency/time method is not able to predict the stability of the solutions it finds.

Ferri studied the stability of multi-DOF systems [Ferri, 1985]. He noticed that stability maps for the initial conditions were extremely difficult to generate since the space of initial conditions has dimension $2N$. Another difficulty is that those modes which possess nodes at the location of the dry friction damper are completely uncoupled from the system. With no positive damping contribution from the friction damper, these modes are always unstable. Moreover, when damping is assumed to be proportional, as in Eq. (5.22), the higher modes, though possessing the same negative viscous damping constants, α and β , feature higher damping, due to the higher frequencies. Therefore, the higher modes are relatively less stable than the lower ones. He found that the response of the dry friction element was dominated by the highest coupled mode included in the numerical integration. Ferri also men-

tioned that prescribing equal damping ratios over all beam modes could be a major reason for the highly unstable nature of negatively damped multi-mode systems. Dowell mentioned that, typically, an actual blade undergoing flutter would acquire negative damping in only one mode while all other modes remain positively damped [Dowell, 1995].

In order to study the stability of the solutions predicted by hybrid frequency/time method method, forward numerical time integration is used. The initial conditions for the time integration are the following. All initial velocities are taken to be zero, and, for each DOF, the initial displacement is taken to be two percent lower or higher than the amplitudes predicted by the hybrid frequency/time method, when five harmonics are used. Since the SNECMA beam considered in the study has three DOF's, there are $2^3 = 8$ such sets of initial conditions for every point of every branch of every mode of vibration. The time integration convergence test is based on the amplitude of the displacements: the steady-state is considered to be reached when, for all DOF's, the difference in amplitude of displacement between two consecutive periods of the motion is smaller than a given percentage of the amplitude, e.g. 1%. A given set of initial conditions is considered to yield an unstable solution when any of the DOF's grow without bound. Finally, there are initial conditions for which the system fails to reach a converged solution at the end of the time integration range but is not unstable: either the solution is aperiodic, or the range of computation should be increased. When the time integration procedure fails to converge, or when the system is unstable, the amplitudes and frequency of the response are shown as zero on all the following figures.

Figures 5.17-5.20 present the results of the stability analysis, as described above, of the sticking branch of the third mode of vibration of the SNECMA beam. Figure

5.17 depicts the first-DOF amplitude of the sticking branches for the three modes of vibration, as predicted by hybrid frequency/time method, and the results of numerical time integration for a few values of the negative viscous damping ratio. For each value of the negative viscous damping ratio, there are eight time integration data points, which correspond to the results of the Runge-Kutta procedure for the eight sets of initial conditions around the corresponding, converged point, predicted by the hybrid frequency/time method for the third mode. As mentioned above, the frequency and the amplitude of the system are shown as zero when the time integration fails to converge or when the system is unstable. It can be seen that, for low values of negative viscous damping, the time integration procedure fails to converge or is unstable: see the first two values of the ratio in Fig. 5.17. For larger values of the ratio, the time integration procedure predicts that, after having started around the converged point on mode 3, the system tends most times towards mode 3. There is a range of damping ratio, 2 to 4.5, for which mode 3 seems to be stable. Outside this range, the system fails to converge or is unstable, or converges towards mode 2 for low values of the negative viscous damping.

The system is unstable for larger values of the negative viscous damping ratio. Whenever one of the modes is unstable, the response of the system becomes unbounded, even if the initial conditions were exclusively in another mode. For example, in Fig. 5.17, for values of the negative viscous ratio damping greater than 4.9, mode 1 is unstable, since no harmonic motion could be found by the hybrid frequency/time method. For values of the viscous damping ratio greater than 4.9, the time integration procedure shows that there is no stable motion, even when the initial conditions are given around mode 3, which should be stable at these viscous damping ratios. Figures 5.18 and 5.19 present, respectively, the second and third

DOF amplitude displacement, as predicted by the hybrid frequency/time method, and by the time integration procedure, using initial conditions around the converged points of mode 3. The same conclusions are reached as for the case of the first DOF: (1) for low values of negative viscous damping, the time integration procedure fails to converge, or converges toward mode 2, (2) mode 3 is stable over an intermediate range of negative viscous damping ratio, and (3) when one mode is unstable (here, mode 1), the system is unstable. Figure 5.20 shows the frequency of the three DOF's of the system, as predicted by the hybrid frequency/time method for the three modes of vibration, and as predicted by numerical time integration for initial conditions around the sticking branch of the third mode. The results are identical to the ones deduced from Figs. 5.17 to 5.19.

As mentioned by Ferri [Ferri and Dowell, 1985], the stability maps are difficult to generate, given the large number of cases to consider. It is also found that the higher mode seems to be the preponderant one in the free response of the system. This is in agreement with Ferri's analysis.

Some of the aperiodic solutions found in Figs. 5.17 to 5.20 can be close to a mode of vibration of the system. For example, Figs. 5.21-5.23 display the time histories of the three DOF's of the beam, as predicted by time integration after a large number of periods, and the time histories of the three DOF's, in the first mode of vibration, as predicted by hybrid frequency/time method with 15 harmonics used. The solution predicted by the time integration procedure was shifted in time in order to ensure phase matching with that predicted by the hybrid frequency/time method. The initial conditions used for the time integration are slightly below (2%) the slipping branch of the third mode of vibration, for a negative viscous damping ratio of 0.361. It is seen that, although the given initial conditions are close to the slipping branch

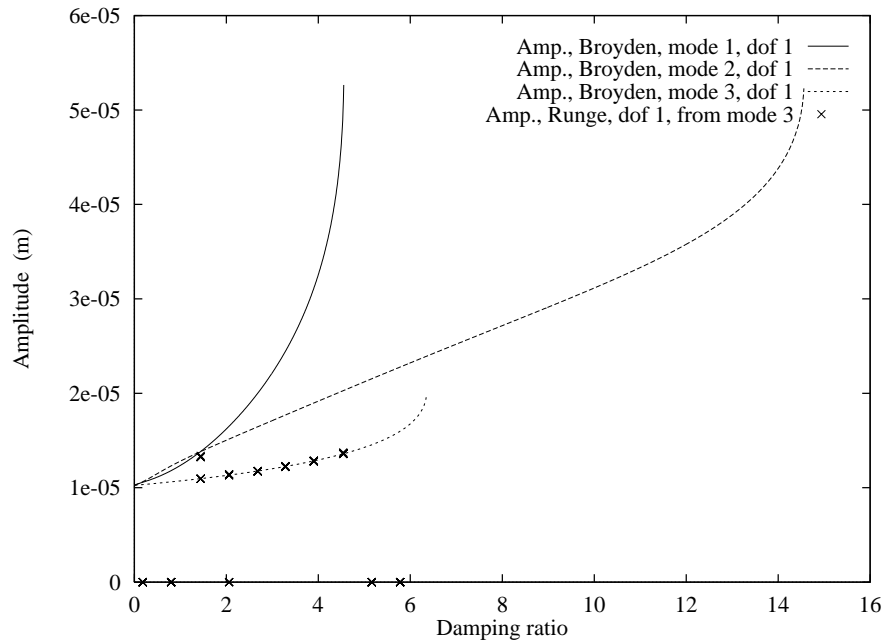


Figure 5.17: Amplitude of the first DOF displacement for the sticking branch of the three modes of vibration of the SNECMA beam, as predicted by the hybrid frequency/time method, with 3 harmonics used, and by forward numerical time integration with initial conditions near mode 3, as a function of the negative viscous damping ratio. When time integration fails to converge or is unstable the amplitude is shown as zero.

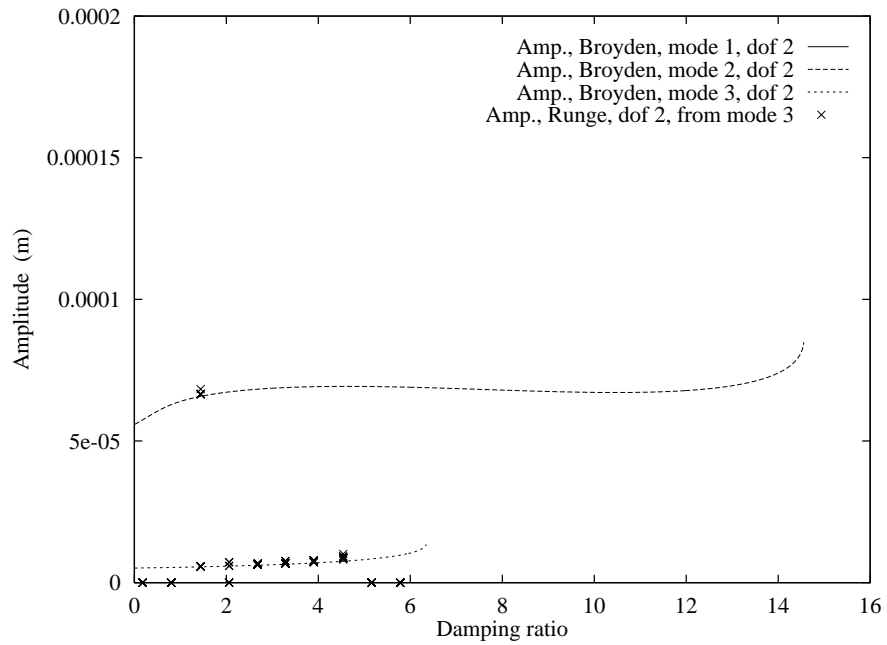


Figure 5.18: Amplitude of the second DOF displacement for the sticking branch of the three modes of vibration of the SNECMA beam, as predicted by the hybrid frequency/time method, with 3 harmonics used, and by forward numerical time integration with initial conditions near mode 3, as a function of the negative viscous damping ratio.

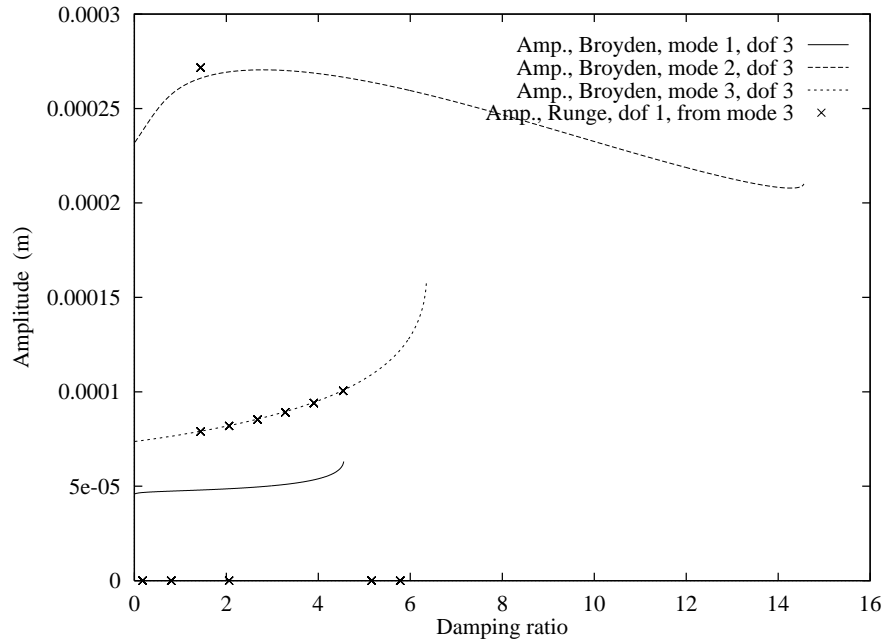


Figure 5.19: Amplitude of the third DOF displacement for the sticking branch of the three modes of vibration of the SNECMA beam, as predicted by the hybrid frequency/time method, with 3 harmonics used, and by forward numerical time integration with initial conditions near mode 3, as a function of the negative viscous damping ratio.

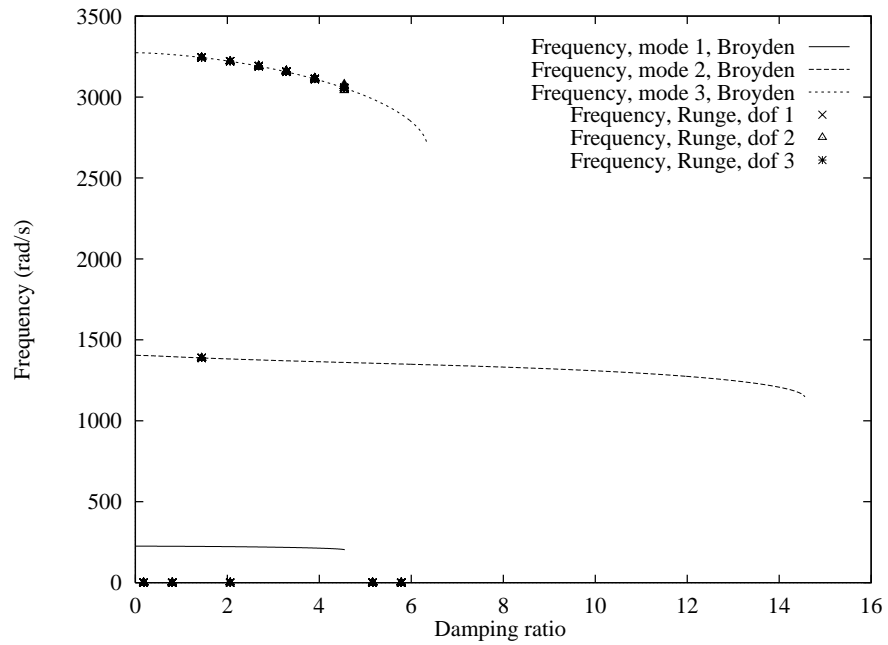


Figure 5.20: Frequency of free motion for the sticking branch of the three modes of vibration of the SNECMA beam, as predicted by the hybrid frequency/time method, with 3 harmonics used, and by forward numerical time integration with initial conditions near mode 3, as a function of the negative viscous damping ratio.

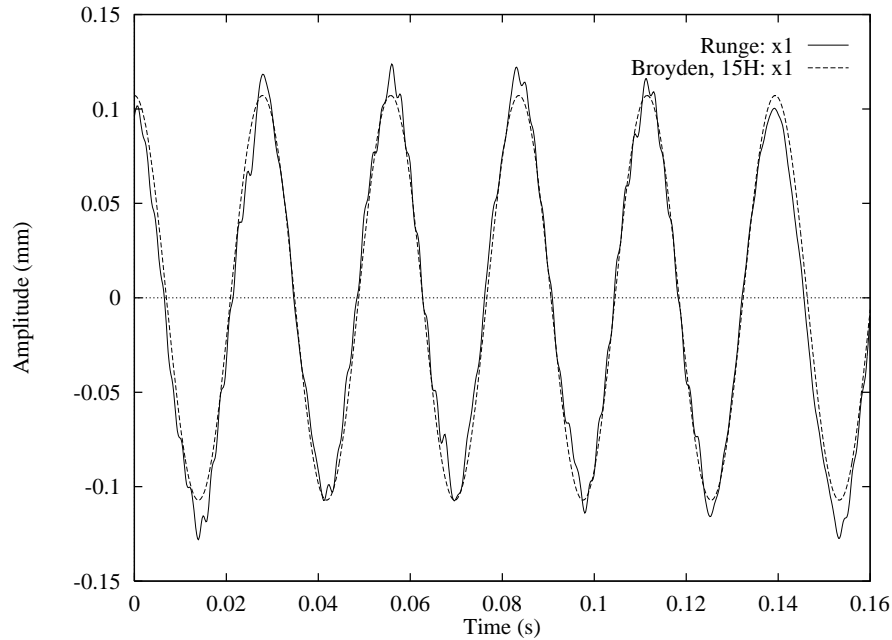


Figure 5.21: Time history of the first DOF of the SNECMA beam, as predicted by hybrid frequency/time method (sticking branch of mode 1), and by time integration (initial conditions 2% below the slipping branch of mode 3). The negative viscous damping ratio is 0.361.

of mode 3, the motion of the system almost converges towards the sticking branch of mode 1. The agreement between time integration and hybrid frequency/time method is almost perfect for the second DOF, and is good for the first and third DOF.

Several possibilities were examined in order to explain the discrepancies between the solution predicted by time integration and by hybrid frequency/time method. The time step used in the Runge-Kutta procedure was reduced by several orders of magnitude, up to several millions steps per cycle, but no improvement was observed. The time integration results were checked after several thousand cycles, but the discrepancies were of the same order of magnitude as after several hundreds of cycles. Figure 5.24 shows the power spectral density of the third DOF displacement time history presented in Fig. 5.23. It is observed that the harmonic content of the signal is

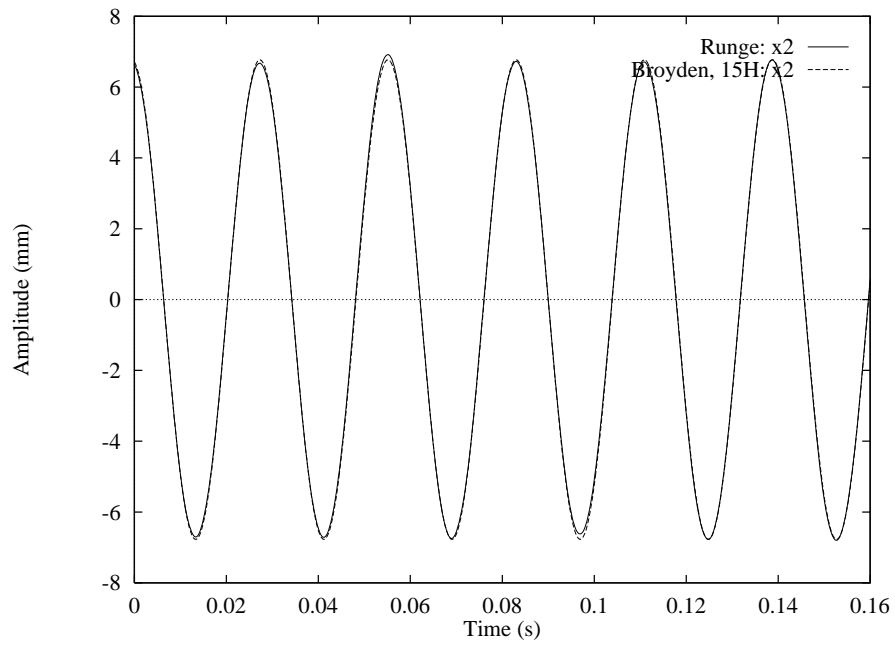


Figure 5.22: Time history of the second DOF of the SNECMA beam, as predicted by hybrid frequency/time method (sticking branch of mode 1), and by time integration (initial conditions 2% below the slipping branch of mode 3). The negative viscous damping ratio is 0.361.

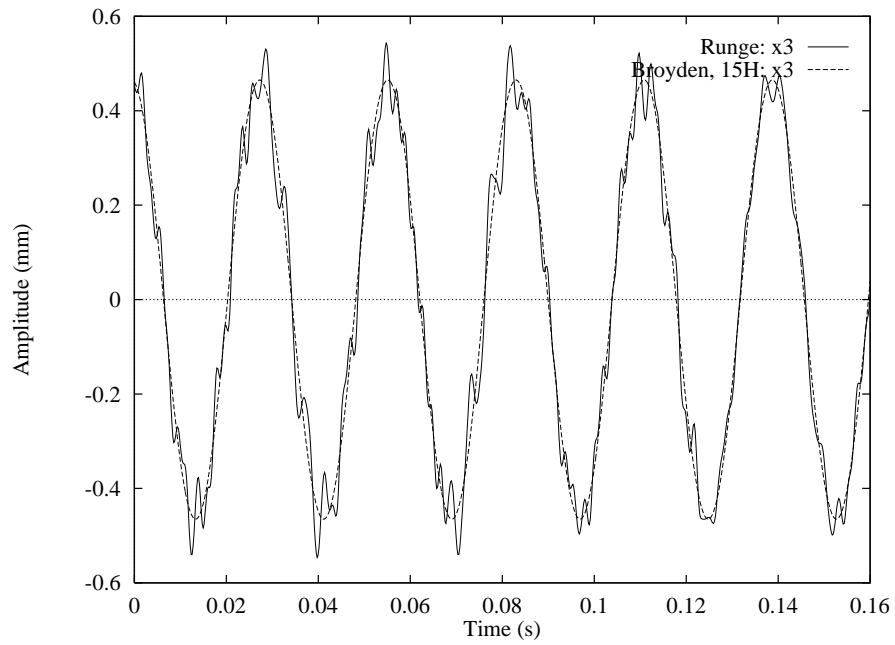


Figure 5.23: Time history of the third DOF of the SNECMA beam, as predicted by hybrid frequency/time method (sticking branch of mode 1), and by time integration (initial conditions 2% below the slipping branch of mode 3). The negative viscous damping ratio is 0.361.

almost exclusively localized around 35 Hz , which corresponds nearly to the sticking frequency of the first mode, equal to 225.42 rad/s , or 35.91 Hz . There is a small amplitude component around 225 Hz , which corresponds to the sticking frequency of the second mode, equal to 1404.38 rad/s , or 223.51 Hz . Finally, there are two other small components around 180 Hz and 250 Hz , which correspond, respectively, to the fifth harmonic and the seventh harmonic of the sticking motion of the first mode. In this case, the hybrid frequency/time method cannot predict the presence of a non-zero component in the second mode of vibration, since it only gives the first mode solution. On the other hand, the multi-harmonic Broyden method should be able to determine the fifth and seventh harmonic components of the first mode. However, the power spectral density analysis of the solution predicted by the hybrid frequency/time method revealed no such components. These higher harmonics may be present in the solution predicted by the time integration because it takes into account the higher frequency second mode and because the modes of vibrations are possibly coupled.

5.4.2 Stability of SNECMA beam with a single negatively damped mode

The free response of the SNECMA beam was studied when only one mode is negatively damped. In this particular study, the damping matrix, $\underline{\mathbf{C}}$, is no longer considered to be a linear combination of the stiffness matrix, $\underline{\mathbf{K}}$, and of the mass matrix, $\underline{\mathbf{M}}$, as defined in Eq. (5.22). The damping matrix is computed as follows. First, the modal damping coefficients of the proportional damping case are computed using a transition matrix, $\underline{\mathbf{T}}$, the matrix of eigenvectors of the beam without friction dampers, which diagonalizes simultaneously the mass and stiffness matrices:

$$\underline{\mathbf{M}} = \underline{\mathbf{T}} \text{Diag}(m_1, m_2, m_3) \underline{\mathbf{T}}^T \quad (5.27)$$

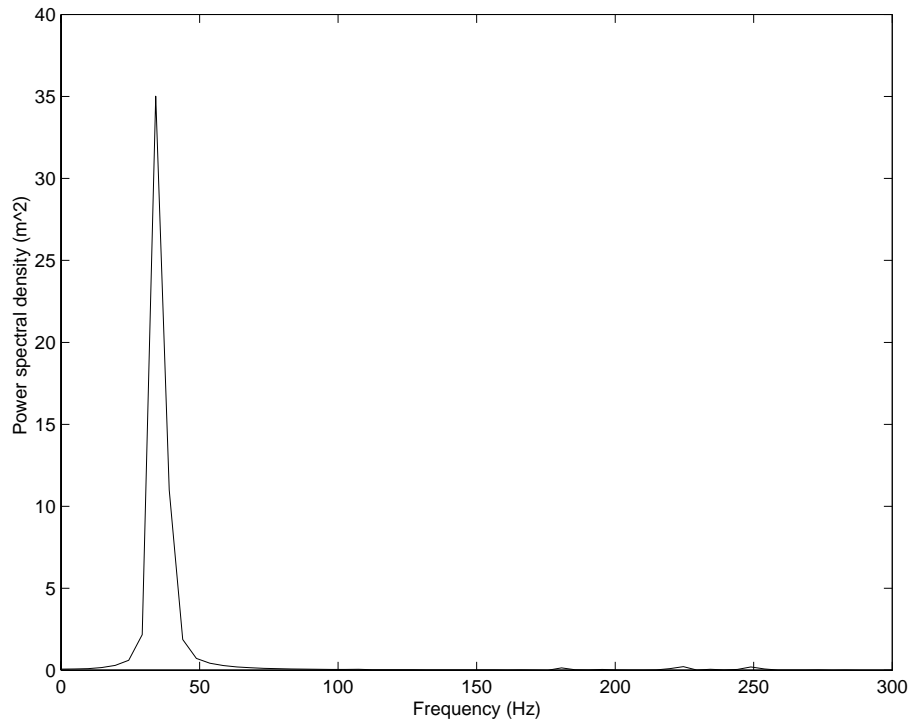


Figure 5.24: Power spectral density of the time history of the third DOF displacement, as predicted by time integration. Same initial conditions as in Fig. 5.23.

$$\underline{\mathbf{K}} = \underline{\mathbf{T}} \text{Diag}(k_1, k_2, k_3) \underline{\mathbf{T}}^T \quad (5.28)$$

where *Diag* denotes a diagonal matrix, and m_i and k_i are, respectively, the modal masses and stiffnesses, $i = 1, 2, 3$. Since the mass and stiffness matrices are symmetric, the transition matrix is orthogonal. Because of Eqs. (5.27) and (5.28), the transition matrix, $\underline{\mathbf{T}}$, also diagonalizes the proportional damping matrix, $\underline{\mathbf{C}}$, defined in Eq. (5.22):

$$\underline{\mathbf{C}} = \underline{\mathbf{T}} \text{Diag}(c_1, c_2, c_3) \underline{\mathbf{T}}^T \quad (5.29)$$

where the c_i are the modal damping coefficients, $i = 1, 2, 3$. In the positively damped case presented in Section 5.4.1, all coefficients c_i , are positive. They are computed from the nominal SNECMA values given in Eq. (2.32):

$$c_1 = 5.789, c_2 = 27.627, c_3 = 12.095 \quad (5.30)$$

In this section, the third mode is assumed to be the only mode negatively damped, so the nominal modal damping coefficient for mode 3 is taken to be $c_3 = -12.095$. In order to study the influence of the negative damping on the free response of the SNECMA beam, the modal damping coefficient is actually equal to:

$$c_3 = -r \cdot 12.095 \quad (5.31)$$

where r is the viscous damping ratio (positive). For each value of the viscous damping ratio, the damping matrix, $\underline{\mathbf{C}}$ is computed using Eq. (5.29), and the periodic solution is found using the method presented in Section 5.3.1. The other two modal damping coefficients, c_1 and c_2 , remain equal to their nominal value given in Eq. (5.30).

Figures 5.25-5.27 present the displacement amplitude of the 3 DOF's of the SNECMA beam, as a function of the viscous damping ratio, when the third mode is

negatively damped. Figure 5.28 depicts the free vibration frequency of the SNECMA beam, as a function of the viscous damping ratio under the same conditions. It can be seen from these figures that the system only vibrates in the third mode of vibration, the one which is negatively damped. This makes sense since the other modes are positively damped. The curves are very similar to the ones obtained in the single-DOF case (see Section 5.2): for each DOF, there is an upper and a lower branch, corresponding respectively to the mostly slipping and mostly sticking motion of the beam. By using a method similar to the one used in Section 5.2, it can be seen that the upper branch determines the stability limit: any motion with an initial displacement larger than the value at the upper branch will be unstable, and any motion initiated below the upper branch will be stable and converge towards to mostly sticking motion. This stability analysis was checked by numerical time integration.

In the case of a single negatively damped mode, the harmonic solution is unique and its stability is the same as the one predicted in the single-DOF case. It is expected that “real” fan blades feature only one negatively damped mode. In this case, the study presented here shows that the hybrid frequency/time method is able to determine the upper and lower branches of the free response, and that the stability of the system can be determined from the results derived for single-DOF systems.

5.5 Conclusion

A multi-harmonic method was developed to study the free response and stability of multi-DOF systems connected to a flexible friction damper and with negative viscous damping. The method is based on harmonic balance and uses the Broyden method to solve the equations in the frequency domain. If several modes of vibrations

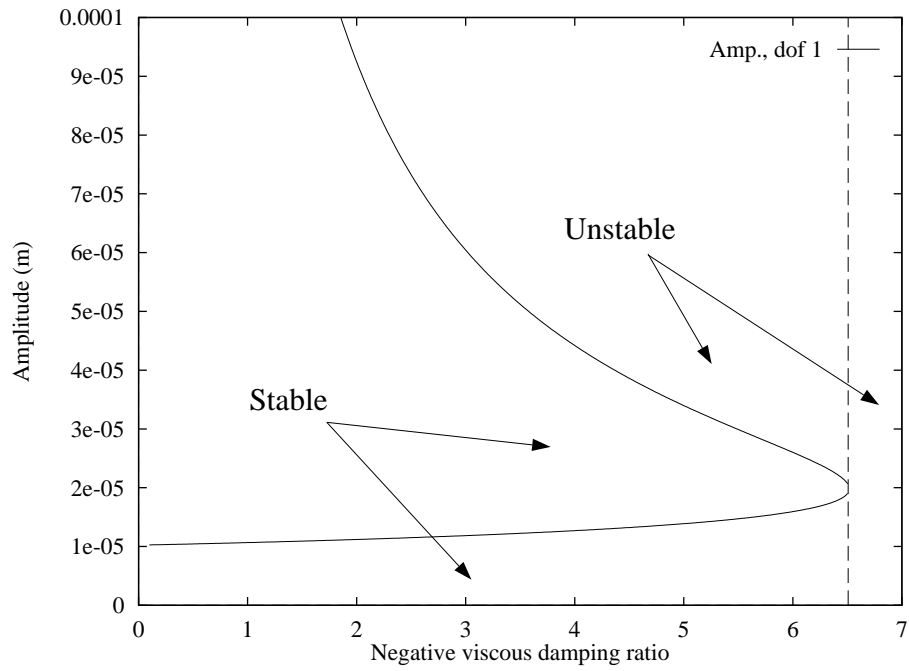


Figure 5.25: Amplitude of displacement of the first DOF of the SNECMA beam, with only the third mode negatively damped, as a function of the negative viscous damping ratio, as predicted by the hybrid frequency/time free response method, with 9 harmonics used.

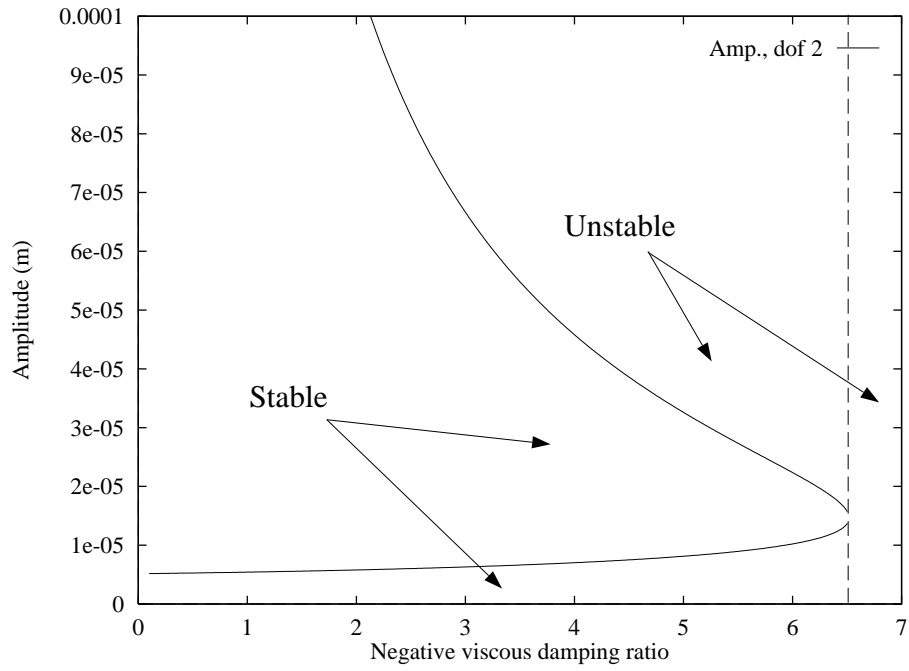


Figure 5.26: Amplitude of displacement of the second DOF of the SNECMA beam, with only the third mode negatively damped, as a function of the negative viscous damping ratio, as predicted by the hybrid frequency/time free response method, with 9 harmonics used.

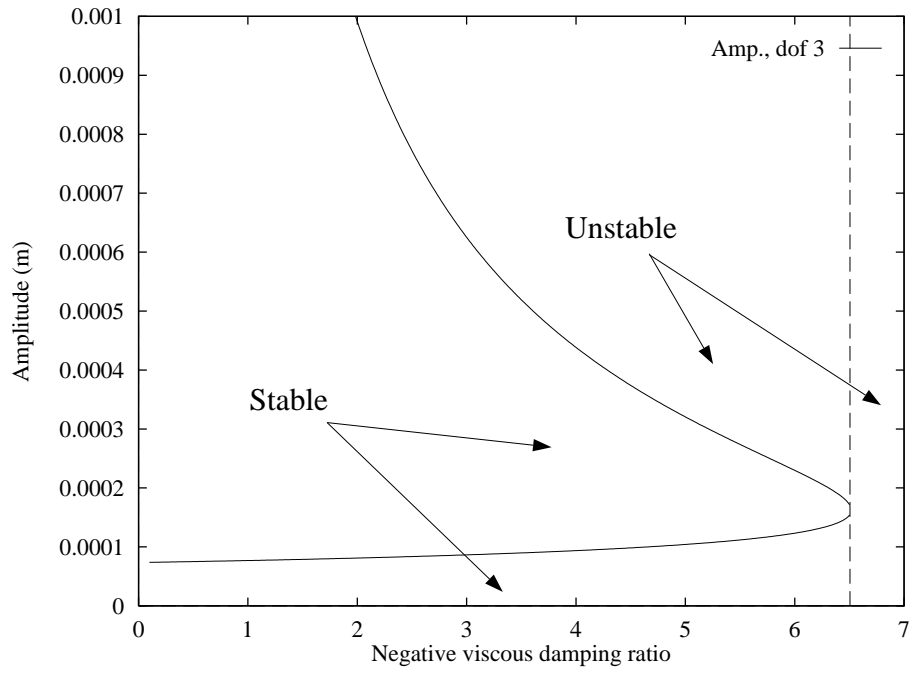


Figure 5.27: Amplitude of displacement of the third DOF of the SNECMA beam, with only the third mode negatively damped, as a function of the negative viscous damping ratio, as predicted by the hybrid frequency/time free response method, with 9 harmonics used.

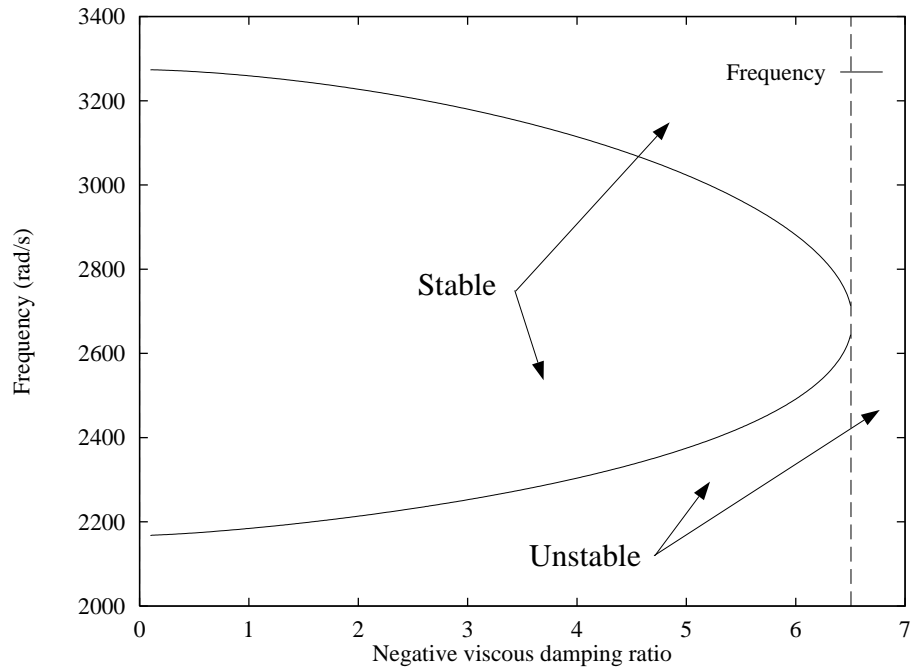


Figure 5.28: Frequency of displacement of the SNECMA beam, with only the third mode negatively damped, as a function of the negative viscous damping ratio, as predicted by the hybrid frequency/time free response method, with 9 harmonics used.

are negatively damped, the solution predicted by the method is non-unique. The stability analysis shows that (1) the overall motion becomes unstable once a single mode cannot be stabilized by friction damping, (2) the higher modes tend to be preponderant in the solution because they are more unstable, (3) the solutions found by time integration often combine several modes and the hybrid frequency/time method is not able to find those. When a single mode of vibration is negatively damped, the multi-DOF results are very similar to the single-DOF ones.

CHAPTER VI

ADVANCED FRICTION DAMPERS

6.1 Introduction

Friction dampers are routinely used in turbomachinery rotors to reduce blade vibrational response. These friction damper elements may be described as rigid friction dampers [Pierre et al., 1985], but they usually consist of a flexible structural element which, for example, is inserted in cavities underneath the platforms of two adjacent blades and is in frictional contact with both blades. The simplest and most widely used model of a flexible friction damper is one-dimensional, and consists of a friction element in series with a linear stiffness. By considering several flexible friction dampers in parallel, this model can take into account microslip [Menq et al., 1986]. The model can also be extended to some particular, elliptical, planar motion, provided that a single temporal harmonic is retained in the solution [Sanliturk and Ewins, 1996]. The hysteretic model, presented in Section 2.2.1 and analyzed in Chapters II-V, essentially characterizes the fundamental shape of deformation of the damper at a particular point of contact with the adjacent structure. However, in general, several such points of contact may be needed to capture effectively the frictional interactions between a damper and its adjacent structures. In such cases the simple hysteretic friction damper model is no longer sufficient, and

the damper itself must be considered as a structure. The elementary flexible friction models presented in Section 2.2.1 and used in the majority of works on friction damped structural systems are not able to represent the damper element as a structure. In this chapter, a new, advanced friction damper model is introduced. Since friction dampers are generally lightweight, it is assumed that the damper inertia forces may be neglected compared to the friction and elastic forces and the damper element is considered massless. Thus, the damper is modeled as a general, massless structure characterized by its own stiffness matrix. The damper is connected to two (possibly more) structural systems at several friction points where slip can occur.

The chapter is organized as follows. First, the force transmitted by the elementary, flexible friction damper used in Chapters II-V is reformulated in a way that permits generalization. Second, the advanced damper element model is introduced and the force it transmits at each frictional interface is evaluated. The multi-harmonic, hybrid frequency/time method is modified to handle this advanced damper model. Finally, the method is applied to a 4-DOF friction damper connecting two beams at four frictional points. Several complex features and properties of the non-linear response are revealed, such as: situations where there is slip at some frictional points and stiction at the other points, and extreme complexity of the frequency response where many modes of vibration can be excited.

6.2 Friction force for elementary damper model

Research efforts on the dynamic response of friction damped structures have mostly considered elementary friction damper models, such as the ones examined in Chapters II-V: these are comprised of a slipping element in series with a stiffness, as depicted in Fig. 6.1. Let x_1 denote the displacement of the structure at one

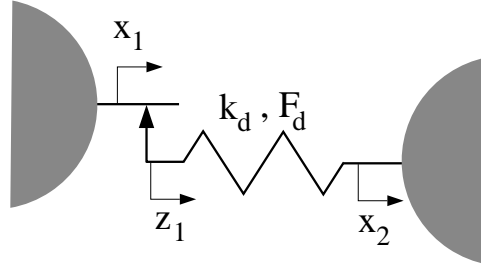


Figure 6.1: Model of the elementary friction damper.

end of the damper, x_2 the displacement of the structure at the other end, f_1 the force transmitted by the friction damper, F_d the maximum force transmitted by the damper, and k_d its stiffness.

The force transmitted by the friction damper is computed by performing the equivalent of a simple numerical time integration over one period of the motion, see Section 3.2. The expression of the force depends on the state of the damper, sticking or slipping, as shown in Table 6.1. Here v_r denotes the relative velocity at the damper, $v_r(j) = \dot{x}_1(j) - \dot{x}_2(j)$.

Damper state	Update	Test for next time step
Sticking	$f_1(j) = f_1(j-1) + k_d(x_1(j) - x_2(j) - x_1(j-1) + x_2(j-1))$	If $ f_1(j) > F_d$
Slipping	$f_1(j) = f_1(j-1)$	If $v_r(j)v_r(j-1) < 0$

Table 6.1: Update for the nonlinear force transmitted by the elementary friction damper in Fig. 6.1.

The force transmitted by the friction damper, f_1 , can be computed from an iteration to the next using the update of Table 6.1. An initial condition must be

given so that the time-marching scheme used to calculate the non-linear friction force over one period is correct. For the elementary damper depicted in Fig. 6.1, it is possible to find an exact initial condition, as follows. When the stretch of the damper stiffness element is maximum, the relative velocity at the damper changes sign. Therefore, according to Coulomb's law of friction, the damper starts sticking. This means that, at the time the damper extension is maximum, the value of the force is known and equal to the maximum force transmitted by the friction damper, F_d , and the state of the damper is sticking. Consequently, the initial condition used to compute the force transmitted by the friction damper is the following:

Property 1 *When the damper relative displacement is maximum, the force transmitted by the friction damper is equal to its maximum value, F_d , and the damper starts sticking.*

If there is no slipping during one period of the motion, then the system is linear and there is no need to use the update presented in Table 6.1.

6.3 Friction force for advanced structure-like dampers

In this section, the elementary damper in Fig. 6.1 is generalized. A damper is modeled as a massless structure, represented by a general stiffness matrix, which is connected to the adjacent structural systems at several slipping or non-slipping interface points. An example of such a structure is depicted in Fig. 6.2: in this particular case, the damper element connects with the adjacent structure at four frictional points, and slipping can take place at any of these points. Let \mathbf{f}_n be the vector of forces transmitted by the damper element to the structure at the N_C points where they interface, \mathbf{D} the stiffness matrix of the damper, \mathbf{z} the vector of damper displacements, $z_i, i = 1, \dots, N_C$, and $x_i, i = 1, \dots, N_C$ the displacement of

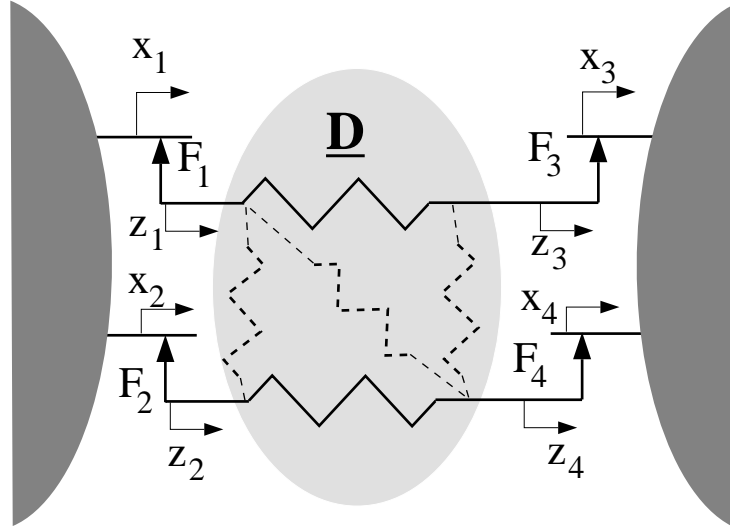


Figure 6.2: Model of an advanced, structure-like friction damper.

the structure DOF connected to the damper at the i -th frictional point. The force transmitted by the damper is expressed as:

$$\mathbf{f}_{nl} = \underline{\mathbf{D}}\mathbf{z} \quad (6.1)$$

For this advanced friction damper model, the damper displacements, z_i , are not readily available. The update used for an elementary friction damper and presented in Table 6.1 cannot be easily extended to structure-like dampers.

6.3.1 New force update for elementary damper

The update presented in Section 6.2 is modified in a way that makes it applicable to structure-like dampers. Denote by Δq the increment of quantity q between the j -th and the $(j + 1)$ -th time step. Table 6.2 presents the update formulas of Table 6.1 using increments.

Since the damper displacement, z_1 , and the displacement at the second end of

Damper state	Update	Test for next time step
Sticking	$\Delta f_1 = k_d(\Delta x_1 - \Delta x_2)$	If $ f_1(j) > F_d$,
Slipping	$\Delta f_1 = 0$	If $v_r(j)v_r(j-1) < 0$,

Table 6.2: Update for the nonlinear force transmitted by the elementary friction damper in Fig. 6.1 using increments.

the damper, x_2 , have the same velocity when the damper is slipping, we have

$$\Delta z_1 = \Delta x_2 \quad \text{when slipping} \quad (6.2)$$

Similarly, the damper displacement, z_1 , and the displacement of the adjacent structure at the first end of the damper, x_1 , have the same velocity when the damper is sticking. Therefore, we have:

$$\Delta z_1 = \Delta x_1 \quad \text{when sticking} \quad (6.3)$$

Using Eqs. (6.2) and (6.3), both updates of Table 6.2 can be written as:

$$\Delta f_1 = k_d(\Delta z_1 - \Delta x_2) \quad (6.4)$$

Equation (6.4) provides an expression to compute the force update, Δf_1 , which is valid for both the sticking and the slipping phases of the motion.

6.3.2 New update for structure-like dampers

The elementary friction damper studied in Section 6.2 and depicted in Fig. 6.1 can be viewed as a structure-like friction damper with two points connecting to the adjacent structure. The second end point of such a damper is always sticking: this may represent for example the case of a damper where the normal load is so large

that the damper is never slipping at this point: $F_2 = +\infty$ (or one with $F_2 > F_1$, as proved below). Therefore, since the damper is always sticking at this point, we have, using the notations previously introduced:

$$z_2(j) = x_2(j), \quad j = 1, \dots, N_{time} \quad (6.5)$$

where N_{time} is the number of sampling points per period of the motion. The stiffness matrix of the elementary damper in Fig. 6.1 is the following

$$\underline{\mathbf{D}} = \begin{bmatrix} k_d & -k_d \\ -k_d & k_d \end{bmatrix} \quad (6.6)$$

where $\mathbf{z} = [z_1, z_2]^T$. Using Eq. (6.5), the single update defined in Eq. (6.4) can be written as

$$\Delta f_1 = k_d \Delta z_1 - k_d \Delta z_2 \quad (6.7)$$

Given the definition of the damper stiffness matrix, Eq. (6.6), Eq. (6.7) leads to

$$\Delta f_1 = D_{11} \Delta z_1 + D_{12} \Delta z_2 \quad (6.8)$$

Since $f_2(j) = k_d(x_2 - z_1)$, Eq. (6.5) leads to

$$\Delta f_2 = k_d \Delta z_2 - k_d \Delta z_1 \quad (6.9)$$

Eqs. (6.6) and (6.9) give

$$\Delta f_2 = D_{21} \Delta z_1 + D_{22} k_d \Delta z_2 \quad (6.10)$$

Hence, from Eqs. (6.8) and (6.10), the new update for the elementary dampers is

$$\Delta \mathbf{f}_{nl} = \underline{\mathbf{D}} \Delta \mathbf{z} \quad (6.11)$$

The update of Eq. (6.11) is valid for both the sticking and slipping periods of the motion, regardless of how many dampers are slipping. In this section, the update of Eq. (6.11) was derived for an elementary friction damper treated as a structure damper. However, this update is also valid for advanced damper elements, as can be proven by “differentiating” the general force expression, Eq. (6.1). Hence, Eq. (6.11) can be used for structure-like dampers, as in Fig. 6.2.

6.3.3 Time-marching procedure for structure-like dampers

Since it is not possible to determine directly the damper displacements, z_i , the update by increments presented in Eq. (6.11) is implemented over one period of the motion in order to compute the force transmitted by the friction damper in the time domain. The procedure is the following:

Procedure 2 *Time-marching step:*

1. *The damper displacement increments, Δz_i , $i = 1, \dots, N_C$, are determined from the state (slipping or sticking) at the various damper interfaces.*
2. *The force increments, $\Delta f_{nl,i}$, $i = 1, \dots, N_C$, are computed using the update formula, Eq. (6.11), from the damper displacement increments, Δz_i , $i = 1, \dots, N_C$.*
3. *The state at the damper interfaces (slipping or sticking) for the next time step is determined from the new values of the friction forces at the damper.*

The second step of this procedure, i.e., the computation of the force increments using the displacement increments, has been presented in Eq. (6.11) and presents no difficulty. The other steps are detailed in the next sections, as follows.

Determination of the displacement increments from the state of the damper

If the i -th damper is sticking, then its velocity is equal to the velocity of the point of the structure to which the damper is attached. Therefore, the i -th increment is

$$\Delta z_i = \Delta x_i \quad \text{when the } i\text{-th damper is sticking} \quad (6.12)$$

If the i -th damper is slipping, then the force it transmits is constant and equal to $\pm F_i$. Therefore, the i -th force increment is equal to zero:

$$\Delta f_i = \sum_{j=1}^{N_C} D_{ij} \Delta z_j = 0 \quad \text{when the } i\text{-th damper is slipping} \quad (6.13)$$

Let S be the set of the N_S friction dampers slipping at a given time step ($N_S \leq N_C$). From Eq. (6.13):

$$\sum_{j=1}^{N_C} D_{ij} \Delta z_j = 0, \quad i \in S \quad (6.14)$$

Eq. (6.14) is a system of N_S linear equations whose N_S unknowns are the displacement increments of the slipping dampers, Δz_i , $i \in S$. Denote by R_i , $i \in S$ the following quantity:

$$R_i = \sum_{j \notin S} D_{ij} \Delta z_j, \quad i \in S \quad (6.15)$$

The R_i , $i \in S$ are computed from the values of the sticking damper displacement increments. From Eqs. (6.14) and (6.15) we have

$$\sum_{j \in S} D_{ij} \Delta z_j = -R_i, \quad i \in S \quad (6.16)$$

Let $\underline{\mathbf{D}}_S$ be the $N_S \times N_S$ submatrix of the damper stiffness matrix, $\underline{\mathbf{D}}$, whose rows and columns correspond to the slipping damper interfaces of set S . Using Eq. (6.16), we have

$$\Delta z_i = - \sum_{j \in S} D_{S,ij}^{-1} R_j, \quad i \in S \quad (6.17)$$

In certain particular cases, it might not be possible to compute the inverse of the stiffness submatrix, $\underline{\mathbf{D}}_{\mathbf{S}}$. In particular, if all N_C dampers are slipping, $\underline{\mathbf{D}}_{\mathbf{S}} = \underline{\mathbf{D}}$, and the inversion is impossible to perform because the stiffness matrix $\underline{\mathbf{D}}$ is singular. However, it is very unlikely that all dampers will be slipping at the same time, unless some very specific conditions are met regarding the symmetry of the damper. Since an actual damper will most certainly not be totally symmetric in terms of geometry and maximum transmitted forces, the potential inversion problems can most likely be overlooked. Section 6.3.3 provides an analysis of the inversion problems possibly caused by damper symmetry.

Equations (6.12) and (6.17) allow to compute all the damper displacement increments for both the sticking and the slipping states. Hence, the first step of Procedure 2 has been explained.

Determination of the state of the damper for next time step

Once the damper displacement increments are computed, as presented in Section 6.3.3, the force increments are computed using Eq. (6.11). The values of the friction forces at the N_C frictional points of the damper are then deduced from their value at the previous time step:

$$\mathbf{f}_{\mathbf{nl}}(j+1) = \mathbf{f}_{\mathbf{nl}}(j) + \Delta \mathbf{f}_{\mathbf{nl}} \quad j = 1, \dots, N_{time} - 1 \quad (6.18)$$

The test to determine whether the i -th damper starts slipping is unchanged with respect to the elementary damper case:

$$\text{If } |f_{nl,i}(j+1)| \geq F_i, \text{ then the } i\text{-th damper is slipping} \quad (6.19)$$

The test to determine whether the i -th damper starts sticking relies on the change of sign of the relative velocity of the damper to the structure at the slipping point.

Since the relative displacement at the i -th damper is $(z_i - x_i)$, the relative velocity is equal to $(\dot{z}_i - \dot{x}_i)$. However, the damper velocity at the i -th friction point, \dot{z}_i , is not readily available. Since time is sampled at N_{time} instants over one period of the motion, the relative velocity test is performed using increments instead of velocities:

$$\text{If } (\Delta z_i - \Delta x_i)(\Delta z_i^- - \Delta x_i^-) < 0, \quad \text{then the } i\text{-th damper starts sticking} \quad (6.20)$$

where Δq^- refers to the increment of the quantity q at the previous time step: $\Delta q^- = q(j) - q(j - 1)$. Equations (6.19) and (6.20) provide the tests to determine whether the friction dampers will be slipping or sticking at the next time step. Hence, the third step of Procedure 2 has been explained.

Problems induced by finite sampling

Since there is a finite number of sampling points, N_{time} , over one period of the motion, the transition times from slipping to sticking might not coincide with the sampling times. Therefore, overshooting might occur. Some of the associated potential problems are:

1. The force transmitted by the i -th friction damper can be greater than its maximum value, F_i , before the slipping increment update, Eq. (6.17), is used.
2. The sum of the friction forces at the N_C points might not add to zero, compromising the overall equilibrium of the system.
3. The upper and lower slipping positions might not be opposite from each other, resulting in an offset of the friction force.

If not addressed, any of these problems hinders the convergence of the method and results in the failure of the solution algorithm. These problems are numerical, and do not arise from the procedure chosen to compute the friction forces.

All the overshooting problems may be corrected by making sure that the slipping value of the i -th friction force is equal to the maximum force transmitted by the friction damper, F_i . To that purpose, Eq. (6.13) is modified as follows:

$$\Delta f_i = \pm F_i - f_{nl,i}(j) \quad \text{when the } i\text{-th damper point is slipping} \quad (6.21)$$

Equations (6.18) and (6.21) lead to

$$f_{nl,i}(j+1) = \pm F_i \quad (6.22)$$

With this simple correction, it is ensured that the slipping values of the friction forces are equal to the maximum values, $\pm F_i$, Eq. (6.22). Equation (6.21) ensures that the symmetry of each damper force and the overall equilibrium of the system are enforced.

Potential problems due to stiffness matrix singularity

As presented in Section 6.3.3, the inversion of a submatrix, $\underline{\mathbf{D}}_{\mathbf{S}}$, is needed to compute the displacement increments of the slipping damper points. If not all dampers are slipping, it is reasonable to assume that the system will be sufficiently asymmetric so that the submatrix, $\underline{\mathbf{D}}_{\mathbf{S}}$, is not singular. This is justified because it is very unlikely that the stiffness of the system at the various friction points will all be equal.

Since the stiffness matrix, $\underline{\mathbf{D}}$, is singular, there might be an inversion problem if all friction dampers are slipping. It is very unlikely that this will ever happen, as we will show now. Given the particular structure of the damper stiffness matrix, we have:

$$\sum_{i=1}^{N_C} D_{ij} = 0, \quad j = 1, \dots, N_C$$

Therefore, the following is true:

$$\sum_{i=1}^{N_C} D_{ij} z_j = 0, \quad j = 1, \dots, N_C$$

By adding up the previous expressions for all N_C values of j , we have

$$\sum_{j=1}^{N_C} \sum_{i=1}^{N_C} D_{ij} z_j = 0$$

Permuting the summation signs and using Eq. (6.1) yields

$$\sum_{i=1}^{N_C} f_{nl,i} = 0 \quad (6.23)$$

From Eq. (6.23), we deduce the following property of the structure-like friction damper:

Property 2 *The sum of the forces transmitted by the damper element to the structure is equal to zero.*

Let us assume that a given time step, $(N_C - 2)$ friction points are slipping. The values of the forces transmitted by these slipping friction interfaces are equal to their maximum values, $\pm F_i$, $i \in S$. Let us assume now that another friction point starts slipping at this particular time and that the i_0 -th friction point is the only interface left sticking. From Property 2 we deduce that

$$f_{nl,i_0} = - \sum_{i \neq i_0} f_{nl,i} \quad (6.24)$$

By assumption, we have:

$$f_{nl,i} = \pm F_i (= \text{constant}) \quad \forall i \neq i_0 \quad (6.25)$$

Therefore, we deduce from Eq. (6.24) that the force transmitted by the i_0 -th friction damper is constant. Since the i_0 -th damper is sticking and its force is constant (below slipping value), the i_0 -th damper remains stuck and cannot start slipping until another damper starts sticking. Therefore, all dampers cannot be simultaneously slipping.

The previous conclusion could be false if one could find a system and a situation where two dampers can start slipping at the same time. This requires some very particular symmetry in the damper and consequently this case is not considered in the present study.

6.3.4 Initial conditions

Procedure 2 allows one to compute the forces transmitted by the damper to the structure from one time step to the next one. However, an initial condition is needed to start the process.

In the case of an elementary friction damper, an exact initial condition can be found, as described in Property 1. When a structure-like damper is considered, it is not possible to find an exact initial condition for the forces transmitted by the friction damper. The proposed alternative is the following. It is assumed that at the beginning of the period, all dampers are sticking and that the forces at all the dampers are equal to zero. These conditions are not correct, but they verify all static and dynamic conditions of the friction dampers:

1. The sum of the forces is indeed equal to zero (Property 2 is verified).
2. The forces being equal to zero, the dampers are indeed sticking.

The time-marching procedure starts from these assumed initial conditions. Since all the dampers are stuck at the beginning, there is no friction damping. Therefore, the amplitude of the displacements will grow until some of the dampers start slipping: at this stage it is assumed that the friction forces will be accurately computed.

By repeating this time-marching procedure over several periods, we assume that the true solution is reached and that the forces are correctly determined. This time integration is performed over a very small number of periods: the intent is not to

wait until the transient regime has died out, but rather to ensure that there is a balance between the energy brought into the system by external forcing and the energy dissipated by friction and viscous damping.

6.4 Results for an example system

6.4.1 Time histories

The system considered in this section consists of two coupled SNECMA beams, each represented by a three-DOF component mode model. Each beam is clamped at one end (base) and subject to external, harmonic excitation at the other end (tip). The characteristics of the beams are given in Section 2.3.4. The two beams are connected through a four-DOF friction damper element. The system is represented in Fig. 6.3. The first and second DOF's of the damper element connect to the first DOF of each beam, that is, to the point where the elementary friction dampers were connected in Chapters II and IV. The third and the fourth DOF's of the friction element connect to the tips of the beams, where the external forcing is applied. The amplitude, F_{ex} , and frequency, ω , of the external forcing are the same for both beams, but the phases are opposite: we are primarily exciting the antisymmetric modes of vibration of the system. The stiffness matrix of the damper element is taken to be the following:

$$\underline{\mathbf{D}} = \begin{bmatrix} 2.88 \cdot 10^7 & -2.4 \cdot 10^7 & 0 & -4.8 \cdot 10^6 \\ -2.4 \cdot 10^7 & 2.64 \cdot 10^7 & -2.4 \cdot 10^6 & 0 \\ 0 & -2.4 \cdot 10^6 & 2.64 \cdot 10^6 & -2.4 \cdot 10^5 \\ -4.8 \cdot 10^6 & 0 & -2.4 \cdot 10^5 & 5.04 \cdot 10^6 \end{bmatrix} \quad (6.26)$$

The maximum friction forces transmitted at the friction points are constant and their values are listed in Table 6.3. Since $F_4 = +\infty$, the force transmitted by the fourth

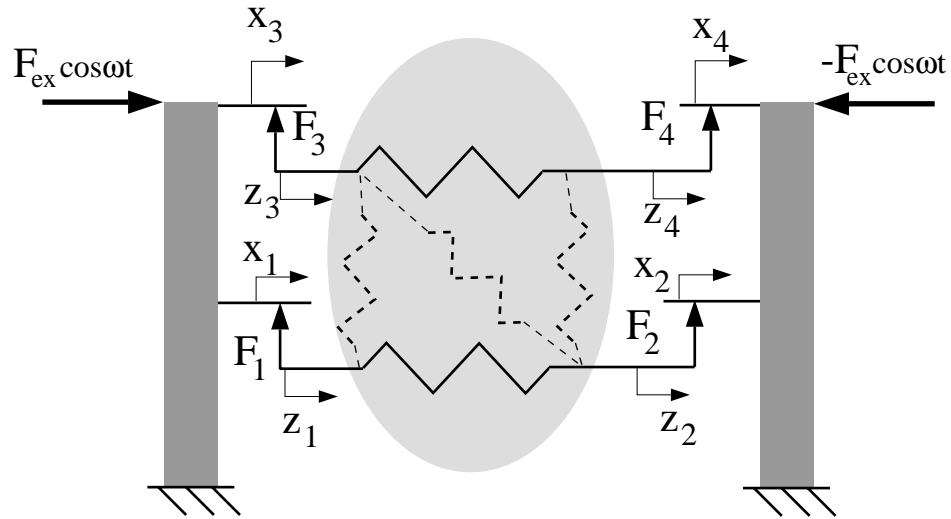


Figure 6.3: 4-DOF damper element connected to two SNECMA beams.

friction damper never reaches its maximum value. Therefore, the fourth friction damper is always sticking and never slips.

Damper friction point, $i =$	1	2	3	4
Maximum force (N), $F_i =$	24.60	100.0	246.05	$+\infty$

Table 6.3: Maximum forces transmitted by the structure-like friction element.

Figures 6.4-6.7 depict, at a particular frequency, the time histories of the forces transmitted by the four friction dampers for various force amplitudes, F_{ex} . Also represented are the time histories of the friction forces if the four dampers were stuck all the time. When all dampers are always stuck, the damper element behaves like an elastic structure and the whole system, beams and damper element, is linear. In Figs. 6.4-6.7, the friction forces computed assuming that there is no slipping at any frictional point are referred to as sticking linear forces. Finally, the sum of the friction

forces at the four interfaces is represented. The case shown in Fig. 6.4 corresponds to a situation where no damper is slipping during the period of the motion. In this case, the forces transmitted by the friction dampers are identical to the forces transmitted if the dampers are stuck all the time. We can verify that the sum of the forces is equal to zero, as predicted in Eq. (6.23). In Fig. 6.4, the damper structure acts like a mere stiffness and there is no non-linearity.

In Fig. 6.5, damper 1 undergoes some slipping during the period of the motion. The time history of the friction force at damper 1 is very similar to the time histories of elementary friction dampers. Since the displacements at the four friction dampers are coupled, the non-linearity introduced by the slipping motion of damper 1 influences the motion of the other friction dampers. In particular, it can be seen that the force at damper 2 is non-smooth, although damper 2 is never slipping. Similarly, the forces at dampers 3 and 4 are offset with respect to the values they would have if all dampers were sticking all the time. Finally, the forces of the 4 dampers add to zero, as predicted in Eq. (6.23).

In the case represented in Fig. 6.6, there are times when damper 1 alone is slipping, times when damper 1 and 2 are slipping, and times when dampers 1 and 3 are slipping. For this particular force amplitude and at this frequency, two dampers at most are slipping at the same time. As in Fig. 6.5, it can be seen that even the force transmitted by the non-slipping damper, damper 4, is non-smooth. It can also be seen that there are discontinuities in the force derivatives due to the rapid change of relative velocities at the damper interfaces. The force transmitted by a slipping damper point can be greater than the force this damper interface would transmit if all the dampers were sticking, see for example damper 2. This never happens with elementary friction dampers: for an elementary friction damper, the friction force is

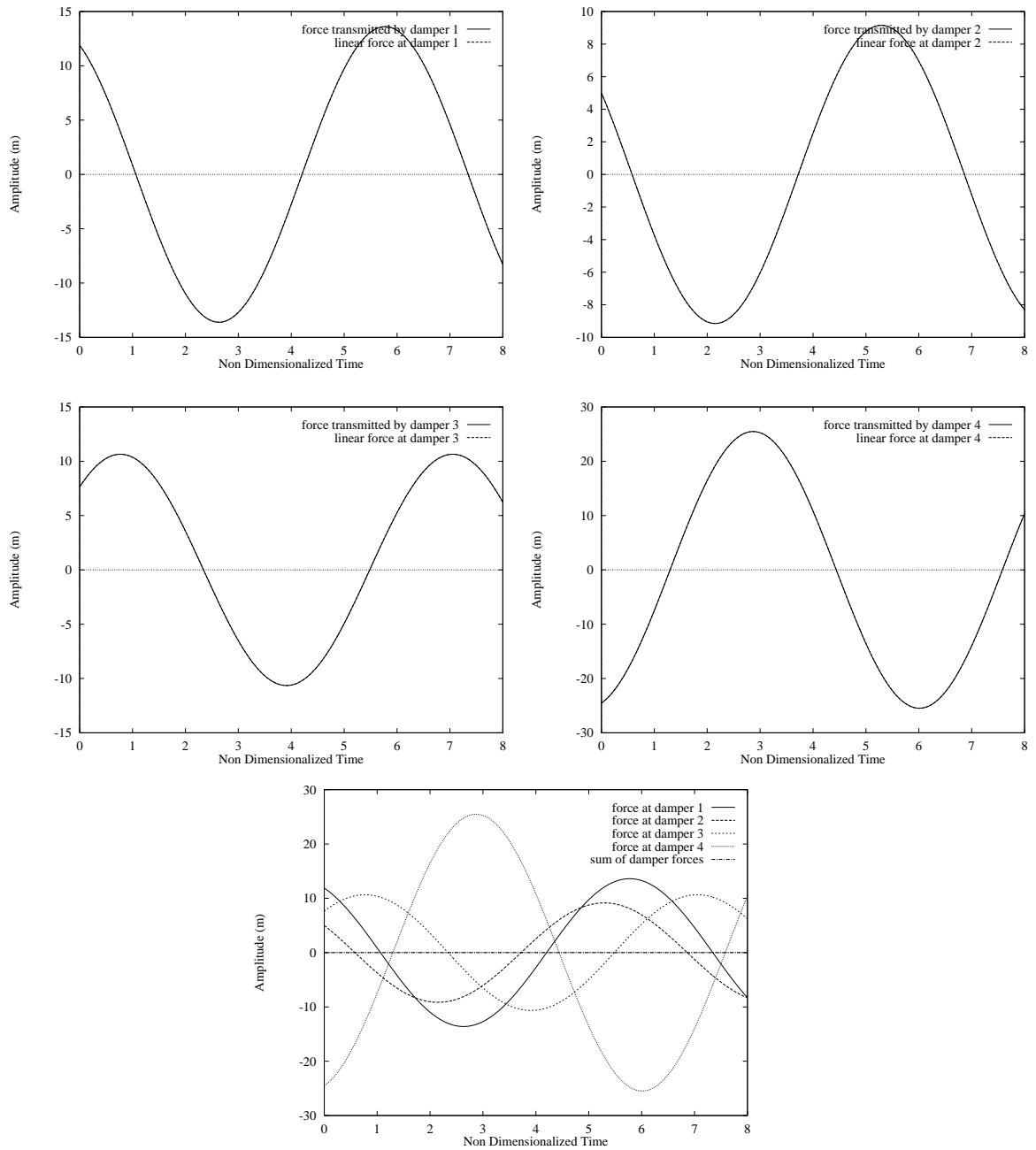


Figure 6.4: Time histories of the four friction forces, of the sticking linear forces at the damper locations, and of the sum of the forces transmitted by the friction element, when no damper is slipping, for $\omega = 250 \text{ rad/s}$ and $F_{ex} = 15 \text{ N}$.

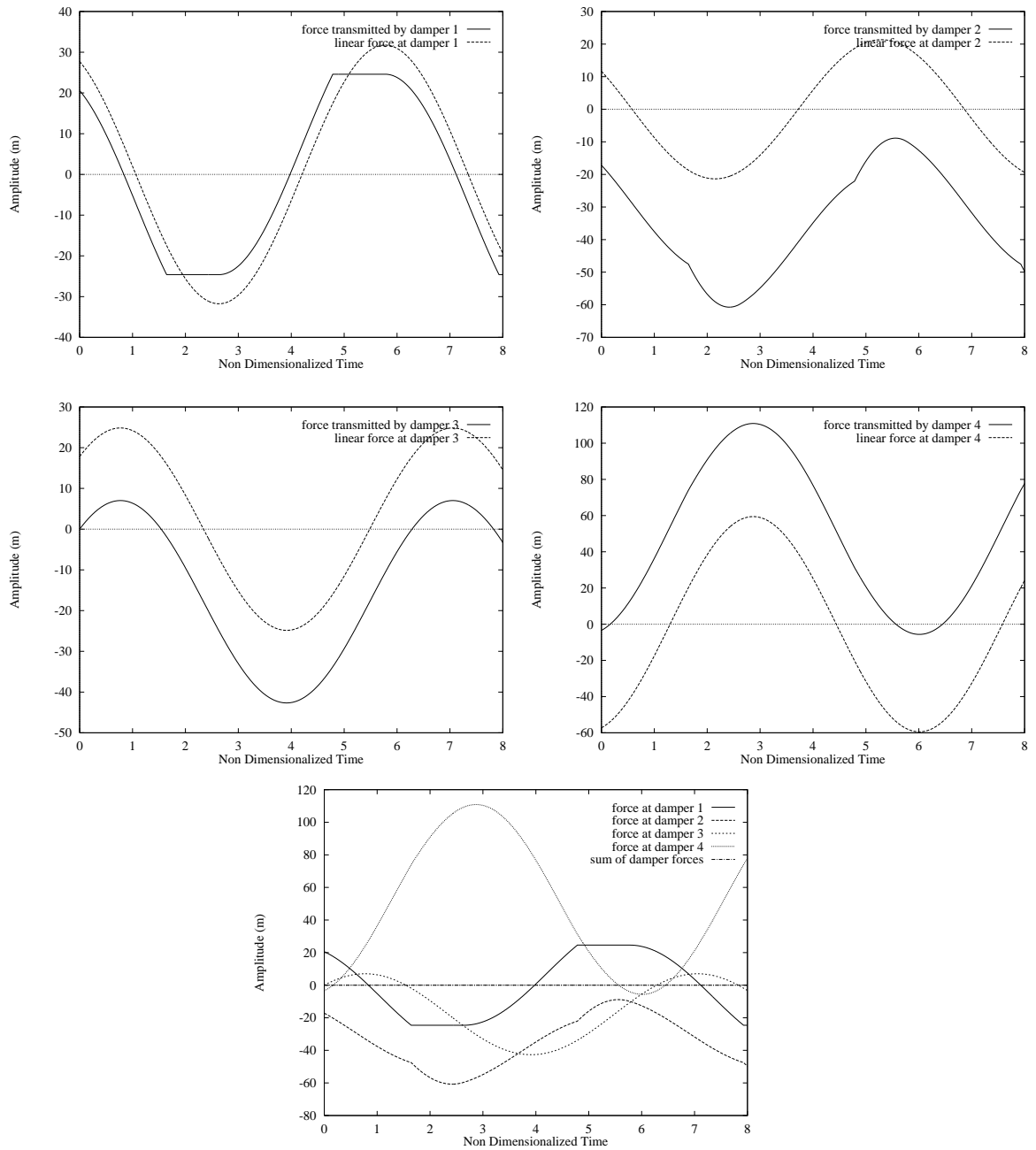


Figure 6.5: Time histories of the four friction forces, of the sticking linear forces at the damper locations, and of the sum of the forces transmitted by the damper element, when only damper 1 is slipping, for $\omega = 550\text{rad/s}$ and $F_{ex} = 35\text{N}$.

always smaller than the force the damper would transmit if it was never slipping. Finally, we can verify again that the sum of the forces transmitted by the dampers is equal to zero.

In Fig. 6.7, the external forcing is large enough to make three dampers slipping at the same time, namely dampers 1, 2, and 3. When three dampers are slipping, the force transmitted by the sticking damper, damper 4, remains constant, as shown in Section 6.3.3. Therefore, when three dampers are slipping, all four friction forces are constant. Once again, we can verify that the sum of the forces transmitted by the damper element is equal to zero.

6.4.2 Frequency response results

In this section, the frequency response of the system considered in Section 6.4.1 is obtained for various amplitudes of external forcing. Figures 6.8 and 6.9 depict the frequency response of the beam system at the locations of dampers 1 and 2, for various force amplitudes, while Figs. 6.10 and 6.11 show the frequency response of the beam system at the locations of dampers 3 and 4.

For a low force amplitude, $F_{ex} = 20N$, none of the dampers slip at any time and the response of the system is linear. In this case, the displacement amplitudes at dampers 1 and 2 on one hand, and at damper 3 and 4 on the other hand, are very similar. As the amplitude of external forcing increases, $F_{ex} \geq 30N$, the displacements at dampers 1 and 2, and 3 and 4, become increasingly different. There starts to be some slipping: the presence of slipping affects drastically the displacements at dampers 3 and 4. For larger amplitudes of external forcing, $F_{ex} = 50N$, as a result of more dampers undergoing slipping, more resonance frequencies of the system are excited and another group of resonances appears. As the force amplitude increases

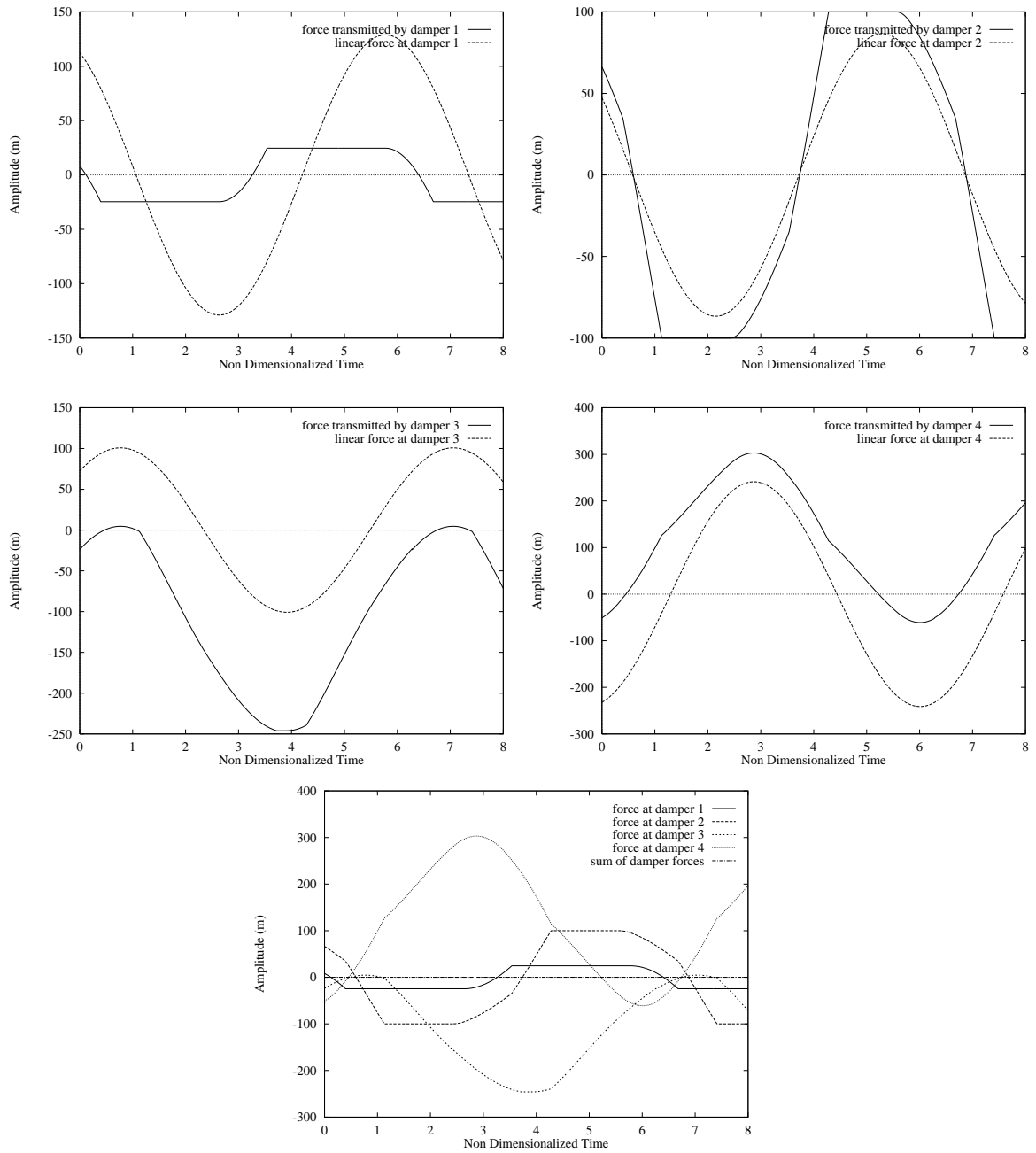


Figure 6.6: Time histories of the four friction forces, of the sticking linear forces at the damper locations, and of the sum of the forces transmitted by the damper element, when only two dampers are slipping at the same time, for $\omega = 550\text{rad/s}$ and $F_{ex} = 140\text{N}$.

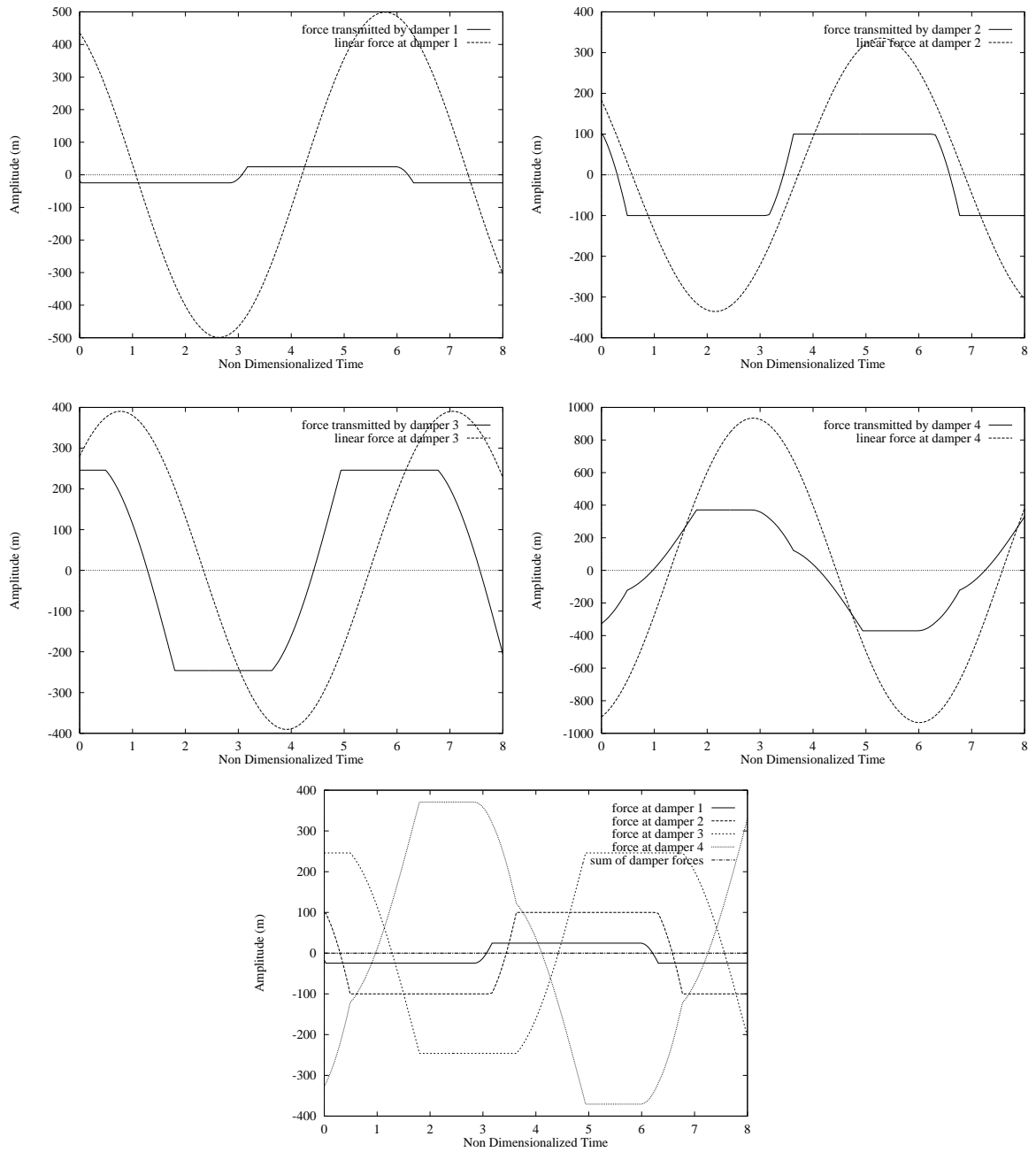


Figure 6.7: Time histories of the four friction forces, of the sticking linear forces at the damper locations, and of the sum of the forces transmitted by the damper element, when at most three dampers are slipping at the same time, for $\omega = 550 \text{ rad/s}$ and $F_{ex} = 550 \text{ N}$.

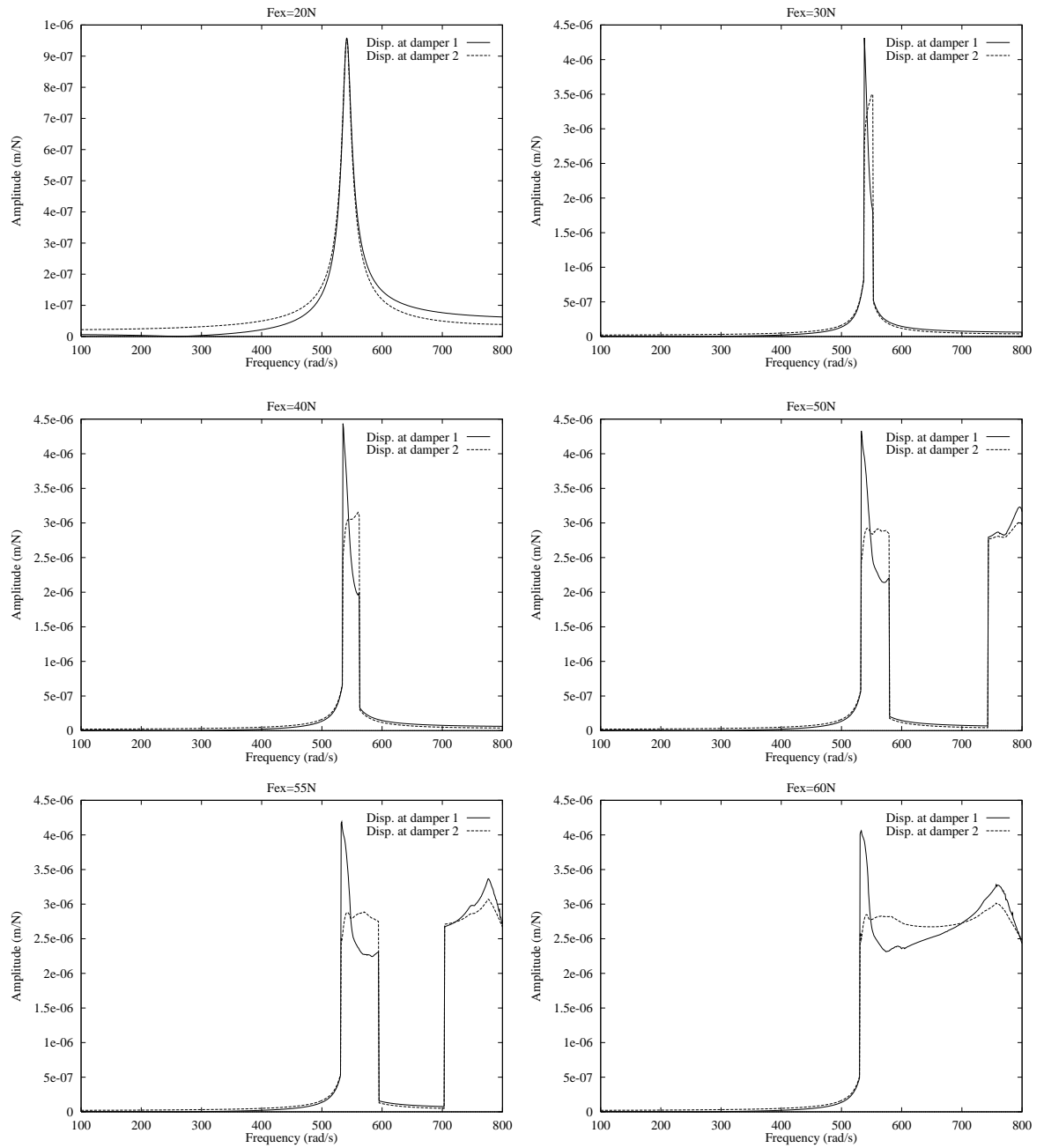


Figure 6.8: Beam displacement amplitude at dampers 1 and 2, as a function of the frequency, for different force amplitudes: $F_{ex} = 20, 30, 40, 50, 55,$ and $60N$ (from left to right, top to bottom).

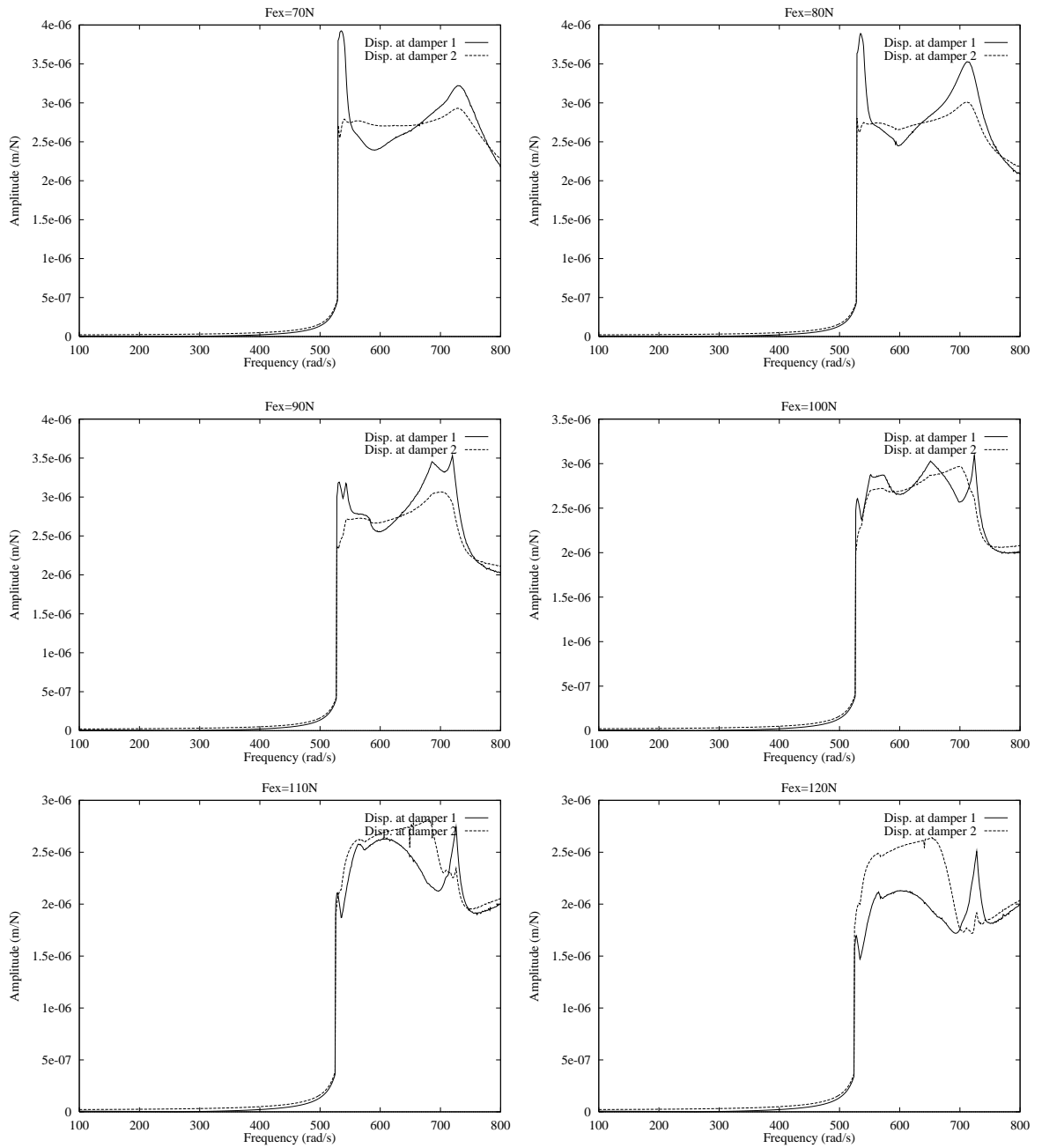


Figure 6.9: Beam displacement amplitude at dampers 1 and 2, as a function of the frequency, for different force amplitudes: $F_{ex} = 70, 80, 90, 100, 110,$ and $120N$ (from left to right, top to bottom).

further, $F_{ex} \geq 60N$, the groups of resonances merge together and it is observed that, depending on the number of friction dampers slipping, many resonance frequencies are excited. The dynamics of this advanced damper are thus significantly richer and more complex than the ones of elementary friction dampers.

In order to understand better the presence of all the resonances observed in Figs. 6.8-6.11, the first three resonance frequencies of the beam system in various configurations are given in Table 6.4. The boldfaced resonance frequencies correspond to frequencies in the interesting ranges of Figs. 6.8-6.11, i.e., from 500 to 700 rad/s . A superscript 2 indicates a multiplicity of order two of a resonance frequency.

Configuration	1 st frequency	2 nd frequency	3 rd frequency
No damper slipping	541.26	1090.2	2026.59
Damper 1 slipping	336.38	680.84	1004.61
Damper 2 slipping	342.83	693.58	1006.11
Damper 3 slipping	191.15	678.17	1358.67
Dampers 1 and 2 slipping	159.59	512.98	901.76
Dampers 2 and 3 slipping	159.59	664.94	901.76
Dampers 1 and 3 slipping	159.59 ²	901.76 ²	2167.54 ²
Dampers 1, 2, and 3 slipping	159.59 ²	901.76 ²	2167.54 ²

Table 6.4: First three natural resonance frequencies of the two-beam/damper system in various slip/stick damper configurations (in rad/s).

There are six separate resonance frequencies from 500 rad/s to 700 rad/s . This might explain the fact that for force amplitudes greater than 60N, there is a con-

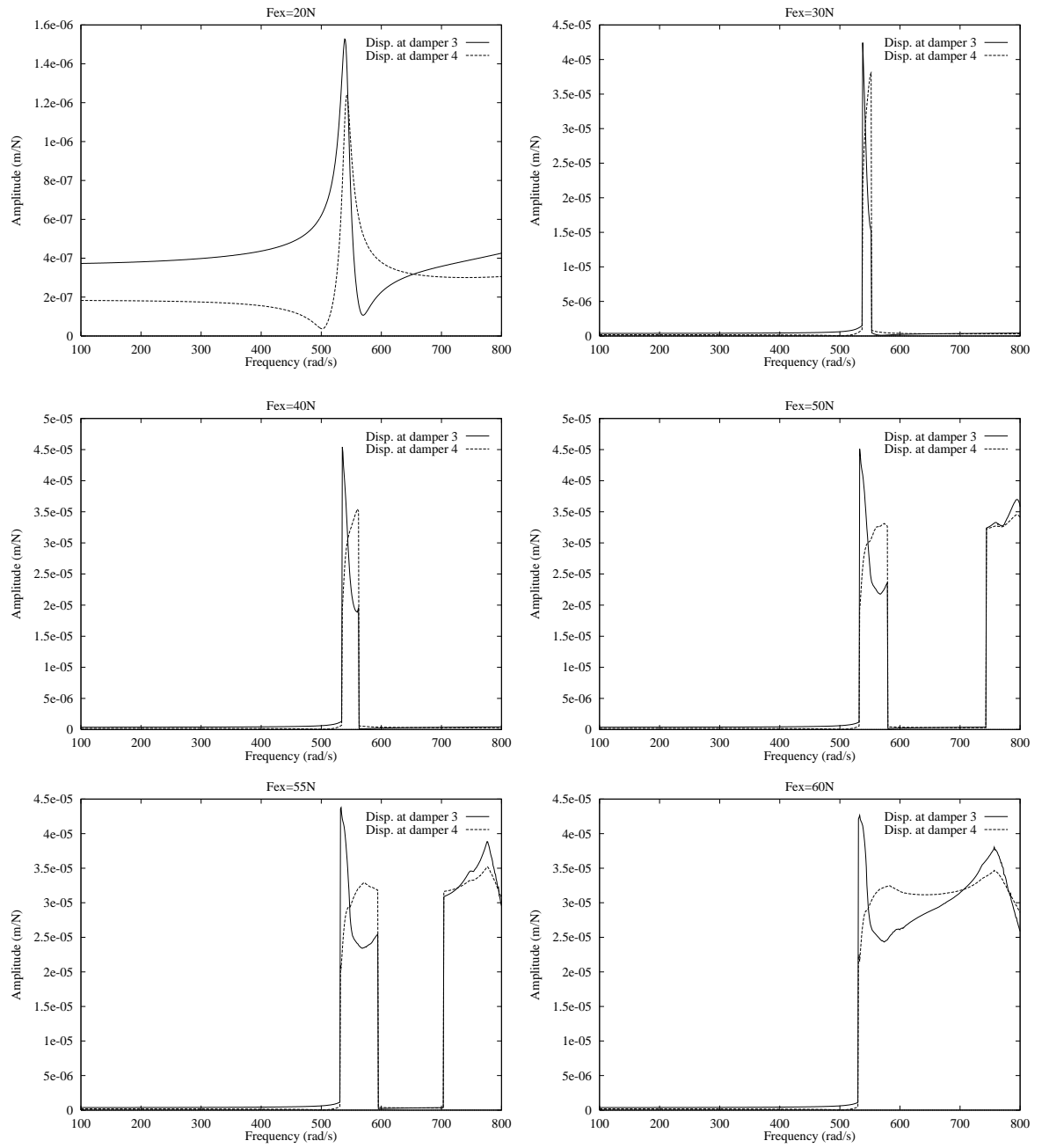


Figure 6.10: Beam displacement amplitude at dampers 3 and 4, as a function of the frequency, for different force amplitudes: $F_{ex} = 20, 30, 40, 50, 55,$ and $60N$ (from left to right, top to bottom).

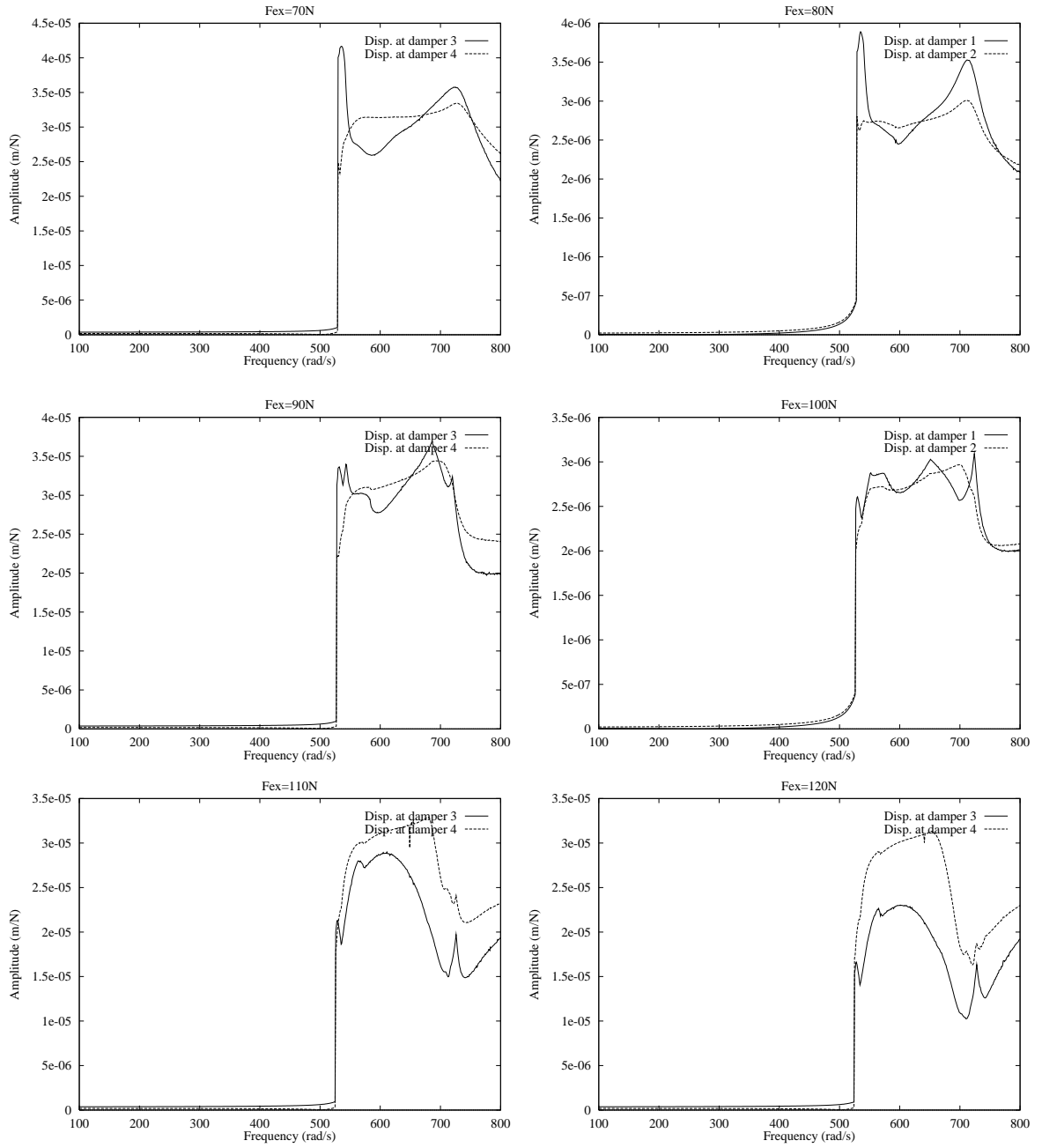


Figure 6.11: Beam displacement amplitude at dampers 3 and 4, as a function of the frequency, for different force amplitudes: $F_{ex} = 70, 80, 90, 100, 110,$ and 120 N (from left to right, top to bottom).

tinuum of resonant response of the beam system. When both dampers 1 and 3 are slipping, the two SNECMA beams are actually independent from each other. We can see in Table 6.4 that the natural frequencies of the system when dampers 1 and 3 are slipping are equal to the natural frequencies of the SNECMA beams not attached to any friction damper.

Finally, one might wonder why the resonant curves are so steep in the case of an advanced friction damper. The external excitation is antisymmetric, i.e., the amplitude of the external forcing is the same for each beam but the phases are opposite of each other. The steepness of the resonant curves may be attributed to the antisymmetry of the external forcing, as similar results were obtained when two beams, each attached to a flexible friction damper and coupled through a linear stiffness were subject to antisymmetric external forcing.

6.5 Conclusions and Future work

A new model of friction damper element was introduced. The advanced friction damper is considered to be a general, massless structure connecting at several friction points to the adjacent structural system, with a possibility of slipping motion at any of these connecting interfaces. A new methodology was developed in order to compute the forces transmitted by an advanced friction damper to an adjacent structure.

Results were obtained for a four-DOF damper element connecting two SNECMA beams. It was found that there are different configurations of the system where several dampers can slip at the same time. Consequently, numerous natural resonance frequencies of the system are excited and the dynamic response of the system is complex.

The case presented in Sections 6.4.1 and 6.4.2 corresponds to an arbitrary system, which might bear little similarity with an actual blade-damper configuration. However, the results presented are interesting, because they demonstrate:

- the applicability of the method developed for elementary friction dampers to advanced, structure-like friction dampers,
- the richness of the dynamics of structures attached to advanced friction dampers.

Future work will focus on the studies of the dynamics of systems attached to advanced, structure-like friction dampers.

CHAPTER VII

CONCLUSIONS

7.1 Main contributions

The main contributions of this work are as follows:

- A one-harmonic approximation was derived for the prediction of the forced response of friction damped structural systems. The computation of the force transmitted by the friction dampers was enhanced with respect to the traditional single-harmonic method by performing a time-marching procedure over one period of the motion. The number of equations to solve was reduced by the introduction of complex, reduced dynamic and force matrices. The procedure was successfully and efficiently applied to multi-DOF systems. Several limitations of the one-harmonic methods were pointed at.
- The force transmitted by a damper element to an adjacent structure was evaluated in the time domain in a new fashion: the friction force is deduced from the relative displacement and velocity of the structure at the damper location. No assumption besides Coulomb's law is made on the friction force, allowing for a high level of accuracy. Several slip and stick phases per period are allowed, and the influence of higher harmonics can be totally accounted

for.

- A new method, based on the harmonic balance procedure and the Broyden algorithm, and a time-domain treatment of the friction force were developed and used to study in an efficient and accurate manner the dynamics of friction damped systems. The method can include as many temporal harmonics as desired to capture the dynamics of the system. The procedure is fast and reliable, and can be applied to large-scale models of turbomachinery elements. To the author's knowledge, this is the first time that the harmonic balance method has been used along with the Broyden method to study the dynamics of friction-damped structures.
- Results were presented for several large-scale systems, under a variety of structural and friction parameters. Complex features of the non-linear response were identified, such as: motions with multiple stick-slip phases during each period, subresonances, and localization. The multi-harmonic, hybrid frequency/time method provides very significant time savings over the more traditional numerical time integration procedures.
- The multi-harmonic method developed for the study of the forced response was expanded to the analysis of the free response and stability of friction damped systems: the procedure is similar to the one used for the forced response, with the frequency of vibration being an unknown. It was observed that the dynamics are very rich when several modes of vibration are negatively damped and that the stability analysis is often not conclusive. When a single mode of vibration is negatively damped –as expected in actual blades undergoing flutter, the hybrid frequency/time method is able to predict in an efficient and

reliable manner the free steady-state response and the stability of the system.

- A new, general model of a friction damper was introduced, which may represent more accurately damped bladed disk assemblies. The new damper element is a massless structure with its own stiffness matrix. The model allows for several contact points at each interface between the damper and the structure. The motions at all the contact points are coupled through the stiffness of the damper element. A new, general method was presented to compute the force transmitted by the general damper element to the adjacent structures: the method is based on a time-marching procedure over a few periods of the motion. Several properties of the forces transmitted by structure-like dampers were identified, such as the fact that the sum of all the forces equals to zero. Results were presented for an example system and revealed rich dynamics.

7.2 Direction for future work

Following are some suggestions of investigation topics that, if addressed, would enhance the analysis of the dynamics of friction damped blade assemblies presented in this dissertation.

- Microslip

In the analysis of friction damped structural systems, single point contact Coulomb friction is often assumed. This model is acceptable as long as gross slip occurs at the interface, usually as a consequence of the normal load being small. However, for high normal loads, partial slip is expected. Since one single-point contact Coulomb damper alone can only represent fully slipping or stuck situations, more refined models of the friction interface have to be used

in order to accurately predict the energy dissipated at an interface undergoing microslip.

In the past, microslip has often been introduced using three different models. Since the main characteristic of micro-slip is that the slope of the loading curve decreases gradually, due to partial slip, as the contact displacement increases, the first approach is to approximate this loading curve by an exponential [Sanliturk et al., 1997]. The second approach is to use distributed element models for hysteresis. One such model is based on an array of elastoplastic elements in parallel or in series. The parallel-series model has been widely used [Iwan, 1967, Sanliturk and Ewins, 1996]. Finally, the third approach is based on a continuous model of the friction interface, represented by an elastoplastic shear layer [Menq et al., 1986]. Even if this third approach seems more general, it does not seem to bring more accuracy than the first two methods and the analytical complexity of this model make it difficult to implement this method for large scale systems.

- Variable normal load

It might be important to consider the effects of the variations of the normal load across the frictional interface. Such effects have been found to be significant [Ferri, 1995, Whiteman and Ferri, 1999]. Yang *et al.* (1998) have introduced a new contact interface model, with a friction contact point and a massless elastic element. The stiffness of the elastic element is characterized by two linear springs, which account for the shear and normal stiffness properties. This model can represent tangential stick slip motion as well as intermittent separation, and the contact interface can either have a preload or initial gap.

Analytical criteria must be developed to predict the transitions between various states of the interface and, with these transitions established, the hysteresis loop can be obtained in order to characterize the stiffness and damping of the interface.

- Two-dimensional friction contact

Most of the research efforts on friction damped structural systems have been directed to analyzing friction interfaces constrained to move in one-dimension: i.e., a contact point which moves back and forth along a straight line. This assumption may not always be valid, especially if there is coupling between motions of the structure in more than one direction: for example bending and torsion of a turbine blade. Menq *et al.* (1991) studied the two-dimensional interface motion when the contacting point moves in an elliptical path. Sanliturk and Ewins (1996) extended the method to more general, planar paths. The friction is supposed to take place between two nodes of the structures whose location is determined by their x - and y - coordinate in the plane of the motion. The damper extension is computed at each iteration over several cycles until the trajectory stabilizes. Once this trajectory is known, the friction force and its direction angle can be computed and resolved into the x - and y - directions. This approach can be generalized to any hysteresis loop and may take into account microslip.

- To represent more accurately the actual assemblies used in turbomachinery equipment, the dampers may need to be considered as wedge elements connecting two adjacent blades. This damper model combines both the structure-like approach presented in Chapter VI and variable normal loads, as defined above.

- In Chapter VI, the damper inertia forces are neglected compared to the elastic and friction forces. In some cases, the mass of the damper may need to be taken into account in the model.

BIBLIOGRAPHY

BIBLIOGRAPHY

- [Allgower and Georg, 1990] Allgower, E. and Georg, K., 1990, *Numerical Continuation Methods*, Springer-Verlag, Berlin.
- [Berthillier et al., 1998a] Berthillier, M., Dupont, C., Chanez, P., and Saurat, F., 1998a, “Réponse Forcée Aéroélastique des Aubes de Turbomachines,” to be published in “Revue Française de Mécanique”.
- [Berthillier et al., 1998b] Berthillier, M., Dupont, C., and Mondal, R., 1998b, “Blades Forced Response Analysis With Friction Dampers,” *Journal of Vibration and Acoustics*, Vol. 120, pp. 468–474.
- [Bladh et al., 1998] Bladh, R., Castanier, M. P., , and Pierre, C., 1998, “Reduced Order Modeling and Vibration Analysis of Mistuned Bladed Disk Assemblies with Shrouds,” *Proceedings of the 43rd ASME Gas Turbine and Aeroengine Technical Congress, Exposition and Users Symposium, Stockholm, Sweden*.
- [Bobylev et al., 1994] Bobylev, N., Burman, Y. M., and Korovin, S., 1994, *Approximation Procedure in Nonlinear Oscillation Theory*, Walter de Gruyter, Berlin.
- [Cameron and Griffin, 1989] Cameron, T. and Griffin, J., 1989, “An Alternating Frequency/Time Domain Method for Calculating the Steady-State Response of Nonlinear Dynamic Systems,” *Journal of Applied Mechanics*, Vol. 56, pp. 149–154.
- [Dowell, 1995] Dowell, E. H., 1995, *A Modern Course in Aeroelasticity*, Kluwer Academic Publishers.
- [Ferri, 1985] Ferri, A., 1985, *The Dynamics of Dry Friction Damped Systems*, PhD thesis, Princeton University.
- [Ferri, 1995] Ferri, A., 1995, “Friction Damping and Isolation Systems,” *Journal of Engineering for Gas Turbines and Power*, Vol. 117, pp. 196–206, Special 50th Anniversary Design Issue.
- [Ferri and Bindemann, 1992] Ferri, A. and Bindemann, A., 1992, “Damping and Vibration of Beams with Various Types of Frictional Support Conditions,” *Journal of Vibration and Acoustics*, Vol. 114, No. 3, pp. 289–296.

- [Ferri and Dowell, 1985] Ferri, A. and Dowell, E., 1985, “The behavior of a linear, damped modal system with a non-linear spring-mass-dry friction damper system attached, part II,” *Journal of Sound and Vibration*, Vol. 101, No. 1, pp. 55–74.
- [Ferri and Dowell, 1988] Ferri, A. and Dowell, E., 1988, “Frequency Domain Solutions to Multi-Degree-of-Freedom, Dry Friction Damped Systems,” *Journal of Sound and Vibration*, Vol. 124, No. 2, pp. 207–224.
- [Griffin, 1980] Griffin, J., 1980, “Friction Damping of Resonant Stresses in Gas Turbine Engine Airfoils,” *Journal of Engineering for Power*, Vol. 102, pp. 329–333.
- [Griffin and Sinha, 1985] Griffin, J. and Sinha, A., 1985, “The Interaction Between Mistuning and Friction in the Forced Response of Bladed Disk Assemblies,” *Journal of Engineering for Gas Turbines and Power*, Vol. 107, pp. 205–211.
- [Griffin et al., 1998] Griffin, J., Wu, W.-T., and El-Aini, Y., 1998, “Friction Damping of Hollow Airfoils: Part I - Theoretical Development,” *Journal of Engineering for Gas Turbines and Power*, Vol. 120, pp. 120–125.
- [Guillen and Pierre, 1996] Guillen, J. and Pierre, C., 1996, “Analysis of the Forced Response of Dry-Friction Damped Structural Systems Using an Efficient Hybrid Frequency-Time Method,” *Proceedings of the International Mechanical Engineering Congress and Exposition, Atlanta, Georgia, November 1996*, volume DE-91, pages 41–50.
- [Guillen and Pierre, 1998] Guillen, J. and Pierre, C., 1998, “An Efficient, Hybrid, Frequency-Time Domain Method for the Dynamics of Large-Scale Dry-Friction Damped Structural Systems,” *Proceedings of the IUTAM Symposium on Unilateral Multibody Dynamics, Munich, Germany*.
- [Iwan, 1967] Iwan, W., 1967, “On a class of models for the yielding behaviour of continuous and composite systems,” *Journal of Applied Mechanics*, Vol. 34, pp. 612–617.
- [Kruse and Pierre, 1996] Kruse, M. and Pierre, C., 1996, “Forced Response of Mistuned Bladed Disks Using Reduced-Order Modeling,” *Proceedings of the 37th AIAA/ASME/ASCE/AHS/ASC Structures, Structural Dynamics, and Materials Conference*, volume 4, pages 1938–1950.
- [Lau et al., 1983] Lau, S., Cheung, Y., and Wu, S., 1983, “Incremental Harmonic Balance Method with Multiple Time Scales for Aperiodic Vibration of Nonlinear Systems,” *Journal of Applied Mechanics*, Vol. 50, pp. 871–876.
- [Lau and Zhang, 1992] Lau, S. and Zhang, W.-S., 1992, “Nonlinear Vibrations of Piecewise-Linear Systems by Incremental Harmonic Balance Method,” *Journal of Applied Mechanics*, Vol. 59, pp. 153–160.

- [Leung and Ge, 1995] Leung, A. and Ge, T., 1995, “Toeplitz Jacobian Matrix for Nonlinear Periodic Vibration,” *Journal of Applied Mechanics*, Vol. 62, pp. 709–717.
- [Ling and Wu, 1987] Ling, F. and Wu, X., 1987, “Fast Galerkin Method and its Application to Determine Periodic Solutions of Nonlinear Oscillations,” *International Journal of Non-Linear Mechanics*, Vol. 22, No. 2, pp. 89–98.
- [Menq et al., 1986] Menq, C.-H., Bielak, J., and Griffin, J., 1986, “The Influence of Microslip on Vibratory Response, Part I: A New Microslip Model,” *Journal of Sound and Vibration*, Vol. 107, No. 2, pp. 279–293.
- [Menq et al., 1991] Menq, C.-H., Chidamparam, P., and Griffin, J., 1991, “Friction Damping of Two-dimensional Motion and its Application in Vibration Control,” *Journal of Sound and Vibration*, Vol. 144, pp. 427–447.
- [Mickens, 1984] Mickens, R., 1984, “Comments on the Method of Harmonic Balance,” *Journal of Sound and Vibration*, Vol. 94, No. 3, pp. 456–460.
- [Muszýnska and Jones, 1983] Muszýnska, A. and Jones, D., 1983, “On Tuned Bladed Disk Dynamics: Some Aspects of Friction Related Mistuning,” *Journal of Sound and Vibration*, Vol. 86, No. 1, pp. 107–128.
- [Natsiavas, 1998] Natsiavas, S., 1998, “Stability of Piecewise Linear Oscillators With Viscous and Dry Friction Damping,” *Journal of Sound and Vibration*, Vol. 217, No. 3, pp. 507–522.
- [Natsiavas and Gonzalez, 1992] Natsiavas, S. and Gonzalez, H., 1992, “Vibration of Harmonically Ecited Oscillators With Asymmetric Constraints,” *Journal of Applied Mechanics*, Vol. 59, pp. 284–290.
- [Nayfeh and Mook, 1979] Nayfeh, A. and Mook, D., 1979, *Nonlinear Oscillations*, John Wiley & Sons.
- [Pierre et al., 1985] Pierre, C., Ferri, A., and Dowell, E., 1985, “Multi-Harmonic Analysis of Dry Friction Damped Systems Using an Incremental Harmonic Balance Method,” *Journal of Applied Mechanics*, Vol. 51, No. 4, pp. 958–964.
- [Ren and Beards, 1994] Ren, Y. and Beards, C., 1994, “A New Receptance-Based Perturbative Multi-Harmonic Balance Method for the Calculation of the Steady-State Response of Non-Linear Systems,” *Journal of Sound and Vibration*, Vol. 172, No. 5, pp. 593–604.
- [Sanliturk and Ewins, 1996] Sanliturk, K. and Ewins, D., 1996, “Modelling Two-Dimensional Friction Contact and its Application Using Harmonic Balance Method,” *Journal of Sound and Vibration*, Vol. 193, No. 2, pp. 511–523.

- [Sanliturk et al., 1997] Sanliturk, K., Imregun, M., and Ewins, D., 1997, “Harmonic Balance Vibration Analysis of Turbine Blades With Friction Dampers,” *Journal of Vibration and Acoustics*, Vol. 119, pp. 96–103.
- [Shiau et al., 1998] Shiau, T., Rao, J., Yu, Y., and Choi, S., 1998, “Steady-State Response and Stability of Rotating Composite Blades with Frictional Damping,” *Journal of Engineering for Gas Turbines and Power*, Vol. 120, pp. 131–139.
- [Shiau and Yu, 1996] Shiau, T. and Yu, Y., 1996, “Frictional Damping on the Dynamic Behaviour of Composite Blades,” *Proceedings of the 6th International Symposium on Transport Phenomena and Dynamics of Rotating Machinery*, volume 1, pages 262–271.
- [Sinha and Griffin, 1983] Sinha, A. and Griffin, J., 1983, “Friction damping of Flutter in Gas Turbine Engine Airfoils,” *Journal of Aircraft*, Vol. 20, No. 4, pp. 372–376.
- [Sinha and Griffin, 1984] Sinha, A. and Griffin, J., 1984, “Effects of Static Friction on the Forced Response of Frictionally Damped Turbine Blades,” *Journal of Engineering for Gas Turbines and Power*, Vol. 106, pp. 65–69.
- [Sinha and Griffin, 1985] Sinha, A. and Griffin, J., 1985, “Effects of Friction Dampers on Aerodynamically Unstable Rotor Stages,” *AAIA Journal*, Vol. 23, pp. 262–270.
- [Sinha et al., 1986] Sinha, A., Griffin, J., and Kielb, R., 1986, “Influence of Friction Dampers on Torsional Balde Flutter,” *Journal of Engineering for Gas Turbines and Power*, Vol. 108, pp. 313–318.
- [Wang and Chen, 1993] Wang, J. and Chen, W., 1993, “Investigation of the Vibration of a Blade with Friction Damper by HBM,” *Journal of Engineering for Gas Turbines and Power*, Vol. 115, pp. 294–299.
- [Wang, 1996] Wang, Y., 1996, “An Analytical Solution for Periodic Response of Elastic-Friction Damped Systems,” *Journal of Sound and Vibration*, Vol. 189, No. 3, pp. 299–313.
- [Wang, 1997] Wang, Y., 1997, “Stick-Slip Motion of Frictionally Damped Turbine Airfoils: A Finite Element in Time (FET) Approach,” *Journal of Vibration and Acoustics*, Vol. 119, pp. 236–243.
- [Wei and Pierre, 1989] Wei, S.-T. and Pierre, C., 1989, “Effects of Dry Friction Damping on the Occurrence of Localized Forced Vibrations in Nearly Cyclic Structures,” *Journal of Sound and Vibration*, Vol. 129, pp. 397–416.
- [Whiteman and Ferri, 1999] Whiteman, W. E. and Ferri, A. A., 1999, “Suppression of Bending-Torsion Flutter Through Displacement-Dependent Dry Friction Damping,” *AIAA Journal*, Vol. 37, pp. 79–83.

[Yang et al., 1998] Yang, B., Chu, M. L., and Menq, C., 1998, “Stick-Slip-Separation Analysis and Non-Linear Stiffness and Damping Characterization of Friction Contacts Having Variable Normal Loads,” *Journal of Sound and Vibration*, Vol. 214, No. 4, pp. 461–481.

ABSTRACT

STUDIES OF THE DYNAMICS OF DRY-FRICTION-DAMPED BLADE ASSEMBLIES

by

Jérôme Guillen

Chairperson: Christophe Pierre

The steady-state response to periodic excitation of multi-degree of freedom (DOF) structural systems with several elastic/perfectly plastic attached dry friction dampers is studied. The force transmitted by a friction damper is deduced in the time domain from the displacement and velocity of the corresponding DOF to which the friction damper is attached. The convergence of the method is ensured by a modified Broyden's algorithm, which is used to solve iteratively the set of multi-harmonic nonlinear equations in the frequency domain. The solution algorithm is thus hybrid in the frequency and time domains. The method proposed can handle both friction dampers that are attached to ground and the general case of dampers that connect two DOF's of the structure. Results are obtained for both tuned and mistuned configurations of large-scale models of dry-friction damped bladed disks used in turbomachinery applications, subject to various traveling wave "engine order" excitations, for a variety

of structural and friction parameters. Interesting, complex features of the nonlinear response are revealed, such as: motions for several stick-slip phases per period; localized motions for mistuned systems, which feature mostly sticking motion at most blades and mostly slipping motion at a few blades; subresonances; effects of higher harmonics. Free response and stability analyses are also presented for structural systems attached to a single friction damper. Finally, a novel, general model of friction damper is introduced: the damper element is a general, massless structure connected at multiple punctual interfaces to the adjacent structures. This model allows for a rich combination of stick/slip dynamic motion at the various interfaces. It is believed to provide an accurate behavior of dry friction-damped blade assemblies.